

ABSTRACT

Title of dissertation: LIDAR REMOTE SENSING OF VERTICAL FOLIAGE PROFILE AND LEAF AREA INDEX

Hao Tang, PhD, 2015

Dissertation directed by: Professor Ralph Dubayah
Department of Geographical Sciences

Leaf Area Index (LAI) and Vertical Foliage Profile (VFP) are among the most important forest structural parameters, and characterization of those parameters in high biomass forests remains a major challenge in passive remote sensing due to signal saturation problem. Recently an active remote sensing technology, light detection and ranging (lidar), has shown a great promise in this task recognizing its accuracy in measuring aboveground biomass and canopy height. This dissertation further expands current application of lidar on ecosystem monitoring, and explores the capacity of deriving LAI and VFP from lidar data in particular.

The overall goal of this study is to derive large scale forest LAI and VFP using data from the Geoscience Laser Altimeter System (GLAS) on board of ICESat, and provide a framework of validating such LAI products from plot level to global scale. To achieve this goal, a physically based Geometry Optical and Radiative Transfer (GORT) model was first developed using high quality airborne waveform

lidar data over a tropical rainforest in La Selva, Costa Rica. The excellent agreement between lidar data and field destructively sampled data demonstrated the effectiveness of the Lidar-LAI model and suggested large footprint waveform lidar can provide accurate vertical LAI profile estimates that do not saturate even at the highest possible LAI levels.

Next, an intercomparative study of ground-based, airborne and spaceborne retrievals of total LAI was conducted over the conifer-dominated forests of Sierra Nevada in California. Good relationships were discovered in their comparisons, following a scaling-up validation strategy where ground-based LAI observations were related to aircraft observations of LAI, which in turn were used to validate GLAS LAI derived from coincident data. Successful implementation of this strategy can pave the way for the future recovery of vertical LAI profiles globally.

LAI and VFP products were then derived over both the entire state of California and Contiguous United States as an efficacy demonstration of the method. These products were the first ever attempts to obtain large scale estimates of LAI and VFP from lidar observations. Such forest structural measurement can be used not only to quantify carbon stock and flux of terrestrial ecosystem, but also to provide spatial information of specie abundance in biodiversity. Results from this study can also greatly help broaden scientific applications of future spaceborne lidar missions (e.g. ICESat-2 and GEDI).

LIDAR REMOTE SENSING OF VERTICAL FOLIAGE PROFILE AND LEAF
AREA INDEX

by

Hao Tang

Dissertation submitted to the Faculty of the Graduate School of the
University of Maryland, College Park, in partial fulfillment
of the requirements for the degree of
Doctor of Philosophy
2015

Advisory Committee:

Professor Ralph Dubayah, Chair
Professor George Hurtt
Professor Shunlin Liang
Dr. Ross Nelson
Professor Joseph Sullivan

© Copyright by
Hao Tang
2015

Dedication

To

My parents,

Changsheng Tang & Ping Xue

and

Jie Zhou

Acknowledgements

I would first express my sincere gratitude to my advisor Ralph Dubayah, without whom I cannot achieve this honor with pains and gains. It is a long journey, and this wizard like Gandalf the Grey led me towards the right path of becoming a genuine researcher and scientist, sentence by sentence, paper by paper. I would also like to pay special gratitude to Shunlin Liang, who brought me into this department and provided invaluable care and advice during my graduate student life. I am also very thankful to all my other committee members: George Hurtt, Ross Nelson and Joe Sullivan for their generous and constructive advice and feedbacks.

Special gratitude goes to John Townshend who always enlightens me with extreme patience and advice. Many thanks to Michelle Hofton, Bryan Blair, Guoqing Sun, Bruce Cook and Chengquan Huang, who have guided me throughout the endless sea of lidar data and waveforms. I would have been drowned without their kind help. I also acknowledge David Clark, Matthew Clark and all their team members for their work in La Selva Biological Station. Acknowledge also goes to Alan Strahler, Crystal Schaff, Sangram Ganguly and Gong Zhang.

A big thank you to Anu Swatantran, Matthew Brolly, Anupam Ananad, Amanda Whitehurst, Laura Duncanson, Steve Flanagan, Katelyn Dolan, Justin Fisk, Christine Kang, Lee Ann King, Mike O'Connell, Naiara Pinto and all VCL & GEL lab members. The days spent with you guys provide sunshine in our windowless lab. Thanks also go to staff of department front office, Bob Crossgrove, Liz Smith, Suzanne Bach, Christine Kang, Rachel Berndtson for their extreme patience and

support.

Many thanks to all my Chinese friends in the department, Wenli Huang, Qiongyu Huang, Maosheng Zhao, Danxia Song, Tao He, Xiaopeng Song, Xin Tao, Qing Ying, Lei Wang, Cheng Fu, Dong Chen, Dongdong Wang, Feng A. Zhao, and Feng R. Zhao. I will also thank all the Chinese students and scholars in our department and CSSA as we are united together to present the culture and spirit of our nation.

It is beyond any verbal description about how fortunate and grateful I am towards all my family, my beloved friends and my special one. They give me the strongest support and warmest love all the time. I love you all!

Table of Contents

List of Tables.....	viii
List of Figures	ix
Chapter 1 An Overview of Current Measurement Methods of LAI and VFP	1
1.1 Motivation	1
1.2 Background	5
1.2.1 Relevance of LAI and VFP to carbon cycle science	5
1.2.2 Relevance of LAI and VFP to terrestrial ecology	6
1.2.3 Relevance of LAI and VFP to biodiversity	7
1.3 Quantifying forest LAI.....	8
1.3.1 From field methods	8
1.3.2 From passive remote sensing	9
1.4 Lidar remote sensing of LAI	11
1.5 Dissertation Outline	14
Chapter 2 Retrieval of Vertical LAI Profiles over Tropical Rain Forests using Waveform Lidar at La Selva, Costa Rica	16
2.1 Introduction	16
2.2 Study Area & Data.....	18
2.2.1 Study area	18
2.2.2 Field data	19
2.2.3 Lidar data.....	20
2.3 Methods.....	21
2.3.1 Cumulative LAI from tower measurements	22
2.3.2 Cumulative LAI profiles from LVIS waveforms.....	22
2.3.3 Scale adjusted cumulative LAI from LVIS waveform.....	25
2.3.4 Distance of tower from lidar footprint center	27
2.4 Results	27
2.4.1 Comparison of lidar and tower LAI	27
2.4.2 Landscape LAI variability	31

2.5 Discussion	35
2.6 Conclusion.....	41
Chapter 3 Deriving and Validating Leaf Area Index (LAI) at Multiple Spatial Scales through Lidar Remote Sensing.....	43
3.1 Introduction	43
3.1.1 LAI using remote sensing.....	43
3.1.2 Proposal for multi spatial scale LAI validation	46
3.2 Study Area and data.....	48
3.2.1 Ground based data: hemispherical photography, LAI-2000 and terrestrial lidar	49
3.2.2 Airborne lidar data: LVIS.....	49
3.2.3 Spaceborne lidar data: GLAS	50
3.3 Methods.....	51
3.3.1 LAI from Ground Based Measurements	52
3.3.2 LAI from LVIS	54
3.3.3 LAI from GLAS.....	56
3.4 Results.....	59
3.4.1 LVIS LAI.....	59
3.4.2 LVIS LAI vs. Ground Based LAI.....	61
3.4.3 LVIS LAI vs. GLAS LAI	63
3.4.4 LVIS LAI vs. MODIS LAI.....	66
3.5 Discussion	68
3.6 Conclusion.....	73
Chapter 4 Large-scale Retrieval of Leaf Area Index and Vertical Foliage Profile from the Spaceborne Waveform Lidar (GLAS/ICESat).....	76
4.1 Introduction	76
4.2 Data and Methods.....	78
4.2.1 GLAS.....	78
4.2.2 Ancillary Input Data.....	79
4.2.3 LAI Derived from Landsat	81
4.2.4 LAI Retrieval Algorithm	81
4.3 Results.....	85
4.3.1 GLAS LAI	86

4.3.2 GLAS Vertical Foliage Profiles (VFP)	89
4.3.3 GLAS vs. Landsat	95
4.3.4 Slope Analysis	97
4.4 Discussion	99
4.5 Conclusion.....	104
Chapter 5 Characterizing Leaf Area Index (LAI) and Vertical Foliage Profile (VFP) across the United States	106
5.1 Introduction	106
5.2 Methods.....	109
5.2.1 GLAS Data	109
5.2.2 Retrieval of GLAS LAI and VFP	110
5.2.3 Comparison Data Set.....	110
5.2.4 Analysis	111
5.3 Results.....	113
5.3.1 GLAS LAI and VFP Comparisons with LVIS and Landsat	113
5.3.2 Aggregated GLAS LAI and VFP at Ecoregions.....	117
5.3.3 GLAS LAI Distributions by Environmental Factors	122
5.4 Discussion	126
5.5 Conclusion.....	131
Chapter 6 Conclusion	133
Appendices.....	140
Bibliography.....	144

List of Tables

Table 2-1 Total LAI from different land cover and land use areas	29
Table 3-1 Site characteristics from ground based data collection at Sierra National Forest, CA, July, 2008 (Zhao et al. 2012).....	48
Table 3-2 Summary of comparison results with LVIS LAI	67
Table 4-1 Statistics of GLAS LAI and LAI strata by biome type (ENF = Evergreen Needle Forest, EBF = Evergreen Broadleaf Forest, DNF = Deciduous Needleleaf Forest, DBF = Deciduous Broadleaf Forest).	94
Table 5-1 Ecoregions with highest total LAI values	118

List of Figures

Fig. 2-1 Land use map of La Selva Biological Station, Costa Rica. 55 LAI measurement towers were constructed across different forest areas, but mainly focused on old-growth forest.	20
Fig. 2-2 Examples of cumulative LAI profile from tower measurements and derived from LVIS.	28
Fig. 2-3 Cumulative LAI estimated from LVIS data against all 55 cumulative LAI measurement towers. The total sampling number is 546, which is the number of total tower bins used to collect leaves. Note that after scale adjustment, many of the value that were underpredicted by LVIS rise.	30
Fig. 2-4 Cumulative LAI estimated from LVIS against cumulative LAI for towers with a distance less than 5 m from the laser pointing center. Cumulative LAI values from 16 towers are marked with different symbols.	31
Fig. 2-5 Total LAI mapped across La Selva as derived from LVIS. Regenerating pastures have the lowest LAI values. Old growth forests have the highest mean LAI value and secondary forests are somewhat lower.	33
Fig. 2-6 Vertical LAI integration maps from 0 to 5m, 5 to 10m, 10 to 20m and above 20m.	34
Fig. 2-7 Box plot of total LAI distribution over different forest successional types. The median LAI value is lowest for earlier succession stages and a reaches maximum value for 30-34 year-old secondary forests. Central lines give the median and boxes above and below the line give the interquartile range. Dashed lines give the 5% and 95% ranges. Non-overlapping median notches indicate significant differences	

between those medians at roughly a 95% confidence interval. 35

Fig. 2-8 An example of LAI profiles derived from LVIS with different values of ρ_v/ρ_g . As the leaf/soil reflectance ratio increases, the LAI value decreases and the profiles shift towards lower values of LAI. The sensitivity of LAI to the ratio changes is about 1. 38

Fig. 2-9 Different sensitivity of moderate LAI (~ 4) (a) and high LAI (~ 8) (b) to different ground noise levels. Ground noise is added to waveforms manually and the total noise value is shown in the legend, ranging from 25% to 100% of the peak value of return energy. The same noise levels have different levels of impact for low and high LAI. 39

Fig. 3-1 Deriving and validating LAI products at multiple-scales. Regional-scale lidar mapping (e.g. LVIS) can bridge the gap between sparsely measured field data and satellite observations. 52

Fig. 3-2 Recursive estimation of LAI from GLAS waveform data. LAI estimate from GLAS data must satisfy the processing conditions defined by independent but inexact LAI sources. 59

Fig. 3-3 Landscape map of effective LAI generated from LVIS, showing large spatial variation of LAI at 30 m scale. The forests in Sierra follow a spatially discontinuous distribution, leaving large gaps of bare ground and rocks between conifer canopies. 60

Fig. 3-4 Frequency distribution of effective LAI from LVIS data over the entire Sierra National Forest area. 61

Fig. 3-5 Plot-level averaged LVIS effective LAI against plot-level LAI estimates

from a) Hemispherical photos, b) LAI-2000, c) Echidna regression LAI and d) Echidna hinge angle LAI. While there are strong relationships, LVIS is biased low, especially with regards to Echidna. 62

Fig. 3-6 a) GLAS LAI derived from non-recursive method; b) GLAS LAI derived from recursive method. The x-axis is averaged LVIS effective LAI and the y-axis is derived GLAS LAI. 63

Fig. 3-7 Correlation statistics of RMSE and r^2 calculated upon comparison of all LVIS LAI and GLAS LAI values as a function of slope threshold (α). For a given slope threshold α , the y-axis represents the RMSE (or r^2) of all GLAS shots with slope $< \alpha$ 65

Fig. 3-8 Averaged LVIS effective LAI against GLAS LAI at the GLAS footprint level for GLAS shots with an average slope $< 20^\circ$ 66

Fig. 3-9 Averaged LVIS total LAI against MODIS LAI at each MODIS 1 km pixel level. 67

Fig. 4-1 Location of ICESat ground tracks over California, USA. ICESat did not provide a wall-to-wall coverage but rather data along transects separated by relatively long distances across track at mid-latitudes. 78

Fig. 4-2 Algorithm flowchart of retrieving LAI and VFP from GLAS data. Parallelograms are input data sets. The recursive method part (within the dash-dotted rectangle) is adapted from Tang et al. (2014). 85

Fig. 4-3 GLAS LAI estimates over California. The majority of GLAS footprints had a LAI value less than 2 but there were also footprints with values greater than 8. The solid line shows the cumulative frequency. 86

Fig. 4-4 GLAS LAI as a function of land-cover type. The width of the boxes is proportional to the number of observations for each type. Forest LAI (both evergreen needleleaf and mixed forest) are significantly larger than any other type. Note that difference between Evergreen needleleaf forest and mixed forest is also significant ($P < 0.001$)..... 88

Fig. 4-5 Boxplot of GLAS LAI distribution as a function of elevation stratification groups. A linear regression analysis (dotted line) of LAI values averaged by elevation groups (red cross) shows a decreasing trend ($r^2 = 0.91$, $P < 0.001$)..... 89

Fig. 4-6 Left: VFP (vertical resolution of 2 m) averaged for all GLAS shots over California for different land cover types. Each profile represents a single land cover type. Mean values are central lines within the color-filled 95% CI envelope. Note the low height of peak LAD is because of the averaging process over the land cover type. Individual profiles have much more variable shapes (see Right). Right: individual VFP examples with foliage density peak occurring at understory (<5 m), middle-story (~ 10 m) and up-story (>20 m)..... 90

Fig. 4-7 GLAS LAI stratified by canopy position. Note that differences between needleleaf forest and mixed forest were only significant at the 10~20 m layer and > 20 m layer ($P = 0.003$ and $P < 0.001$ respectively). Note differing y-axis scales..... 91

Fig. 4-8 Variability of GLAS LAI strata as a function of elevation for different canopy positions. The decreasing patterns were consistent in the 0-5 m, 5-10 m, 10-20 m and >20 m groups with slightly different rates. Note differing y-axis scales. 92

Fig. 4-9 Density scatter plot of Landsat LAI and GLAS LAI over California. The comparison reveals a fair agreement between the two data sets, but Landsat appears to

saturate at about LAI = 5, and overestimates lower values relative to GLAS. Kernel density color bar refers to the distribution of LAI pairs with darker color indicating more clustered footprints.95

Fig. 4-10 Histogram of LAI difference between GLAS and Landsat. The red dashed line gives the bias (0.26). However, this low bias does not reflect the systematic differences apparent in Fig. 4-9.....96

Fig. 4-11 An example of GLAS LAI and Landsat LAI at small scale. Overlaid GLAS LAI data is given by circles showing the sensor footprint to actual scale.97

Fig. 4-12 Correlation statistics of r^2 and RMSD calculated upon comparison of GLAS LAI and Landsat LAI values by slope groups. Histogram gives distribution of slope groups. About 80% of the data had slopes less than 20°98

Fig. 5-1 Comparison between LVIS LAI and GLAS LAI at different sites across US (N = 318). Each point represents a comparison at GLAS footprint while different colors indicate different sites. The comparison result ($r^2 = 0.60$, bias = -0.23, and RMSE = 0.82) reveals a good agreement between the two data sets. 114

Fig. 5-2 Comparison between LVIS VFP and GLAS VFP integrated at 5 m height interval over different sites in CONUS (N = 1272). The comparison result ($r^2 = 0.36$, bias = -0.043, and RMSE = 0.26) has a relatively lower agreement than that of LAI. 114

Fig. 5-3 Comparison between LVIS and GLAS LAI density integrated at every 5 m height interval. Their agreements increase as the height interval moving upward: 1) 0 - 5 m: $r^2 = 0.04$, bias = 0.09, RMSE = 0.31; 2) 5 - 10 m: $r^2 = 0.33$, bias = -0.13, RMSE = 0.29; 3) 10 - 15 m: $r^2 = 0.53$, bias = -0.08, RMSE = 0.22; 4) 15 - 20 m,

$r^2 = 0.66$, bias = -0.05, RMSE = 0.20. 115

Fig. 5-4 Comparison between Landsat LAI and GLAS LAI over Contiguous US: a) density scatter plot of Landsat and GLAS LAI; b) histogram of LAI difference between Landsat and GLAS. Darker kernel density color refers to more clustered distribution of LAI pairs. Despite a low bias value of 0.18 (red dot-line in b), the comparison ($r^2 = 0.18$, RMSE = 2.02) reveals a relatively low level agreement between the two data sets. In particular, Landsat appears to saturate at about LAI = 4 relative to GLAS. 116

Fig. 5-5 GLAS LAI distributions by WWF ecoregions. LAI values decrease from eastern (or western) coast towards inner land. 117

Fig. 5-6 LAI strata distributions by WWF ecoregions. Despite similar total LAI values, the southeastern forests show different LAI values at stratified height intervals. 119

Fig. 5-7 Distribution of total LAI across different land cover types. The width of the boxes is proportional to the number of observations for each type. 121

Fig. 5-8 Averaged GLAS VFP for different land cover types across US: non-forest vegetation types (left) and forest types (right). Mean values are central lines within the color-filled 95% CI envelope. 122

Fig. 5-9 Distribution of GLAS LAI and forest ratio (GLAS shots over forest divided by total shot numbers) as a function of elevation stratification groups. Overall, there is a decreasing trend of LAI values as elevation increases ($r^2 = 0.59$, $adj\text{-}r^2 = 0.56$, $P < 0.01$) despite an observed variation. Such variation pattern of total LAI coincides with the distribution of forest ratio at elevation groups ($r^2 = 0.45$, $adj\text{-}r^2 = 0.40$, $P <$

0.01)..... 123

Fig. 5-10 Distribution of GLAS LAI as a function of precipitation stratification groups. A linear regression analysis of LAI values averaged by precipitation groups shows a very significant increasing trend (1.84 unit per 1000 mm, $r^2 = 0.96$, $adj\text{-}r^2 = 0.95$, $P < 0.001$) at areas with annual precipitation less than 2400 mm but almost no increase above that. 124

Fig. 5-11 Example of a combined environmental effect on GLAS total LAI and VFP. GLAS transects selected from Western Cascade, Eastern Cascade and northern Rocky Mountain areas have averaged LAI values of 4.90, 2.75 and 3.99. Heights in the second and third rows are multiplied by 10 to show foliage distribution within canopy..... 126

Chapter 1 An Overview of Current Measurement Methods of LAI and VFP

1.1 Motivation

Forests play an important role in both human social activities and environmental systems. Not only do they provide raw material of food, medicine and fuel, but also shelters for endangered species according to Millennium Ecosystem Assessment (2005). Forests are also major sinks for anthropogenic carbon emissions and help mitigate the effects of climate change. All these functions of forests fundamentally rely on the development of canopy structure at individual leaf level, where photosynthesis takes place. A detailed quantitative measurement of canopy structural attributes is among the top priorities in terrestrial ecology, biodiversity and carbon cycle studies. This involves the measurement and derivation of many biophysical parameters for current ecosystem experiments and models. Among them are Leaf Area Index (LAI) and Vertical Foliage Profile (VFP).

LAI, defined as one half of the total leaf area projected per unit horizontal surface (Chen et al. 1997), has been widely applied in ecology and remote sensing community in describing biosphere-atmosphere interactions of carbon dioxide, water and energy. It has already been proven to be an efficient representative of canopy foliage content and crown structure, and has been widely applied to estimate radiation attenuation, plant photosynthesis and respiration with considerable accuracy (Gower and Norman 1991). Large scale LAI measurements are typically required in

ecological, hydrological and climate models. For example, LAI is a major input parameter driving ecosystem models to simulate ecological responses at regions with limited field measurements in particular (Hurt et al. 2004). Hydrological models require estimates of LAI to simulate terrestrial evapotranspiration (ET), which plays a key role in regional water and energy balance. Accurate LAI measurements also help establish and improve the relationship between Gross Primary Production (GPP) and remote sensing spectral reflectance observations to reduce the uncertainty of terrestrial carbon fluxes (Turner et al. 2006).

VFP (vertical foliage profile or vertical LAI profile) is essentially the vertical variation of LAI closely related to foliage-height profiles (Aber 1979), and an integration of VFP through canopy will get the LAI value. Compared with LAI, it is a more realistic representation of 3D canopy structure and determined to be among the most critical determinants of energy and material flows in ecosystems (Parker et al. 2001; Stark et al. 2012). A significant improvement in terrestrial carbon and ET estimate should be expected with further application and incorporation of VFP into current models rather than LAI alone. This is because foliage at different height intervals contribute differently towards total photosynthesis and canopy carbon storage (Ellsworth and Reich 1993). Previous work has indicated that the use of a uniform foliage distribution instead of the actual LAI profile could result in an underestimated GPP value (up to 50%) under diffuse radiation condition (Chen et al. 1999; Kotchenova et al. 2004). VFP have also been widely applied in biodiversity conservation and proven to be important metrics in studies of breeding bird survey (Bradbury et al. 2005; Goetz et al. 2007; Hyde et al. 2006; Swatantran et al. 2012).

These studies indicate that further application of VFP has the potential to better refine current carbon and ecological models.

Large scale LAI and VFP measurements are among basic requirements in studies of global environmental change acknowledging their importance in ecosystem modeling. However direct measurements of LAI and VFP are spatially limited at field campaigns largely due to both complexity of natural environment and limitation of costs. An alternative solution is to derive those ecosystem structural parameters based on their relationship spectral signatures derived from remote sensing images. Tremendous efforts from the remote sensing community have been made to derive LAI products at different spatial and temporal scales since the 1980s, focusing largely on the use of passive remote sensing data. To date there have been a large number of regional to global scale LAI data sets available, including MODIS (Myneni et al. 2002), LANDSAT (Ganguly et al. 2008), CYCLOPES (Baret et al. 2007) and many others. These products have been widely used in studies of terrestrial ecosystems and have greatly improved our knowledge and understanding of global environment and climate change (Fang et al. 2013; Mu et al. 2007; Myneni 2001; Zhao et al. 2005). However, three key issues remain unsolved despite such great progress and successes with passive remote sensing: first, spectral signals of satellite images saturate over high LAI areas; secondly, LAI products from different sensors are inconsistent (Abuelgasim et al. 2006); and finally, vertical foliage structure or VFP products are not available. While these problems have long been discovered, they cannot be easily solved within the regime of traditional remote sensing technology.

In the past decade, LiDAR (Light Detection and Ranging) has emerged as a

new remote sensing technology to derive different forest characteristics (e.g. canopy height and aboveground biomass) with unprecedented accuracy (Drake 2002a; Hyde et al. 2005; Lefsky 1999a). The penetration ability of active laser energy emitted from the lidar sensor allows a 3D measurement of entire canopy structure that is impossible from traditional passive remote sensing data. As a result, deriving highly accurate LAI and VFP products from lidar remote sensing is a promising field with many efforts being made by different groups (Morsdorf et al. 2006; Ni-Meister et al. 2001; Strahler et al. 2008). Spaceborne lidar missions, such as the Ice, Cloud, and land Elevation Satellite (ICESat) or the upcoming Global Ecosystem Dynamics Investigation (GEDI), provide a unique opportunity for exploring the efficacy of deriving LAI and VFP at continental to global scale. Large scale LAI and VFP products, once derived and validated appropriately from such spaceborne lidar, can greatly help improve our understandings of ecosystem structure and dynamics and address current science priorities endorsed in NRC Decadal Survey (NRC 2007).

The overall goal of my dissertation is to develop an approach to map forest LAI and VFP at large scale using data from the Geoscience Laser Altimeter System (GLAS) on board of ICESat. In particular, the following objectives will be addressed:

- 1) Derive LAI and vertical foliage profile from waveform lidar using a physically based model.
- 2) Develop a robust Lidar-LAI model and validation framework for deriving LAI and vertical foliage profile from GLAS.
- 3) Derive and validate GLAS LAI products at different scales across major forest

types.

1.2 Background

1.2.1 Relevance of LAI and VFP to carbon cycle science

Carbon emissions from human activities have been continuing to change climate system for the past decades, leading to a significant increase of globally averaged temperature and sea level (IPCC 2007, 2013). In particular, fossil fuel use, forest deforestation and land-use change are determined to be the major sources of increased carbon in atmosphere with an annual rate of 4.1 ± 0.1 GtC (IPCC 2013). However, large measurement uncertainties ($> 50\%$) remain in current estimates of land-to-atmosphere flux (-0.9 ± 0.6 GtC) and carbon stocks in terrestrial forests (Houghton 2007). This leads to an imbalance of more than 1 GtC within global carbon cycle known as "missing carbon" (DeFries et al. 2002; Houghton et al. 1998; Schindler 1999). Significant efforts have been made to reduce the unbalance and uncertainty in carbon cycles. For example, recent reports from long-term forest inventory data suggest an annual carbon sink of 2.4 ± 0.4 GtC in global forests from 1990 to 2007 (Pan et al. 2011). Although such field estimates are approaching the equivalent magnitude of inversion model (deduced from fossil fuel emissions and land-use change sources minus ocean and atmospheric sources), there remains a large uncertainty, in tropical forests particularly, regarding the sparse sampling at local scales and subsequent up-scaling estimates. Additionally, deployments of these field campaigns are highly costly and usually take a long time to complete the mission. As a result there are critical requirements for higher density supplemental data products

for ground sampling and more accurate terrestrial carbon stock estimates over large scale. Those requirements may be achieved through either direct products from remote sensing data or indirect estimates from ecosystem models (Hurt et al. 2004), both of which would require an accurate characterization of ecosystem parameters. Canopy height, LAI and vertical foliage profile are among the most important biophysical parameters closely related to the terrestrial carbon stocks and aboveground biomass based on allometric equations (Drake 2002a; Dubayah and Drake 2000; Lefsky et al. 2002). They have been widely used to derive national level or continental scale aboveground biomass products (Baccini et al. 2012; Kellndorfer et al. 2012; Saatchi et al. 2011).

1.2.2 Relevance of LAI and VFP to terrestrial ecology

Terrestrial ecosystems are sensitive towards climate change due to their low tolerance and vulnerability towards environmental change (Bonan 2008). Since an increase in temperature, CO₂ concentration and nitrogen (N) deposition as well as changes in precipitation pattern will be expected under current scenario (IPCC 2013), it is thus critical to understand how forests respond to the ongoing climate change. Factors associated with climate change and variability have different impacts on terrestrial ecosystems, and can lead to both a long-term effect on changing forest structure and function as well as a short-term effect characterized by disturbance regimes, mainly including fire risk, insect infestation and drought (Dale et al. 2001; Lindner et al. 2010; Vose et al. 2012). However, adaptations of terrestrial ecosystems towards the changing climate system have not been fully understood yet. For

example, increase of atmospheric carbon dioxide could enhance forest productivity known as carbon fertilization effect, but this effect can be largely offset by the increased temperature and drought. Debates arise whether tropical forests play as carbon sources or sinks under changing climate and there has been no clear answer yet (Clark 2004; Lewis et al. 2009). The exact mechanism is still under further examination and requires a considerable effort considering the complex interactions among ecosystem, atmosphere and human activities (Bonan 2008; Cramer et al. 2001). Two fundamental requirements will be needed to achieve such goal, including 1) coupling of human and environmental systems, and 2) consistent measurements and monitoring of system parameters. Biophysical variables including LAI and VFP are such important parameters in terrestrial ecosystems (Arora and Boer 2005; Randerson et al. 2009; Running et al. 1999). For example, they are the key parameters used to estimate fraction of absorbed PAR, GPP/NPP and ET across different biomes and provide a great knowledge of global carbon, water and energy fluxes between biosphere and atmosphere (Knyazikhin et al. 1998c; Mu et al. 2007; Myneni et al. 2002; Zhao et al. 2005).

1.2.3 Relevance of LAI and VFP to biodiversity

Global biodiversity has been under consistent threats primarily from anthropogenic land use change and climate change (Sala et al. 2000). The speed of biotic diversity loss does not slow down in the new millennium; instead it continues at an alarming speed of about 50,000 species according to the Millennium Ecosystem Assessment (2005). The massive loss of biodiversity will lead to the reduction and

simplification of biological heterogeneity and ecological complexity from individuals to regions, and ultimately jeopardize the function and stability of ecosystems and human society (Adams et al. 2004; Walker 1992). It is therefore of critical importance to monitor the biodiversity of wild species and their associated living environments. Because biodiversity is not evenly distributed with some areas far richer than the others, hotspots where most severe threats happen, in tropics particularly, should be set higher conservation priorities (Mittermeier et al. 1998). Identification and mapping of these hotspots are hence imperative in biodiversity and conservation studies. Remote sensing systems are highly suitable for this task acknowledging their high spatial and temporal mapping capabilities. Existing studies of species distribution using remote sensing data can essentially be categorized into following three types: 1) direct mapping of individuals, 2) predictions based on habitat requirements and 3) pattern explorations between field observations and remote sensing data (Nagendra 2001). It is not until recently that vertical canopy structure information was adopted into the observation framework of essential biodiversity variables due to the development of lidar remote sensing (Goetz et al. 2007; Pereira et al. 2013; Turner et al. 2003). In particular, canopy height, vertical foliage profiles and associated 3d measurements derived from lidar remote sensing have been demonstrated as important stratification indicators for forest bird species (Hyde et al. 2006; Swatantran et al. 2012).

1.3 Quantifying forest LAI

1.3.1 From field methods

The most accurate LAI values can be obtained by collecting and measuring

leaves with planimetric or gravimetric (Gobron and Verstraete 2009). Such direct LAI measurements, traditionally by either destructive sampling or leaf litter collection, are labor-intensive and time-costing. As a result, LAI data collected from those direct methods usually are at limited sites but of great scientific values. Alternative indirect methods have been developed to improve the efficiency of field measurement while maintaining its accuracy. Among them, the most popular indirect methods are based on the relationship between radiation transmission and foliage amount in canopy layers discovered by Monsi and Saeki (1953). Various field instruments have been developed and commercially available, such as LAI-2000 Plant Canopy Analyzer (Licor, Inc.), hemispherical photos and TRAC (Tracing Radiation and Architecture of Canopies) (Jonckheere et al. 2004). Nowadays the indirect methods are becoming the primary in situ LAI measurements at plot or site scale considering a balance between efficiency and accuracy. A large amount of LAI data have been acquired across all major biomes in the past decade. These data are both important in landscape ecological studies, and serve as the most critical ground verification data for satellites products as well. In order to monitor global terrestrial ecosystem and the changing climate, many national and international observation networks and programs (e.g. FLUXNET and BigFoot) have also been deployed to conduct field LAI measurements using both direct and indirect methods.

1.3.2 From passive remote sensing

Remote sensing could provide large spatial and multi-temporal scale LAI products, and has played an important role in studies of terrestrial ecosystem and

climate change. The earliest work could trace back to Tucker's (1979) method of combining red and photographic infrared channels into vegetation index for vegetation monitoring, which was later famously known as NDVI. An explosive amount of research followed up then with a great advance in both data quality of satellite images as well as method development. Nowadays there have been a large number of global and regional LAI products available from various sensors including MODIS, Landsat, CYCLOPES, ECOCLIMAP and others. Methods of deriving LAI from those satellite images fall into three main categories: 1) empirical methods which builds relationships between field measured LAI and satellite vegetation indices (Chen and Cihlar 1995; Chen et al. 1997; Cohen et al. 2003; Morisette et al. 2006); 2) canopy radiative transfer modeling and physical model inversion (Ganguly et al. 2008; Knyazikhin et al. 1998a; Knyazikhin et al. 1998b; Koetz et al. 2005; Myneni et al. 2002); and 3) hybrid methods combining the previous two methods (Fang and Liang 2003; Walthall et al. 2004). However, LAI products from different sensors are not quite consistent with each other, and a detailed assessment of these products suggests a considerable spatial variation in their accuracies (Abuelgasim et al. 2006). It is particularly true over high biomass and closed canopy forests, such as tropical rain forests where satellite signal saturates quickly and becomes insensitive to canopy structural changes (Steininger 1996). In addition, most of the algorithms only make empirical assumptions about the actual distribution of vertical canopy structural. This simplification could contribute a large error and uncertainty in deriving LAI products considering the heterogeneity of natural forests. All these errors and uncertainties in remote sensing based LAI products should be carefully studied to assess their

propagation effects on the accuracy of the higher level analysis and simulations in terrestrial ecosystems research. Consequently, it is imperative for the community to derive both highly accurate LAI products as evaluation benchmarks as well as vertical LAI distribution for ecosystem modelers.

1.4 Lidar remote sensing of LAI

Lidar is an active remote sensing technology and it calculates the distance between a target and the sensor by measuring the roundtrip traveling time of emitted laser pulse. According to the type of information collected from the return signal, lidar can be broadly classified as discrete-return systems or waveform-recording systems. Discrete-return lidar records one or a small number of height metrics by identifying major peaks in the return signal while waveform lidar measures the complete height distribution of illuminated objects by recording the entire returned signal (Lefsky et al. 2002). Lidar systems can also be classified as terrestrial, airborne and spaceborne lidar depending on the type of platform, and all the three types will be used in this study.

Terrestrial laser scanning (TLS) or terrestrial lidar system quickly becomes a popular 3D measurement tool in earth sciences. At each survey plot, they could provide a rapid, complete and precise documentation of geometric properties of natural surfaces including forest structure information (Brodu and Lague 2012). Typically terrestrial lidar systems have demonstrated the capability of accurately measuring canopy height, diameter at breast height (DBH), LAI and VFP (Cote et al. 2009; Douglas et al. 2012; Strahler et al. 2008; Zheng and Moskal 2012). The

Echidna Validation Instrument (EVI) is one such example of conducting field measurement and validation for airborne/spaceborne mapping. EVI is a ground-based, up-ward-scanning, full-waveform-digitizing lidar, built by CSIRO Australia (Jupp et al. 2009). The rotation design allows a scanning of the entire upper hemisphere and a significant portion of the lower hemisphere of the instrument (Strahler et al. 2008). Echidna has been applied to retrieve different forest stand structural parameters, including LAI, vertical foliage profile and clumping index (Yang et al. 2013; Zhao et al. 2012; Zhao et al. 2011).

Airborne lidar systems play the most important role in 3D measurements of terrestrial ecosystems. The commercialized discrete return airborne lidar systems (e.g. ALTM and RIEGL) have been widely used in generating high quality canopy height and topographical DEM data (Asner et al. 2005; Naesset 1997, 2002; Nilsson 1996; Popescu 2007; Sorin et al. 2004). However, there is a potential drawback of the conflicts in data-processing algorithm and sensor configuration between specific scientific objects and commercial usage (Lefsky et al. 2002). For example, airborne lidar usually fly during leaf-off seasons to generate more accurate DEM while leaf-on data is more desirable for ecological and carbon cycle studies (Sexton et al. 2009). Its emitted laser could miss the top of canopy occasionally leading to an underestimated measurement of forest height. In contrast, the waveform-recording lidar systems have the advantage of enhanced canopy penetration capability, full scanning of entire vertical structure and larger mapping coverage (Lefsky et al. 2002). The Laser Vegetation Imaging Sensor (LVIS) is one such example of waveform-recording lidar

systems. LVIS is an airborne medium footprint (~25 m) lidar designed and developed at NASA's Goddard Space Flight Center (GSFC) (Blair 1999). It has been demonstrated highly suitable for the studies of vegetation structure with different ecosystem structure parameters (e.g. canopy height, aboveground biomass, VFP and LAI) derived from its canopy height metrics (Drake 2002a; Hyde et al. 2005; Swatantran et al. 2011).

Spaceborne lidar systems provide unique observations of terrestrial ecosystem structure at global scale. Measurements from these systems can greatly deepen current understanding of ecosystem dynamics and global environmental change. The Geoscience Laser Altimeter System (GLAS) on board of Ice Cloud and Elevation Satellite (ICESat) was previously the only spaceborne lidar providing global 3D measurements of ecosystem structure from 2003 to 2009. There have been several global canopy height products available derived from GLAS data in recent years (Lefsky 2010; Los et al. 2012; Simard et al. 2011). A descendant mission ICESat-2, equipped of a photon-counting lidar system ATLAS, is planned to launch in 2015 but with a primary focus on global ice sheet observation (Abdalati et al. 2009). A DESDynI mission was originally designed for the ecosystem monitoring in parallel to ICESat-2 but terminated due to budget sequestration of NASA (Hall et al. 2011). Fortunately, a new spaceborne Global Ecosystem Dynamics Investigation (GEDI) lidar will be developed for the International Space Station (ISS) to obtain a 3D view of the Earth's vegetated ecosystems (Dubayah et al. 2014). By then end of the mission, billions of vertical forest profiles will have been measured to further

understand ecosystem dynamics and its effect on climate change and biodiversity resources.

Lidar remote sensing provides an unprecedented 3D measurement capability of structural characteristics of ecosystem, and has demonstrated its potential of deriving highly accurate LAI and vertical forest structure products. Previous researches focus on deriving LAI from airborne discrete return lidar (Farid et al. 2008; Jensen et al. 2008; Morsdorf et al. 2006; Richardson et al. 2009; Solberg et al. 2009). In most of the studies, empirical relationships between field measured LAI values and predictor variables derived from different lidar metrics were explored through regression analysis. It was not until more recently that physical models based on the gap fraction method were developed to calculate LAI and VFP from both airborne and terrestrial lidar systems (Morsdorf et al. 2006; Ni-Meister et al. 2001; Zhao et al. 2011). Such physical models have the potential to derive LAI and VFP products at global scale from spaceborne lidar mission (ICESat/ ICESat-2 and GEDI) to help better address the most critical environmental problems through balancing the carbon cycle and investigating biodiversity abundance.

1.5 Dissertation Outline

This central objective of the dissertation is to derive large scale LAI and VFP products from the spaceborne waveform lidar GLAS on board of ICESat. In Chapter 2, a theoretical physical lidar-LAI model is developed and validated in a tropical rainforest. In Chapter 3, an inter-comparison study of ground-based, airborne and spaceborne retrievals of LAI is conducted over the conifer-dominated forests of

Sierra Nevada in California. The encountered effectiveness of these relationships allows the implementation of a scaling-up strategy where ground-based LAI observations are related to aircraft observations of LAI, which in turn are used to validate GLAS LAI derived from coincident data. In Chapter 4, the potential of large scale retrieval of LAI and VFP from GLAS observations are demonstrated with the implementation of the developed physically based method over the entire state of California. In Chapter 5, a GLAS LAI and VFP product is derived over Contiguous United States and examined by data sets from airborne lidar at major forest types. The final chapter summarizes this dissertation and discusses its potential linkage and guidance towards future spaceborne lidar missions.

Chapter 2 Retrieval of Vertical LAI Profiles over Tropical Rain Forests using Waveform Lidar at La Selva, Costa Rica

2.1 Introduction

Tropical forests store 13% of the global carbon and play an important role in terrestrial carbon dynamics and other ecosystem processes (Clark and Clark 2000). Leaf Area index (LAI), commonly defined as the maximum projected leaf area per unit ground surface (Chen et al. 1997), is an important ecosystem model parameter strongly linked to plant respiration and photosynthesis (Gower and Norman 1991). In addition, LAI is often used to parameterize surface energy balance and hydrological models for effects such as radiation attenuation and precipitation interception.

The vertical variation in LAI is related to foliage-height profiles (Aber 1979) which have been shown to be important determinants of energy, water and nutrient flows (Parker et al. 2001). This is because foliage at different height intervals contribute differently towards total photosynthesis and canopy carbon storage (Ellsworth and Reich 1993). The vertical distribution of leaf material may also play a role in determining habitat suitability and species abundance and diversity (Swatantran et al. 2011).

The importance of LAI has thus led to considerable efforts by the remote sensing community to map its distribution over a variety of spatial and temporal scales. Passive remote sensing data have been used to derive LAI using empirical relationships between reflectance and field measured LAI (Chen and Cihlar 1995;

Chen et al. 1997; Cohen et al. 2003; Morisette et al. 2006), and using physically-based radiative transfer modeling (Koetz et al. 2005). However, results from different sensors are not consistent. Their accuracies vary considerably (Abuelgasim et al. 2006) and drop significantly in dense tropical forests where LAI is high. In addition, passive remote sensing systems do not adequately capture vertical variation in LAI. In contrast, lidar (light detection and ranging) potentially provides this vertical dimension information.

Lidar has been successfully used to derive forest structural characteristics such as canopy height, forest structure and aboveground biomass in different forest types (Drake 2002a; Hyde et al. 2005; Lefsky 1999a). Recent studies have used lidar data to derive LAI (Farid et al. 2008; Jensen et al. 2008; Morsdorf et al. 2006; Richardson et al. 2009; Solberg et al. 2009). Predictor variables (often called “lidar metrics”) are generally derived from discrete return or waveform-based small footprint lidar data (e.g. canopy height) to perform regression analysis in these studies. Zhao and Popescu (2009) combined lidar data and other optical remote sensing metrics (e.g. NDVI) but found adding such metrics did not improve LAI estimates significantly. Riano (2004) compared LAI values from both airborne lidar and hemispherical photography in central Spain, and found that LAI was better estimated using a radius size of lidar sampling scale from 7.5 - 12.5 m. Their results suggested LAI could be better predicted using a medium footprint lidar. However, there has been little research using lidar data to estimate LAI in tropical rain forests, where the saturation problem for passive remote sensing is significant (Abuelgasim et al. 2006). Furthermore, the use of medium to large footprint waveforms to derive LAI, such as

those from the airborne Laser Vegetation Imaging Sensor (LVIS) has not been explored.

Our research goal is to study the spatial and vertical distribution of LAI over the La Selva Biological Station in Costa Rica using the airborne scanning waveform lidar from LVIS. We first derive vertical LAI profiles from LVIS waveforms using the physically-based Geometric Optical and Radiative Transfer (GORT) model (Ni-Meister et al. 2001). Next, we validate the vertical LAI profiles derived from lidar with field-based measurements of destructively sampled LAI at towers and then map LAI spatially across the landscape. Finally, we assess the accuracies and sensitivity of LAI retrieval from lidar waveforms and discuss their implications for large-scale mapping.

2.2 Study Area & Data

2.2.1 Study area

La Selva Biological Station is located in the Atlantic lowlands of Costa Rica. It is one of the most extensively studied field sites in tropical forests, with a well-documented history of its biological data sets. The area receives an annual rainfall of 4000 mm and has a mean temperature of 26 °C. The topography of this study site is relatively low (<150m), but there are some areas with slopes exceeding 30 degrees. The station has a mixture of old growth and secondary lowland tropical wet forests along with remnant plantations and various agroforestry treatments. Most canopy trees here are evergreen or only briefly deciduous. Detailed site characteristics can be found in Clark et al. (2008) and Dubayah et al. (2010).

2.2.2 Field data

LAI was measured in a 515 ha section of upland tropical wet forest at the La Selva Biological Station by Clark et al. (2008). A modular walk-up tower was built to harvest all leaves and branches in 55 vertical transects from ground to canopy top (Fig. 2-1). The tower footprint was 1.30 m × 1.86 m for the first four transects (June - August 2003) and it was expanded to 2.45 m × 1.86 m for the next 51 transects (August 2003 - March 2005). Because data from the two configurations did not differ significantly in LAI or forest height, they were processed together. The tower locations were selected by strict stratified random sampling. The landscape was divided in 9 classes of cells based on high, medium and low GIS-predicted phosphorus and high, medium and low GIS-predicted slope. 10 x 10 m cells were selected at random (with predetermined constraints such as no streams) with each of the 9 classes. An additional 10 low canopy sites were selected with a different semi-random protocol. Tower sites were geolocated using differential GPS and the La Selva base station. Nominal geolocation accuracy with differential correction was < 1 m. Tower sites were separated by an average of 153 m from their nearest neighbor, so they represented independent samples of forest conditions within a given forest type. Leaf areas of all species were measured at each height section (1.86 m per section) in laboratory after destructive sampling (discussed below).

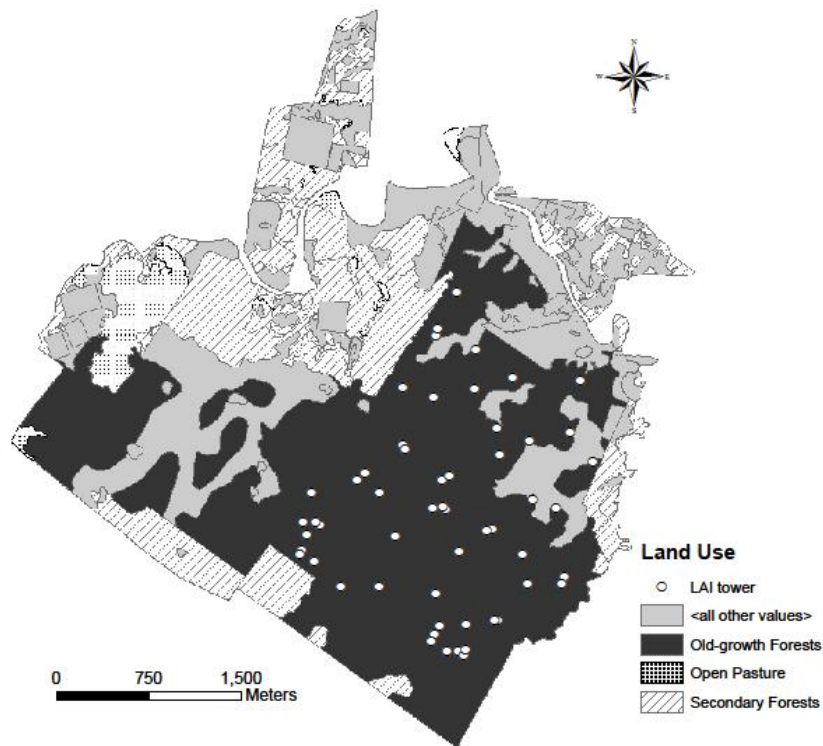


Fig. 2-1 Land use map of La Selva Biological Station, Costa Rica. 55 LAI measurement towers were constructed across different forest areas, but mainly focused on old-growth forest.

2.2.3 Lidar data

LVIS is a medium footprint (~25 m), waveform digitizing, scanning laser altimeter focusing on the study of surface topography and vegetation structure (Blair 1999). LVIS digitizes the entire outgoing and return signal to provide a waveform from which attributes such as ground elevation, canopy height, canopy cover and canopy height profiles can be derived. Standard products from LVIS include both fully digitized waveforms as well as height metrics at different waveform energy returns (Hofton 2002; Hofton et al. 2000). Many studies have shown the ability of

LVIS in mapping forest structure and habitat characteristics in tropical and temperate forests (Drake 2002b; Hyde et al. 2005), but direct derivation of LAI from LVIS waveforms has not been attempted. The LVIS instrument was flown over the entire La Selva in both 1998 and 2005. The swath width in 2005 was 2 km and nominal footprint diameter was 25 m. In this study, we used only the 2005 LVIS waveform data to derive LAI in contemporaneous with the field data collection. We did not consider the temporal lags or seasonal discrepancy between field and lidar data because wet tropical forests are evergreen or only briefly deciduous and LAI values at tall sites (>21 m) did not differ between sites sampled in the dry season (January–May) or in the wet season ($P > 0.51$, $n = 10, 28$) for the 2003–2005 sample period (Clark et al. 2008).

2.3 *Methods*

We derived cumulative LAI profiles from both destructive sampling and LVIS data and then compared them at the same vertical and spatial scales. Areas of collected leaves from the ground to a particular height were integrated to ascertain tower-cumulative LAI, which could then be compared to LVIS-cumulative LAI derived from GORT model. The derived LVIS LAI profiles were adjusted to better match the scale of the LAI tower measurements, as the latter has a far smaller area than an LVIS footprint. Lastly we filtered tower locations as a function of their distance from the center of the nearest LVIS footprint to explore the degree to which their non-coincidence affects LAI retrieval accuracy.

2.3.1 Cumulative LAI from tower measurements

Leaves harvested at each section of tower height were measured in the laboratory according to different plant functional groups: *Pentaclethra* (dominant trees), other trees, palms, lianas, herbaceous climbers, herbs, ferns, non-woody epiphytes and woody epiphytes (Clark et al. 2008). A LI-COR-3100 leaf area meter was used to measure the one-sided leaf area. LAI for a certain height section was quantified through the measurement of total leaf area present within that tower sector. Cumulative LAI profiles were then calculated with an integration of LAI per height sector from the ground to a particular height section. There were a total of 546 tower-cumulative LAI values at different heights from all 55 towers (i.e. each tower provided multiple cumulative LAI estimates, one every 1.86 meters from the ground to the top of the canopy). However, because not all towers were sufficiently co-located with LVIS footprints, some were removed from the validation data set (discussed below).

2.3.2 Cumulative LAI profiles from LVIS waveforms

In this section, we derive cumulative LAI profiles from lidar waveforms using gap theory (Chen and Cihlar 1995; Chen et al. 1997; Gower and Norman 1991; Miller 1967; Nilson 1971, 1999) which quantifies the relationship between LAI and the gap frequency for horizontally homogenous canopy layers according to the general formula:

$$P(\theta) = e^{-G(\theta) \cdot LAI / \cos(\theta)} \quad \text{Eq. 1}$$

where $P(\theta)$ is the gap probability within canopy with a view zenith angle of θ

and $G(\theta)$ is the projection coefficient representing unit leaf area on the canopy layer perpendicular to the view direction. For LVIS we assume the viewing zenith angle is constant at 0, and hence we only need information of gap probability and projection coefficient to obtain LAI.

Ni-Meister et al. (2001) developed a method to derive gap probability and canopy cover from lidar waveforms. The basic assumption of the model is that gap probability is the reverse of the vertical canopy profile as laser energy can only penetrate into the lower canopy layer or ground through gaps (including both within-crown gaps and between-crown gaps). Using this relationship, canopy closure is calculated using the cumulative laser energy return for a known ratio of canopy and ground reflectance as follows:

$$P(z) = 1 - \text{fcover}(z) = 1 - \frac{R_v(z)}{R_v(0) + \frac{\rho_v R_g}{\rho_g R_v(0)}} \quad \text{Eq. 2}$$

where $P(z)$ and $\text{fcover}(z)$ represent the gap probability and canopy cover percentage above a particular height z within canopy respectively. The terms $R_v(z)$, $R_v(0)$ and R_g are the integrated laser energy returns from the canopy top to height z , from canopy top to canopy bottom, and from the ground return individually. The canopy and ground reflectance are ρ_v , ρ_g respectively. This model in general measures Plant Area Index, not Leaf Area Index, since branches and trunks also reflect laser energy. But we did not explicitly consider the difference between the two in this research as the large majority of energy (93%) reflected back towards the sensor comes from the leaves with only 7% from other areas of the plant (Note: both

leaf and plant area data were destructively sampled to determine this ratio, but the plant area data are not published and are unavailable).

We applied a similar approach to the LVIS data to get gap probability and canopy cover at La Selva. Mean signal noise level was first subtracted from raw waveforms to reduce noise. We then applied Gaussian decomposition of waveforms to separate R_v and R_g (Hofton et al. 2000). This method may not accurately provide a separation if topographic slopes are present and we examine this effect using a sensitivity analysis as described in the discussion section. The quantity of ρ_v/ρ_g was calculated from ASD FieldSpec spectrometer (Analytical Spectral Devices, Boulder, CO, USA) measurement of soil and leaves in our study area by Clark et al. (2005). The ground reflectance ρ_g was calculated as an average value of 0.14 (SD = 0.03) for 19 soil reflectance samples at 1064 nm. For ρ_v , we only considered the dominant species, *Pentaclethra*. Only 4 ASD measurements of *Pentaclethra* were available (0.31, 0.34, 0.38 and 0.51 at 1064 nm). The 0.51 value was too large for single leaf reflectance and hence was not accurate, possibly because of multiple scattering (Clark et al. 2005). As a result, we calculated the average (0.34) of the first three values. Then we obtained the ρ_v/ρ_g value of 2.5 at 1064 nm and used it as the mean value for the whole study area. With the relevant information regarding canopy and ground energy separation as well as ρ_v/ρ_g , the cumulative gap probability and canopy cover was then calculated using Eq. 2.

Finally we calculated the apparent foliage profiles and cumulative LAI profiles based on the derived gap probability. The apparent foliage profile was

defined by the following equation:

$$F_{app}(z) = \frac{d \log P(z)}{dz} \quad \text{Eq. 3}$$

The log transformation of gap probability follows MacArthur and Horn (1969): the density of foliage may be estimated from the distribution of first leaf distance. Note that it is actually a transformation of Eq. 1. The cumulative LAI profile was then calculated through the actual foliage profile (or foliage area volume density), which is a projection adjustment of $F_{app}(z)$ (Ni-Meister et al. 2001) using the following equation:

$$LAI_{cum}(z) = C * \int_{z_0}^z F_a(z) dz = C * \int_{z_0}^z \frac{F_{app}(z)}{G} dz \quad \text{Eq. 4}$$

where $LAI_{cum}(z)$ is the cumulative LAI as a function of height z and z_0 is the height location of the canopy bottom. The term $F_a(z)$ is the foliage area volume density with units of m^2/m^3 and G is the projection coefficient used to adjust the apparent foliage profile $F_{app}(z)$ to $F_a(z)$. Assuming a random foliage distribution within the canopy, we set the projection coefficient G to be 0.5 (Ni-Meister et al. 2001). Clumping index C is another important parameter which adjusts the linear relationship between effective LAI and true LAI (Chen et al. 1997). Chen et al. (2005) derived global foliage clumping indices from multi-angular satellite POLDER data and we chose the mean clumping index value of 1.58 for broadleaf & evergreen forest.

2.3.3 Scale adjusted cumulative LAI from LVIS waveform

LAI estimates from lidar and measurements from field towers have different

footprint areas ($\sim 500 \text{ m}^2$ for LVIS vs. less than 5 m^2 for tower). A direct comparison between these two datasets may be problematic, especially in areas with low canopy cover or high canopy cover variability. For example, the LAI value from LVIS would be smaller than from a tower because tower footprints include only trees whereas LVIS footprints cover both trees and gaps. Therefore, it is necessary to convert cumulative LAI derived from LVIS to the same scale of tower measurement by adjusting for these footprint discrepancies.

We performed a scale adjustment from LVIS LAI to tower using LVIS canopy cover (Eq. 5).

$$\text{LAI}_{\text{scale}}(z) = \frac{\text{LAI}_{\text{cum}}(z)}{f_{\text{cover}}(0)} = \left(1 + \frac{\rho_v}{\rho_g} \frac{R_g}{R_v(0)}\right) * C * \int_{z_0}^z \frac{d \log P(z)}{dz} * \frac{1}{G} dz \quad \text{Eq. 5}$$

The adjustment is based on the assumption that foliage distribution within the tower is the same as all other canopy-covered areas within an LVIS footprint. We divided LVIS LAI by the canopy cover to approximate the same foliage distribution as the tower LAI. This has the effect of excluding between-tree gap areas in the calculation of LAI in an LVIS footprint. Total canopy cover (f_{cover}) was calculated using Eq. 2. Note that canopy cover derived here is only an approximation because we cannot separate within-crown gaps and between-crown gaps directly. LVIS LAI has also been integrated from original vertical resolution (about 0.3 m) to tower section height (1.86 m).

Total LAI for an LVIS footprint was directly calculated by setting the height variable z to the maximum canopy height in $\text{LAI}_{\text{cum}}(z)$. It can also be calculated in Eq. 6 after solving the differential lidar equations of Eq. 3 and Eq. 4.

$$LAI_{total} = \frac{c}{G} \times \ln \left(1 + \frac{R_v(0)}{\frac{P_v}{\rho g} \times R_g} \right) \quad \text{Eq. 6}$$

This total LAI value is at LVIS footprint scale and is unadjusted for scale differences with the towers (i.e. not divided by total canopy cover). Landscape scale LAI was then mapped using the total LAI derived in Eq. 6.

2.3.4 Distance of tower from lidar footprint center

Not all towers may be suitable for validating LVIS LAI because they may be too far away from the centers of the laser footprints (i.e. not coincident). The distance between LAI towers and laser shot center may also have a significant effect on canopy height measurement and the accuracy of LAI retrieval. The canopy height retrieval accuracy may drop significantly when the distance between field measurement and laser pointing center is greater than about 5 m (Blair and Hofton 1999; Frazer et al. 2010; Hyde et al. 2005). We thus examined results after filtering out those towers farther than 5 m. This resulted in the removal of 16 towers and reduced the total validation points from $N = 546$ to 185.

2.4 Results

2.4.1 Comparison of lidar and tower LAI

Representative examples of cumulative LAI are shown in Fig. 2-2. The vertical resolution of cumulative profiles from LVIS is 1.86 m to match that of the towers. Cumulative LAI profiles from towers and LVIS generally showed the same trend for all types of LAI distribution (e.g. in Fig. 2-2 with low LAI ≈ 3 , medium LAI ≈ 6 and high LAI ≈ 10). Cumulative LAI values generally increase as canopy height

increase within a profile, but there can be a large difference of total LAI values for the same canopy height level (as it is the case for medium LAI ≈ 6 and high LAI ≈ 10 in Fig. 2-2).

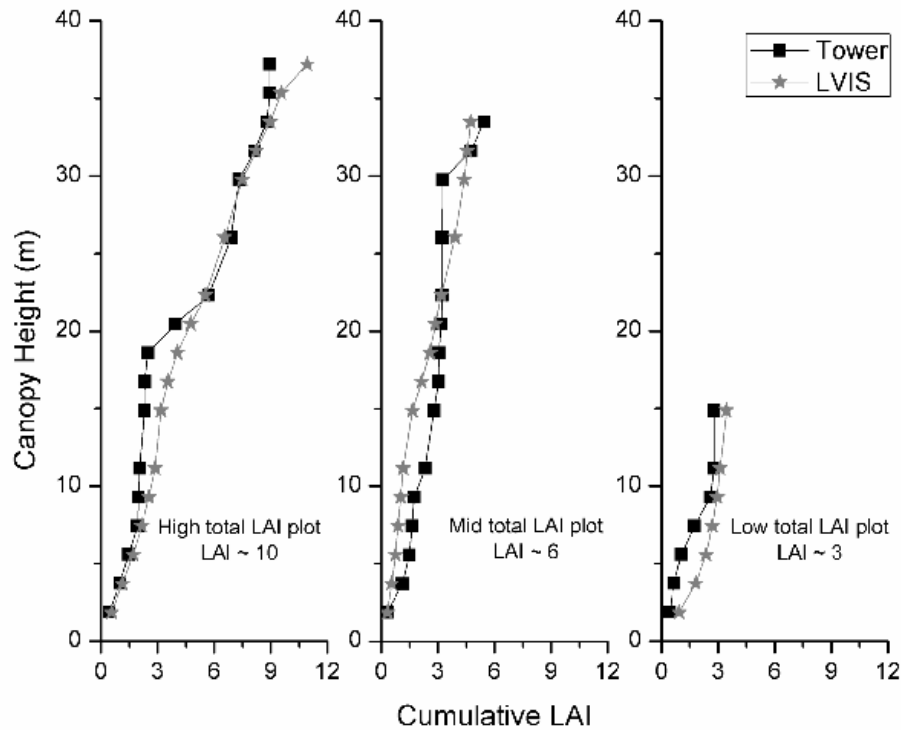


Fig. 2-2 Examples of cumulative LAI profile from tower measurements and derived from LVIS.

Both original GORT derived cumulative LAI and scale-adjusted cumulative LAI were plotted against the tower measured cumulative LAI (Fig. 2-3). The original GORT model explains about 42% of the total variance with a bias of -0.32 and root mean square error (RMSE) of 1.91. The scale-adjusted model slightly improves this result explaining about 50% of total variance with a bias of 0.27 and RMSE of 1.79. Results further improved upon filtering out towers more than 5 m away from laser

pointing center (Fig. 2-4). After adjustment for both scale and coincidence, our model explained about 63% of the total variance with a bias of 0.00 and RMSE of 1.36.

Table 2-1 Total LAI from different land cover and land use areas

Land Cover	LVIS shots	MEAN (m²/m²)	STD (m²/m²)
Open Pasture	3228	1.74	2.72
Secondary Forests	13919	5.20	3.20
Successional Plots	77	2.31	3.29
Selectively-logged Forests	7068	5.41	2.82
Old-growth Forests	35842	5.62	2.99
Abandoned Agroforestry	1415	4.13	2.81

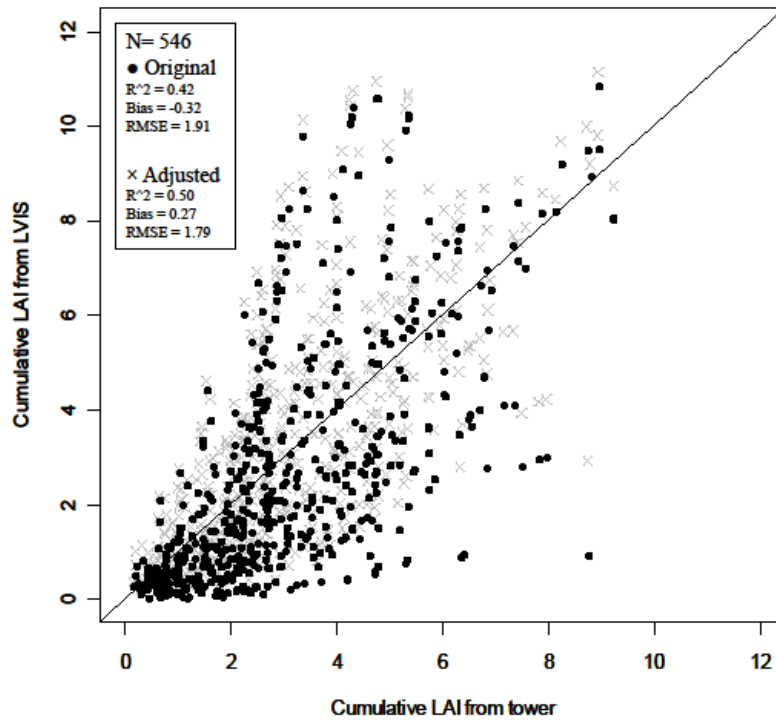


Fig. 2-3 Cumulative LAI estimated from LVIS data against all 55 cumulative LAI measurement towers. The total sampling number is 546, which is the number of total tower bins used to collect leaves. Note that after scale adjustment, many of the value that were underpredicted by LVIS rise.

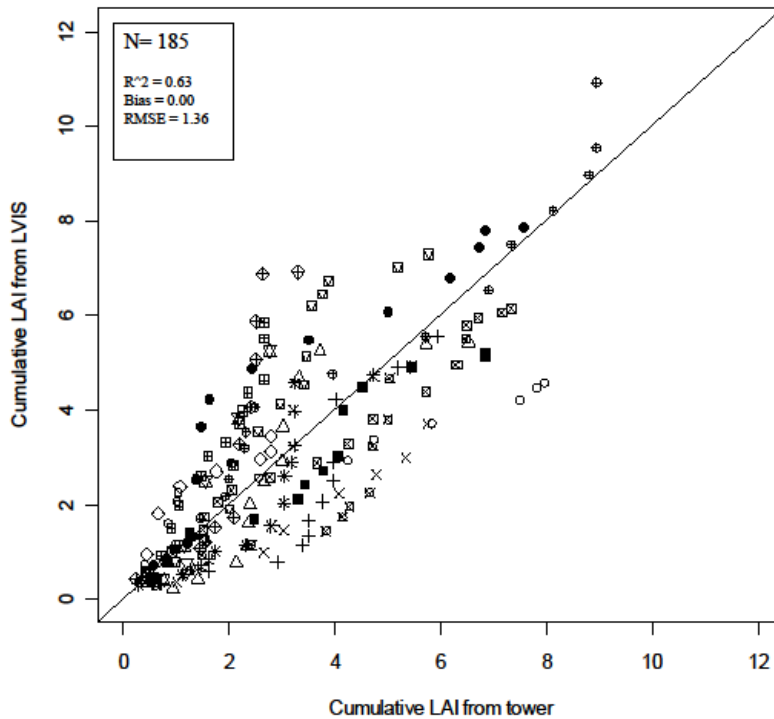


Fig. 2-4 Cumulative LAI estimated from LVIS against cumulative LAI for towers with a distance less than 5 m from the laser pointing center. Cumulative LAI values from 16 towers are marked with different symbols.

2.4.2 Landscape LAI variability

We mapped spatial variations of total LAI (Fig. 2-5), as well as vertical LAI integrations from 0~5m, 5~10m, 10~20m and 20m~top canopy (Fig. 2-6) over the entire landscape. LAI values show great spatial variability both within and between land cover types at the scale of LVIS footprints (25 m). Total LAI distributions over different land cover and land use areas are summarized in Table 2-1 Total LAI from different land cover and land use areas and Fig. 2-7. We found that the lowest LAI values were over open pastures (mean = 1.74, s.d. = 2.72). LAI of successional plots

were somewhat higher (mean = 2.31, s.d. = 3.29).

Regeneration forests from selective-logging had much higher LAI values (mean = 5.41, s.d. = 2.82). Secondary forests showed variability in LAI as a function of forest age (ranging from 6 years to 39 years), but also considerable variability of LAI within successional stages (Fig. 2-7). In general, LAI increases rapidly at early successional stages from about 6 years to 22 years, reaching a maximum at about 30 to 34 years before tapering off as stands mature. This is consistent with the concept of gap development as forests age (Kellner et al. 2011). The mean LAI value of all secondary forests was 5.20, close to the mean LAI value of old-growth forests (5.62). A t-test performed between the total LAI of old-growth and that of all the secondary forests combined resulted in a p-value <0.05, indicating the difference was significant. Vertical LAI distributions also exhibit differences across different land cover types (Fig. 2-6). For example, integrated layer LAI for the top-most layer (20 m and above) tended to be much smaller than for old-growth forests (panel 4, Fig. 2-6).

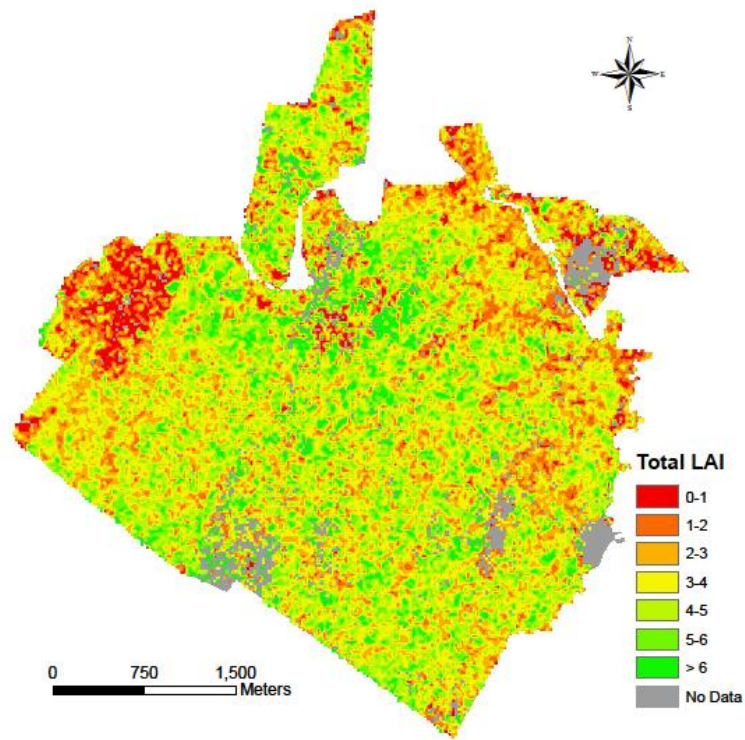


Fig. 2-5 Total LAI mapped across La Selva as derived from LVIS. Regenerating pastures have the lowest LAI values. Old growth forests have the highest mean LAI value and secondary forests are somewhat lower.

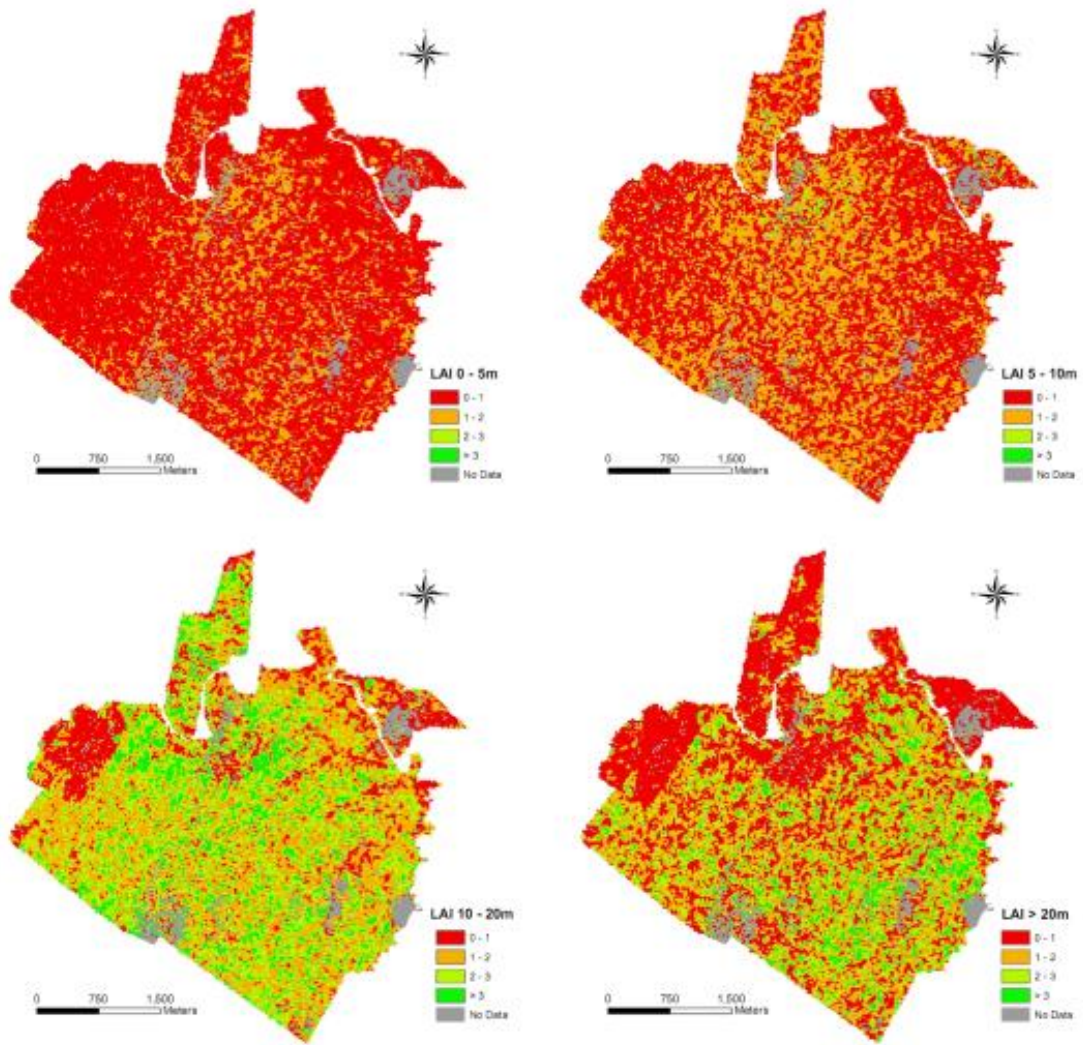


Fig. 2-6 Vertical LAI integration maps from 0 to 5m, 5 to 10m, 10 to 20m and above 20m.

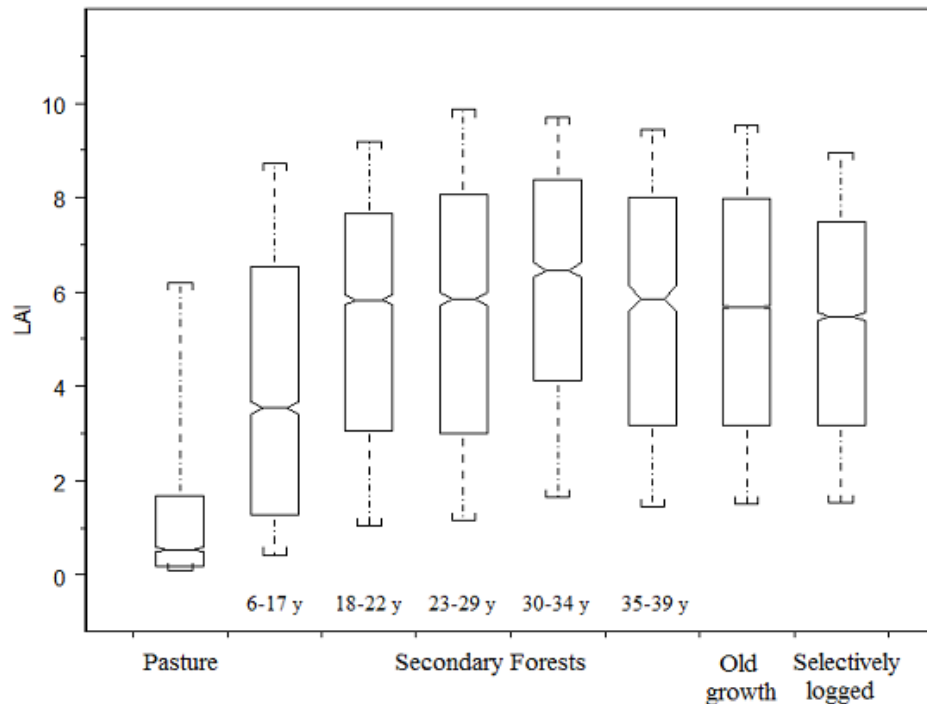


Fig. 2-7 Box plot of total LAI distribution over different forest successional types. The median LAI value is lowest for earlier succession stages and reaches a maximum value for 30-34 year-old secondary forests. Central lines give the median and boxes above and below the line give the interquartile range. Dashed lines give the 5% and 95% ranges. Non-overlapping median notches indicate significant differences between those medians at roughly a 95% confidence interval.

2.5 Discussion

Both vertical LAI and total LAI were derived from LVIS waveforms with the GORT model (Ni-Meister et al. 2001). Our results demonstrate that vertical LAI distributions may be derived from lidar waveforms, in addition to total LAI. We stress here that these results are entirely based on physical derivation of LAI, not statistically based regression methods, as is commonly done. Our methodology thus provides a potential pathway for measuring LAI profiles without the need for field-

measured LAI values to develop model relationships, though ancillary data (or assumptions) are required to parameterize our model (e.g. the ratio of vegetation to ground reflectance).

There were differences between the LVIS-derived cumulative LAI profiles and field measurements with about 37% of the total variance unexplained by our model. Even so, our results are comparable to results found in temperate and boreal needle forests using small footprint lidar (Jensen et al. 2008; Morsdorf et al. 2006). These results are encouraging considering the spatial and vertical heterogeneity of tropical rainforests and their high LAI values.

One source of unexplained variance in our model may be the large differences of footprint sizes between the towers and LVIS data. Even though we attempted to adjust for these differences, our method was only an approximation and thus could lead to errors in validation. Another source of error compounded with the difference in footprint size may be related to the non-coincidence of LVIS footprint centers with tower centers. While we tried to minimize this effect by including only those towers within 5 m of an LVIS footprint, errors may still be present. Consider shifting a 2 m x 2 m column a few meters in a tropical forest, the forest structure captured in the column may change considerably even under a small shift. Note that geolocation of either the towers or the footprint was done with high accuracies (< 1 m) and is not considered as a significant source of error.

Another source of error may be the use of incorrect input parameters in our model (i.e. model error in contrast to the errors just discussed). To assess this, we analyzed model sensitivity to variations in one key parameter in the model known to

affect canopy cover retrieval and LAI: leaf/soil reflectance ratio.

The spatial variation of leaf/soil reflectance ratio ρ_v/ρ_g could have a large impact on the model performance. The ρ_v/ρ_g value often varies for different sites or even within sites due to different environmental conditions. It may also vary temporally as well: foliage has different spectral responses and structural distribution in different growing periods, and the ground reflectance also varies according to the water content and ground cover. We applied a mean value of 2.5 to the whole study area, and this may have introduced errors into the model. The relative high soil moisture in La Selva decreases the soil reflectance and gives a relatively high leaf/soil reflectance ratio (Monteith and Unsworth 2008; Stoner and Baumgardner 1981). Ni-Meister et al.(2001) found that a smaller ratio value would lead to a smaller gap probability. Morsdorf et al. (2006) did not take the variation of leaf reflectance into consideration because their study area was considered to be homogenous for both canopy and understory.

We varied ρ_v/ρ_g from about 1 to 3 to evaluate its effect on LAI (Fig. 2-8). We found that for a moderate LAI (about 4) the range would be about less than 1 (varying from 3.3 to 4.2). Recall our model results had RMSE values that ranged from about 1-2; thus, it is possible much of our average error may be explained by spatial variation in ρ_v/ρ_g . Unfortunately, without detailed measurements of this value it is impossible to further assess its impact relative to other sources of error.

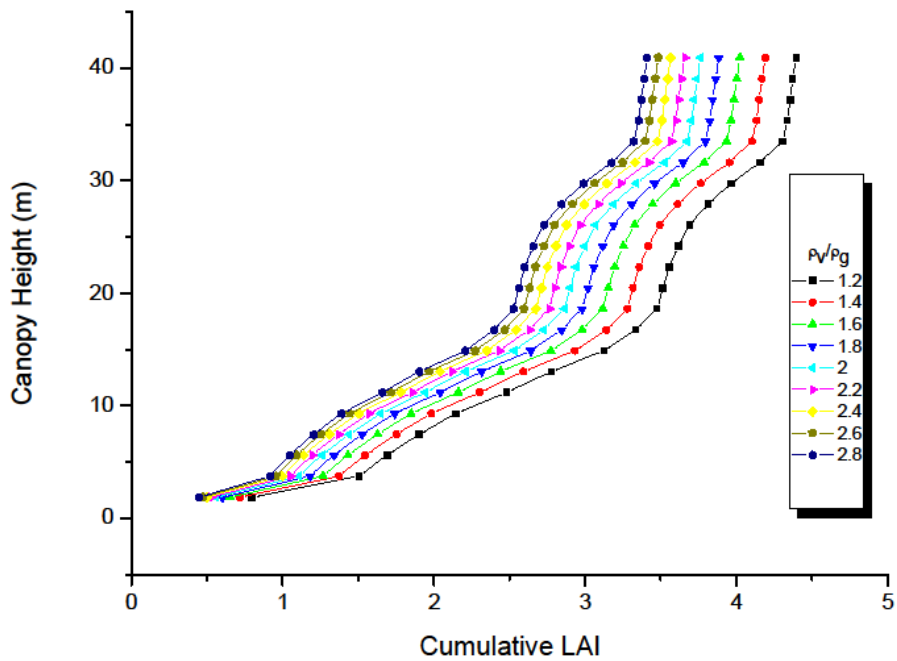


Fig. 2-8 An example of LAI profiles derived from LVIS with different values of ρ_v/ρ_g . As the leaf/soil reflectance ratio increases, the LAI value decreases and the profiles shift towards lower values of LAI. The sensitivity of LAI to the ratio changes is about 1.

The ratio of ground return energy in total reflected energy ($R_g/(R_g + R_v(0))$) is another key element in the LAI retrieval model. This ratio is not a parameter, per se, because it is derived from the waveform itself. However, it is highly sensitive to signal noise in certain situations. A high ratio of ground return energy is caused by low vegetation cover and a low total LAI value. But the relationship is nonlinear, and theoretically retrieved LAI does not saturate with decreasing ground energy ratio. However the LAI value becomes quite sensitive to the fluctuation of ground energy ratio when the ground energy ratio becomes small. A small change in $R_g/R_v(0)$ will

change the derived LAI value significantly. As canopy cover (and LAI) increases the ground energy necessarily becomes smaller. If noise values increase, or if topographic slopes are present (reducing returned ground energy) (Harding 2005; Lefsky et al. 2007; Pang et al. 2006) then errors may occur.

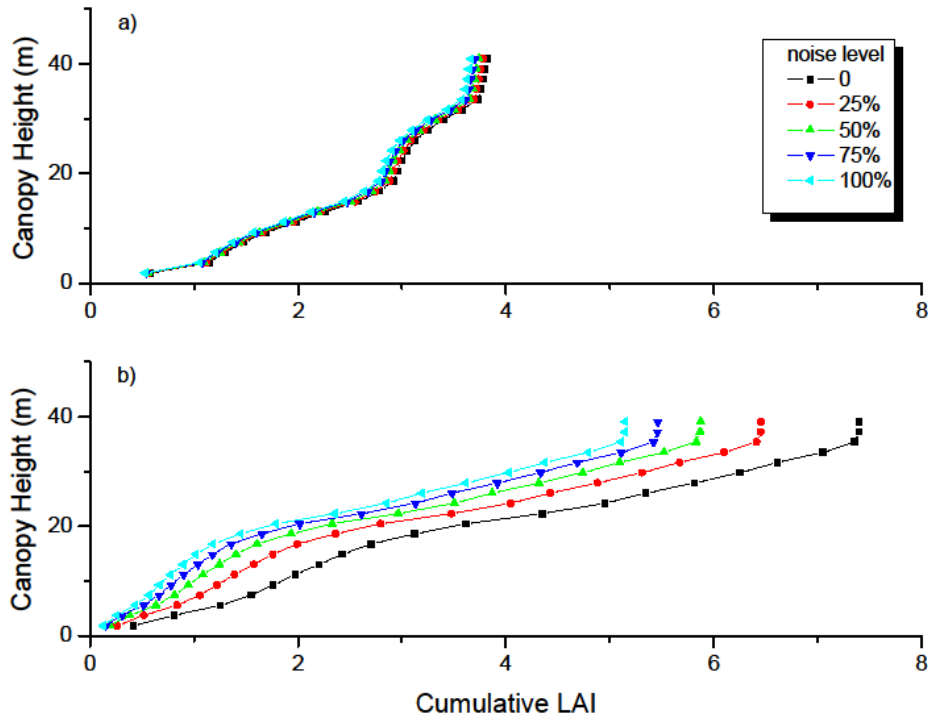


Fig. 2-9 Different sensitivity of moderate LAI (~ 4) (a) and high LAI (~ 8) (b) to different ground noise levels. Ground noise is added to waveforms manually and the total noise value is shown in the legend, ranging from 25% to 100% of the peak value of return energy. The same noise levels have different levels of impact for low and high LAI.

We applied different levels of noise into the ground portion of waveforms to analyze the sensitivity of LAI to $R_g/R_v(0)$. We found that for moderate and lower LAI (about 4) there was little sensitivity to noise (Fig. 2-9a). In contrast, for high LAI (about 8) (Fig. 2-9b) LAI values could be reduced by about 1.5 when the same level

of noise was introduced. This is then another possible source for the scatter in *c*. One implication of this sensitivity is that our LAI retrieval method may be less accurate over densely vegetated areas on steep slopes (and these occur at La Selva). There is no easy solution to this problem. If laser energy is increased to enable canopy penetration for dense forests, there is a subsequent risk of saturation for less dense areas, either from the canopy portion of the waveform or the ground return. Next generation waveform lidars may use dual channels (one low gain and one high gain) to avoid this issue.

Considering again Fig. 2-4, based on our discussion above, we would expect errors to increase starting around LAI values of 4 or so. There is no clear relationship between error and LAI however in this figure, although some heteroscedasticity appears around LAI values greater than 2. The great decrease in scatter from Fig. 2-3 to Fig. 2-4 is based on removing non-coincident comparisons, and the decreased bias and RMSE show how strong this effect is. The remainder of the scatter in Fig. 2-4 is thus a combination of any remaining non-coincidence (which may be as large as 5 m), variations in the ground to canopy reflectance ratio, and signal noise induced by topography and/or high canopy cover. Without knowing the true variability of these factors it is difficult to partition errors between these remaining sources. We note only that the resulting RMSE value of 1.36 m is consistent with and bounded by our sensitivity analyses.

Landscape level mapping of LAI may help to distinguish between some successional forest types and degraded forests. Differentiating among these over tropical areas has been difficult using optical remote sensing (Asner 2005). While

total LAI shows some ability to classify successional states (Fig. 2-7), it ignores the vertical distribution of LAI which may help better distinguish between classes. For example, consider Fig. 2-6 which shows the vertical LAI distribution of La Selva that incorporates all land cover types. LAI integration values at different height stratification layers suggest that the vertical structure of the canopy varies by land cover types and successional states: it is a function not just of total LAI, but of how the LAI is arranged vertically. In particular, distinguishing between older secondary forests and old-growth forests, while difficult using canopy height alone, may be possible using vertical canopy information from lidar. The efficacy of such an approach remains to be tested and is beyond our scope here, but has significance for efforts to map and monitor successional forests and degraded areas (for example, as part of REDD+ activities (Edwards et al. 2010)).

2.6 Conclusion

The vertical distribution of foliar material, as represented by LAI, has been hypothesized as a critical variable for many biophysical processes, yet it has been largely unattainable at landscape scales. As a result, our ability to understand vertical canopy organization and assess its importance in a variety of theoretical and applied domains has been severely limited at all but the most local scales. Our research is one of the few attempts to derive LAI profiles using lidar data based on physical model retrieval rather than through empirical methods. Our study has shown that large footprint waveform lidar can provide estimates of vertical LAI distribution in a tropical rainforest, even under conditions of high canopy cover. Further research is

required to assess the efficacy of our methods across varying landscapes and biomes. The validation of our approach was greatly aided by having actual, destructively sampled LAI measurements. Such data sets are rare indeed but their value is well worth the effort involved in obtaining them as they allow for direct comparison of models with reality. Ground-based lidar holds great promise for providing detailed LAI observations and may be an attractive alternative to destructive sampling (Strahler et al. 2008). The increased use of airborne lidar for forestry and carbon surveys, as well as the potential of retrieving these observations from space, underscores the urgency of continued model development. If successful this may lead to vastly improved data sets of LAI profiles across large areas and provide inputs for a variety of ecological, hydrological and climatological models that currently often use indirect and inaccurate parameterizations of this important attribute.

Acknowledgements

This research was funded by a grant from NASA's Terrestrial Ecology program (NNX08AP55G). The LAI field data were developed with support from NSF (0223284). We thank M. Clark for acquiring and processing leaf and soil spectral data. We also thank W. Ni-Meister for valuable suggestions on the model.

Chapter 3 Deriving and Validating Leaf Area Index (LAI) at Multiple Spatial Scales through Lidar Remote Sensing

3.1 Introduction

3.1.1 LAI using remote sensing

Leaf area index (LAI), defined as one half of the total leaf area projected per unit horizontal ground area, is an important biophysical parameter within ecosystem models due to its impact on energy and mass transfer between the canopy and the atmosphere (Chen et al. 1997). LAI has been proven to be representative of canopy foliage content and crown structure (Gower and Norman 1991) and has been widely used for the estimation of radiation attenuation, plant photosynthesis, and precipitation interception among others.

Large-scale (wide-area) LAI estimates are typically required to drive such ecosystem and other distributed models (Hurt et al. 2004) with efforts to derive LAI products at different spatial and temporal scales using passive optical remote sensing data ongoing since the 1980s. At present there are a large number of global and regional LAI products available from different sensors, such as MODIS (Myneni et al. 2002), LANDSAT (Ganguly et al. 2008), CYCLOPES (Baret et al. 2007). Methods of deriving LAI using remote sensing mainly fall into two categories: 1) building empirical relationships between ground based LAI measurements and satellite vegetation indices (Chen and Cihlar 1995; Chen et al. 1997; Cohen et al. 2003; Morisette et al. 2006); and, 2) inversion methods based on canopy radiative

transfer modeling (Ganguly et al. 2008; Koetz et al. 2005). Hybrid methods also exist that combine both (Fang and Liang 2003).

While these efforts have been largely successful, the accuracy and consistency of regional and global products have been limited by saturation over canopies with high LAI, and variability introduced by the use of different satellite sensors (Abuelgasim et al. 2006). The problem is exacerbated by the lack of independent datasets for validation and product intercomparison. Passive remote sensing retrievals of LAI used for validation will themselves saturate in high LAI conditions. Ground-based derivations provide an alternative, though such methods by their very nature will be spatially limited and are often time consuming to implement. For example, two common ground-based methods of validation are hemispherical photography and optical LAI estimation using a sensor such as the LAI-2000. These in turn have their own limitations: most notably that they are highly sensitive to exposure and solar illumination conditions (Jonckheere et al. 2004)). The most accurate retrieval, destructive sampling, is rarely performed given its cost and impracticality.

Active optical methods, in particular lidar remote sensing, have seen increasingly widespread use for quantifying vertical and horizontal canopy structure, including aspects of canopy height, canopy cover and biomass (Dubayah et al. 2010; Lefsky 2010; Ni-Meister et al. 2010; Saatchi et al. 2011). Of particular interest is the ability to derive canopy (foliar and branch) profiles from waveform and discrete return lidar. This has led to efforts to derive LAI from airborne lidar datasets as well as through terrestrial scanning lidar systems (e.g. see (Jensen et al. 2008; Riano 2004; Solberg et al. 2009; Zhao and Popescu 2009).

In the majority of lidar LAI studies, empirical relationships between ground based measured values and predictor variables derived from lidar metrics have been related through statistical (mainly regression) analysis. More recently gap fraction based physical models and radiative transfer models have been incorporated to derive LAI and vertical foliage profiles using both airborne and terrestrial lidar systems (Morsdorf et al. 2006; Ni-Meister et al. 2001; Tang et al. 2012; Zhao et al. 2011). The ability to derive LAI from such physically-based modeling opens the door to large-scale LAI mapping using lidar, as it frees these efforts from the requirement for associated field data to develop statistically-based lidar/LAI relationships of a spatially non-stationary nature (i.e. the relationships vary with location, species, canopy structure and the like).

While airborne lidar data are increasingly widespread, they are not available globally. Thus, it is of interest to develop and test methods of deriving LAI from space-based lidar where global coverage is possible, both for data set generation as well as for independent validation of existing global LAI products generated from passive optical sensors. The only existing set of such lidar data were obtained by the GLAS instrument on-board ICESAT (Abshire et al. 2005). GLAS data have been used to generate several global height products (Lefsky 2010; Los et al. 2012; Simard et al. 2011), and have been integrated with other data for pan-tropical biomass estimation (Baccini et al. 2012; Saatchi et al. 2011). While GLAS observations were not optimized for the vegetation measurement there remain millions of waveforms obtained across every biome. They thus represent an attractive and potentially powerful source of validation data for total LAI values. Importantly they may also be

used to estimate the LAI profile through the canopy. A global compendium of LAI profiles from GLAS, even given its observational constraints, would provide an unprecedented data set on a key component of canopy structure. These profiles could then be used to initialize ecosystem model parameterizations of leaf area profiles, or serve to validate existing parameterizations.

3.1.2 Proposal for multi spatial scale LAI validation

The development of a physically based method to derive LAI and LAI vertical profiles (Tang et al. 2012) from waveform lidar suggests a potential pathway for obtaining global LAI data from GLAS. Tang et al. (2012) found excellent agreement between LAI derived from the Laser Vegetation Imaging Sensor, LVIS (Blair et al., 1999), an airborne waveform lidar, and destructively-sampled LAI profiles. The success of this effort has led us to examine the feasibility of applying such an algorithm globally using GLAS data. An effort of this scale is complicated by the lack of ground validation data sets that are coincident with GLAS footprints. A potentially attractive alternative exploits the fact that airborne lidar datasets, while geographically spatially limited, are generally continuous (that is wall-to-wall within the flight area). This then allows a scaling-up strategy to be implemented where ground-based LAI observations are related to aircraft observations of LAI, which in turn are used to validate LAI derived from GLAS tracks that intersect the aircraft coverage.

There is a considerable level of uncertainty regarding the efficacy of such an approach. First, ground-based LAI derivations from photos, LAI sensors, and

terrestrial scanning lidar may be inconsistent amongst themselves. Second, the algorithm of Tang et al. (2012) has not been validated outside of its initial application for tropical forests in Costa Rica, nor for the different instrument parameters of GLAS in comparison to LVIS. Third, these different data sources have varying spatial footprints and viewing geometries that may complicate intercomparisons. Thus, a necessary first step is a scale-based comparison of LAI derived from ground, LVIS and GLAS, and is the primary focus of this paper. Such a study should inform eventual efforts to derive a global LAI and LAI-profile data set from GLAS, while also illuminating the utility of aircraft and space-based lidar observations for the validation of passive optical retrievals of LAI.

In this paper we present the results of a study comparing ground-based, LVIS and GLAS retrievals of total LAI over conifer-dominated forests of the Sierra Nevada in California. We first describe our study area and data sources. We use three different forms of ground estimates, hemispherical photography, LAI-2000 measurements, and a terrestrial scanning lidar, along with airborne and spaceborne waveform data from LVIS and GLAS. We next present our methods for retrieving LAI from the three ground-based sources, and briefly review the LVIS algorithm presented in Tang et al. (2012). Implementation of this algorithm for GLAS requires a recursive method to separate ground and canopy returns, a result of the larger footprint size of GLAS, and is described in detail. Our results are organized around a series of comparisons that focus on relating LVIS-derived LAI maps with the different ground-based LAI estimates, and those from GLAS. We next illustrate how our methods may be used to validate LAI estimates from MODIS at much larger

scales. Lastly, we discuss the limitations of our approach and comment on its potential application towards the generation of space-based LAI estimates from GLAS, and the utility of lidar in general as a validation source for passive optical LAI products.

3.2 *Study Area and data*

The study area is located in Sierra National Forest, California, USA and covers an area of approximately 20,000 ha. Being a mountainous area ground elevations are variable, ranging from approximately 1000 to 2500m. The major forest types include Red Fir (*Abies magnifica*), White Fir (*Abies concolor*), Ponderosa Pine (*Pinus ponderosa*), Giant Sequoia (*Sequoiadendron giganteum*), and California Black Oak (*Quercus kellogi*) (Hunsaker et al. 2002).

Table 3-1 Site characteristics from ground based data collection at Sierra National Forest, CA, July, 2008 (Zhao et al. 2012).

Site No.	Stem density (tree/ha)	Dominant species
305	~248	Red Fir
301	~231	Red Fir
801	~125	White fir
406	~256	White fir, Incense cedar, Sugar pine
23	~110	Jeffery pine, Black oak
168	~570	Red fir

3.2.1 Ground based data: hemispherical photography, LAI-2000 and terrestrial lidar

LAI data were acquired from 6 conifer sites comprising varied species and densities within the Sierra National Forest (Table 3-1), using EVI (Strahler et al. 2008), hemispherical photographs, and the LAI-2000. Within each site, 5 plots of 20 to 25 m radius were delineated for the purpose of measuring tree characteristics, acquiring an EVI scan, and observing LAI using hemispherical photos and the LAI-2000 instrument. LAI retrievals from these instruments are discussed in the Methods in Section 3.

3.2.2 Airborne lidar data: LVIS

LVIS (Blair 1999) is an airborne, medium footprint (~25 m) full waveform scanning lidar system designed and developed at NASA's Goddard Space Flight Center (GSFC). LVIS emits laser pulses of 5 mJ with a 1064 nm wavelength at 10 ns bursts with repetition rates of up to 500 Hz. It operates at altitudes of up to 10 km above ground level with a 7° field-of-view (FOV). Standard LVIS products include fully digitized emitting and return waveforms, and ground DEMs, as well as canopy height metrics described at quartile energy returns derived from Gaussian decomposition methods (Hofton et al. 2000). Ecosystem structure parameters such as canopy height, aboveground biomass, vertical foliage profile and LAI have been derived across different biomes using metrics derived from LVIS waveforms (Drake 2002a; Hyde et al. 2005; Swatantran et al. 2011; Tang et al. 2012). LVIS was flown

over the western slope of Sierra National Forest in the summer of 2008. LVIS footprints were collected along and across track to enable a contiguous dataset. The actual footprint density on the ground varied somewhat, based on flight line and swath overlap.

3.2.3 Spaceborne lidar data: GLAS

The Geoscience Laser Altimeter System (GLAS) is a spaceborne lidar developed for the Ice, Cloud and land Elevation Satellite (ICESat) mission (Abshire et al. 2005). GLAS operated at a wavelength of 1064 nm and 40 Hz recording the returned energy from a footprint ~65 m in diameter with a centroid separation of ~165 m (Neuenschwander, 2008). The GLAS footprint follows an elliptical energy distribution of $1/e^2$ with its size varying throughout the mission with computed sizes of about 110, 90 and 55m for laser campaigns 1, 2, and 3) (Abshire et al. 2005; Schutz et al. 2005). Canopy height, aboveground biomass and LAI have been estimated using GLA01 waveform products or GLA14 Land/Canopy Elevation products at different scales (Garcia et al. 2012; Lefsky 2010; Lefsky et al. 2005; Los et al. 2012; Simard et al. 2011). GLA01 waveform products typically include 544 bins providing vertical resolution of 1 ns or 15 cm for land surface products. GLA14 products include surface elevation, footprint centroid coordinates and fits of the GLA01 waveform using up to 6 Gaussian peaks (Harding 2005). The GLAS system operated with a 33-day sub-repeat and 91-day full repeat cycle with the intensity of the laser energy emitted from the sensor known to have decreased significantly after 2007, marking an obvious degradation in the sensor's capabilities and leading to a

shorter than expected system lifetime. To compensate for the annual LAI differences from ground based measurements and sensor degradation problems we selected GLAS shots only from Laser 2C, 3C, and 3F campaigns (May ~ Sep. of 2004, 2005 and 2006). GLAS data were filtered to overlay the study area based on geographic coordinates from GLA14 products. Products of GLA01 and GLA14 were also merged based on the record index and shot number. Shots with saturated waveforms were excluded. Following pre-processing a total of 145 valid GLAS shots were available for this study.

3.3 Methods

While previous work by Tang et al. (2012) has shown the potential for LAI profile derivation, our focus here is only on an intercomparison of total (integrated) LAI to help inform the viability of a validation framework incorporating ground, airborne, and spaceborne LAI estimates. The establishment of such a multi-scale validation framework using total LAI is a first step towards vertical LAI profile estimation using spaceborne lidar.

Note that we do not explicitly consider the difference between LAI and PAI (Plant Area Index). Plant Area Index is the variable derived from LVIS and GLAS as they cannot distinguish between leaves and branches. It is assumed throughout that the two values differ insignificantly, as suggested by Dufrene & Breda (1995), Gower et al. (1999) and Tang et al. (2012).

The comparison procedure progresses across scales from local field-level ground LAI measurements to regional airborne lidar LAI to the LAI products derived

from GLAS (Fig. 3-1). We add a further step to compare our LVIS and GLAS LAI estimates to those from MODIS to assess the ability of lidar to serve as a large scale validation for global, passive optical LAI retrievals.

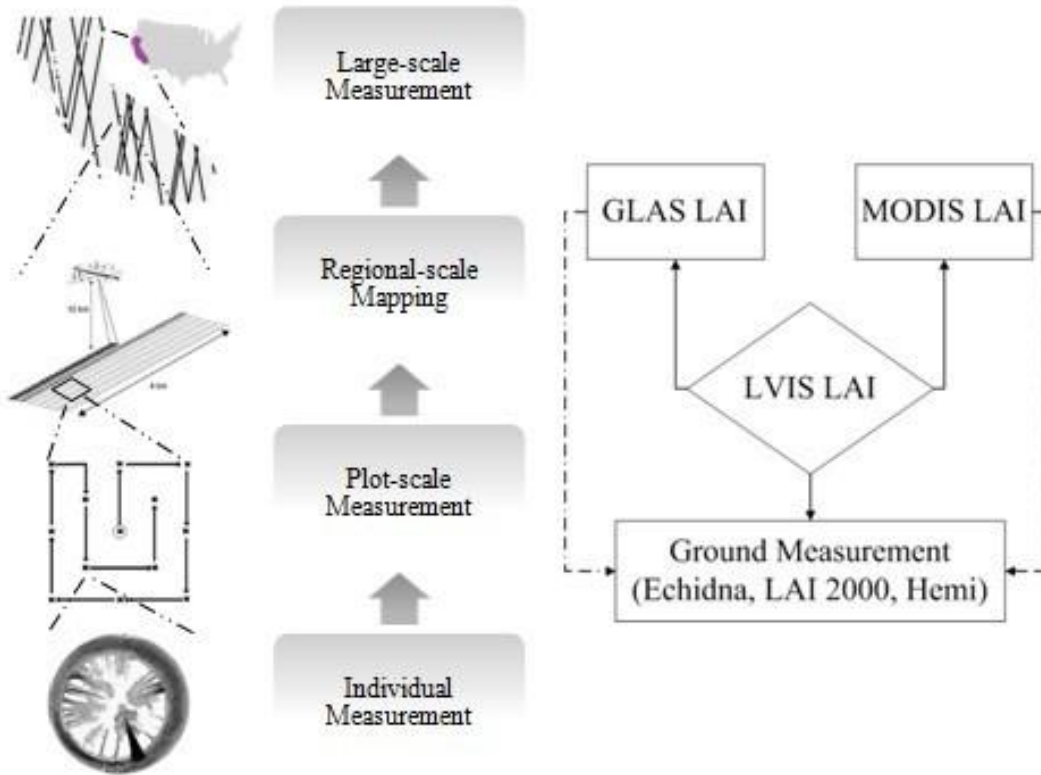


Fig. 3-1 Deriving and validating LAI products at multiple-scales. Regional-scale lidar mapping (e.g. LVIS) can bridge the gap between sparsely measured field data and satellite observations.

3.3.1 LAI from Ground Based Measurements

Ground measurements of LAI were acquired from 3 independent sources described below. There is no assertion that any of these are ground "truth". Rather each represents, per se, an established method of observation that may reasonably be used for characterization of canopy structure, and therefore as validation of remotely sensed retrievals. That said, the limitations in each method have been noted

elsewhere, and arise from differences in measurement approach, spatial scale, viewing geometry and underlying model assumptions. These same limitations are manifest in comparisons with remotely sensed LAI, with the added complication that airborne and space borne sensors look down from above the canopy, while most ground-based characterizations look-up from below. We thus expect a priori, to find some discrepancies among all of the methods and accept this as a limitation of any intercomparison, including our own. That said there is considerable value in quantifying the degree of divergence or convergence in results, and in seeking to understand the mechanisms behind these.

Hemispherical Photography and LAI-2000

Hemispherical photographs and data from the LAI-2000 Plant Canopy Analyzer are collected from two conventionally adopted instruments that use optical techniques for LAI estimation (Jonckheere et al. 2004). In this study hemispherical photographs were processed using Digital Hemispherical Photography (DHP) software to estimate LAI retrievals (Leblanc et al. 2005). Each photograph was divided into 10 azimuthal rings of constant zenith angle range, thus each ring has a 9° range. Each ring was analyzed separately to determine two thresholds, represented by gap fraction, and LAI estimation.

The LAI-2000 Plant Canopy Analyzer, operated in single-instrument mode, calculates LAI using radiation measurements made with a “fish-eye” optical sensor. Measurements were made at 5 angles below the canopy determining light interception. LAI was then computed using a radiative transfer model as part of the

FV2000 software (Li-Cor). Multiple below-canopy readings were taken, following a set spatial sampling procedure, to characterize LAI throughout the plot. Measurements were made starting and ending with reference readings of unobstructed skylight that were linearly scaled with time to match under-canopy readings. This method of LAI retrieval has been employed in studies such as Stenberg et al. (1994) and Zhao et al. (2011).

Echidna terrestrial scanning lidar

The Echidna Validation Instrument is a ground-based, upward scanning, full-waveform-digitizing hemispherical lidar, built by CSIRO, Australia. It emits a pulse of laser energy for which the intensity of return is recorded as a function of distance from the sensor. Scans are completed over the full hemisphere above the instrument with waveforms recorded for every direction within the hemisphere. It has been previously used to provide effective foliage profile, stand height and other forest structural parameters (Jupp et al. 2009; Strahler et al. 2008). It shows relatively consistent LAI retrievals to those obtained from both hemispherical photography and the LAI-2000 Plant Canopy Analyzer (Zhao et al. 2012; Zhao et al. 2011). In this study, methods proposed by Jupp et al. (2009) were followed in calculating LAI from Echidna waveform retrievals.

3.3.2 LAI from LVIS

Tang et al. (2012) implemented a methodology to derive total LAI and vertical LAI profiles using waveform lidar from LVIS. The accuracies found suggested that LVIS could potentially produce more accurate LAI profiles than that

associated with conventional, non-destructive ground measurements. Total LAI values are derived from canopy gap probability while vertical LAI profiles are estimated by taking the inverse of the vertical gap probability distribution as a function of height (Chen et al. 1997). Vertical gap probability is calculated from lidar waveforms using the geometric optical and radiative transfer (GORT) model (Ni-Meister et al. 2001), which is also applicable for derivation of total LAI and vertical LAI profiles. These are obtained from LVIS waveforms through consideration of foliage projection coefficients and the canopy clumping indices. LAI and canopy foliage profiles derived from this method have been validated using destructively sampled data in the La Selva Biological Station, Costa Rica (Tang et al. 2012).

The effective LAI at the LVIS footprint scale was derived using the following equation:

$$LAI_{\text{effective}} = \frac{1}{G} * \ln \left(1 + \frac{R_v(0)}{\frac{\rho_v}{\rho_g} * R_g} \right) \quad (1)$$

where $R_v(0)$ and R_g are the integrated laser energy returns from the canopy, and ground respectively. The default LVIS Gaussian decomposition method (Hofton et al. 2000) is then applied to the waveform to separate the individual energy contributions of canopy and ground. The parameters of ρ_v and ρ_g represent the canopy and ground reflectance. The ratio of canopy to ground reflectance ρ_v/ρ_g was set to be 1.6 for the Sierra site, a value estimated empirically using high spatial resolution Quickbird imagery (Hyde et al. 2005). The projection coefficient G is typically set to 0.5 when assuming a random foliage distribution within the canopy crown. This spherical foliage orientation allows an adequate representation of many

real canopy types and assumes a constant projected foliage surface with respect to inclination angle (Olthof et al. 2003).

As noted in Tang et al. (2012) this algorithm is sensitive to slope when LAI values are large. Therefore, values of effective LAI > 5 were removed where terrain slopes exceeded 40°. Slope data was calculated from ground elevations derived from LVIS.

Vertical gap probability $P(z)$ and effective cumulative LAI profile $LAI_{cum}(z)$ were calculated using the following equations where z_0 is the height location of the canopy bottom (Ni-Meister et al. 2001; Tang et al. 2012).

$$P(z) = 1 - \frac{R_V(z)}{R_V(0)} \frac{1}{1 + \frac{\rho_V R_G}{\rho_G R_V(0)}} \quad (2)$$

$$LAI_{cum}(z) = \int_{z_0}^z \frac{1}{G} * \frac{d \log P_{LVIS}(z)}{dz} dz \quad (3)$$

The LAI values from individual LVIS footprints could then be aggregated to achieve various spatial mappings appropriate for comparison with ground, GLAS and MODIS estimates of LAI. The number of LVIS footprints incident within ground plot boundaries varied from 3 to 9 with an average of 6 shots, and those intersecting GLAS footprints varied from < 5 up to 50 shots with an average of 14.

3.3.3 LAI from GLAS

LAI products can be estimated from GLAS data through separation of canopy and ground energy using the same model as that applied to the LVIS waveforms (Eq. 1). Consideration of several factors must precede this process. The default 6-Gaussian-curves fit applied as part of the LVIS LAI estimation process may fail to

correctly distinguish between canopy and ground return energy in the presence of complex topography or highly heterogeneous vegetation cover when using GLAS (Duncanson et al. 2010). Large errors may occur if direct use is made of the first (or second) Gaussian fit as a representation of the ground return. This could lead to a consistent overestimation of canopy height and therefore LAI as the Gaussian decomposition method would be influenced by multiple-scattering delays incorrectly identified as ground. This would be especially true for situations where the incident energy reaching the ground is low because of turbid atmospherics, degraded GLAS laser energy outputs (which occurred through time), and other factors related to slope and canopy cover (Los et al. 2012). Previous studies only applied empirical cutoff thresholds (e.g. 2 m above the first Gaussian peak center) to separate the ground energy from the canopy return (Garcia et al. 2012; Los et al. 2012). However the reliability of such empirical methods is uncertain.

For this study, a recursive analysis method was developed to facilitate the separation of canopy and ground return energy from GLAS waveforms. Prior knowledge of the LAI distribution (e.g. maximum potential LAI value) obtained from field knowledge or independent data sources (e.g. MODIS LAI) can be used to refine the LAI estimate. The method incorporates 3 major steps. The prior LAI estimates are not required to be exact, but are rather used as inputs into a fuzzy logic system to refute false LAI predictions:

Step 1: Initial estimate of LAI. Both total LAI and vertical LAI profile can be calculated using Eq. 1 and Eq. 3. The ground return energy is calculated as the first Gaussian curve fit from GLA14. The canopy return waveform is calculated as the

difference between original GLA01 waveform and the fitted ground Gaussian curve.

Step 2: Inspection of LAI estimate. The initial LAI estimates must satisfy both of the following prior conditions to be set as the final estimate. The first condition is that the LAI estimate does not exceed the upper limit of total LAI. The upper limit is calculated at 1 km scale using the maximum values of MODIS LAI from 2004~2006. Note that MODIS LAI value (already corrected from clumping effect) is considered to be consistently greater than effective GLAS LAI estimates, and hence can appropriately serve as the upper limit threshold. The second condition is that no anomaly value is detected in the vertical LAI profile. Assuming vertical LAI profile values (not the shape) follow a normal distribution, the maximum value of LAI profile is expected to be less than $\tau = \mu + 3\delta$ with a probability of 99.7% (μ and δ are mean and standard deviation of the LAI profile values). Any derived LAI profile value greater than τ is defined as an anomaly value.

Step 3: If the estimates from the second step fail to satisfy both of the above conditions, it is marked as a "false" estimate and the algorithm will return to Step 1. The LAI calculation process will restart by taking the next Gaussian fit as the representation of the ground return.

This 3-step process as visualized in Fig. 3-2 will continue until one or more of the following situations occur: 1) the conditions of step 2 are satisfied and the "true" LAI estimate is found; or, 2) the applied ground Gaussian fit possesses the largest amplitude among all fits. The second scenario guarantees that the algorithm will not miss the major signal as it is assumed that the strongest Gaussian curve is a result of interaction either with the canopy or the ground.

All 145 GLAS shots were processed using the recursive method, and only GLAS footprints intersected by > 10 LVIS shots were selected for LAI comparison to ensure data quality (number of corresponding footprints, 99).

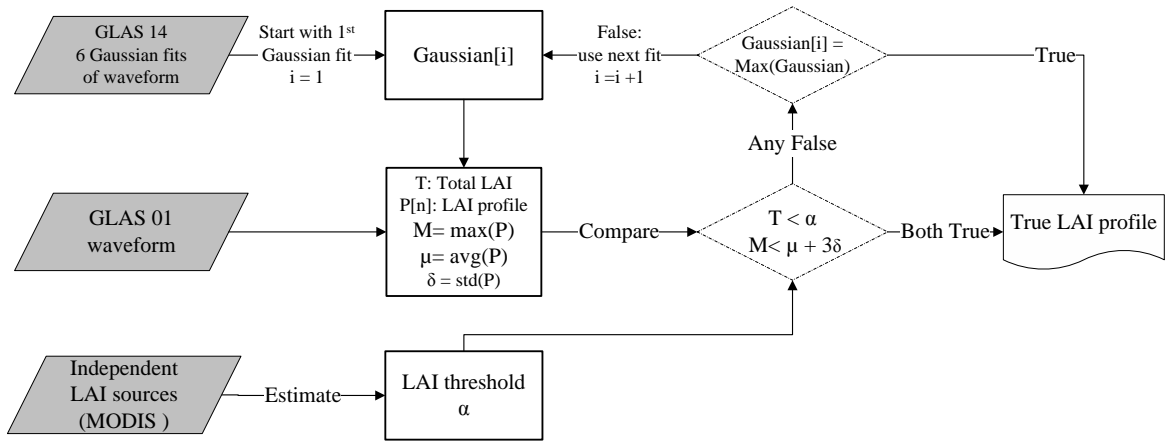


Fig. 3-2 Recursive estimation of LAI from GLAS waveform data. LAI estimate from GLAS data must satisfy the processing conditions defined by independent but inexact LAI sources.

3.4 Results

In this section we present LAI data from the multiple sources featured in this study. These include maps and data comparisons. The results are presented in 3 comparison sections exploring the link between LVIS LAI and LAI values collected from ground-based observation, GLAS and MODIS.

3.4.1 LVIS LAI

Effective LVIS LAI values were averaged over 30 m grids and mapped over the landscape (Fig. 3-3). The 30m LVIS LAI map captures the spatial variation of LAI over all low, medium and high LAI areas. These low LAI areas are dominated by

non-vegetated area such as rocks and bare ground. Medium and high LAI areas are covered by sparsely distributed tree stands and high stand density forests respectively. The Landscape LAI shows a Poisson distribution of LAI values, with a mean value of 1.00 and a standard deviation of 0.98 (Fig. 3-4). Such Poisson distribution and low mean LAI values are expected in the discontinuous distributed conifer forests in our study area.

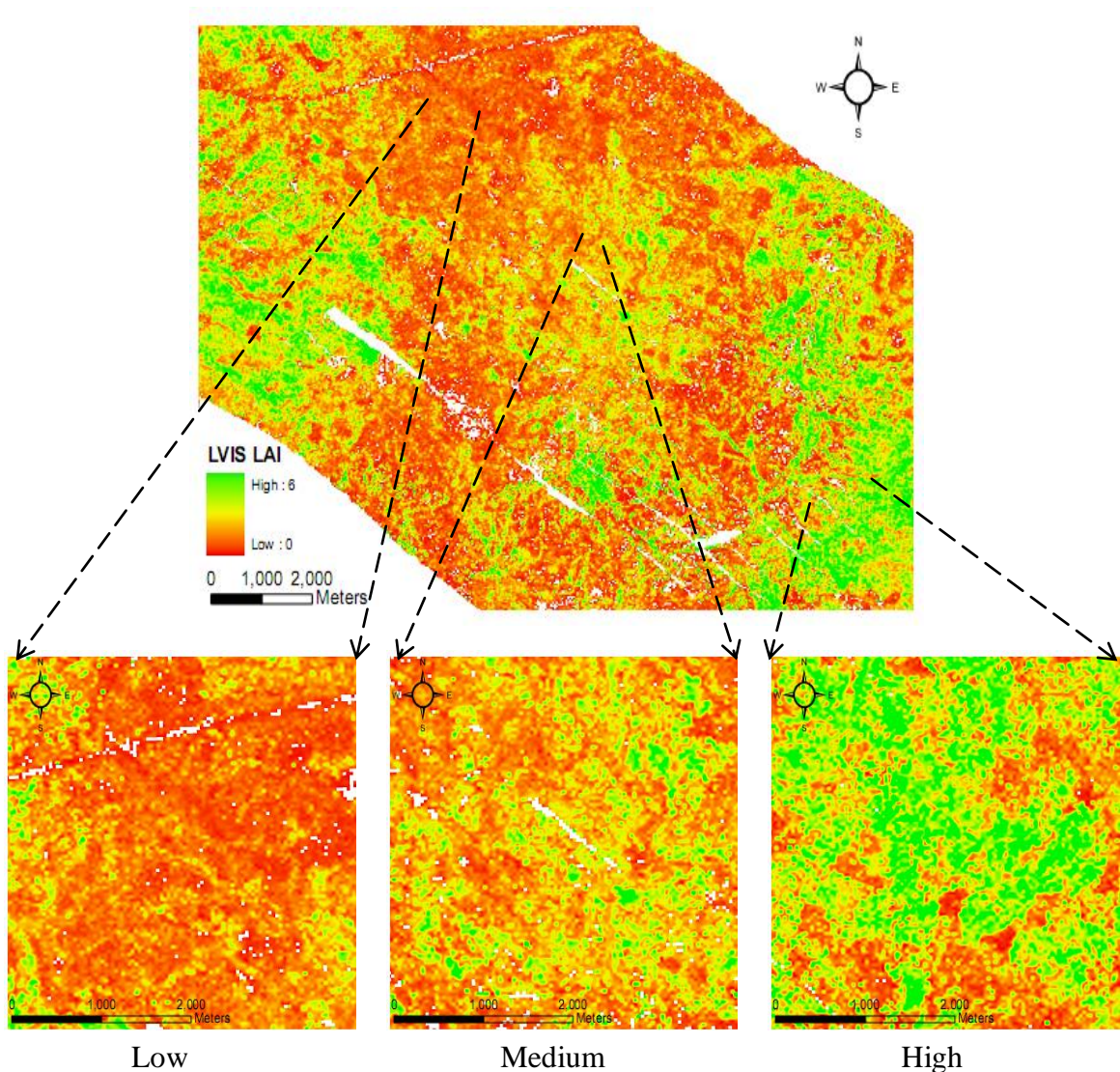


Fig. 3-3 Landscape map of effective LAI generated from LVIS, showing large spatial variation of LAI at 30 m scale. The forests in Sierra follow a spatially discontinuous

distribution, leaving large gaps of bare ground and rocks between conifer canopies.

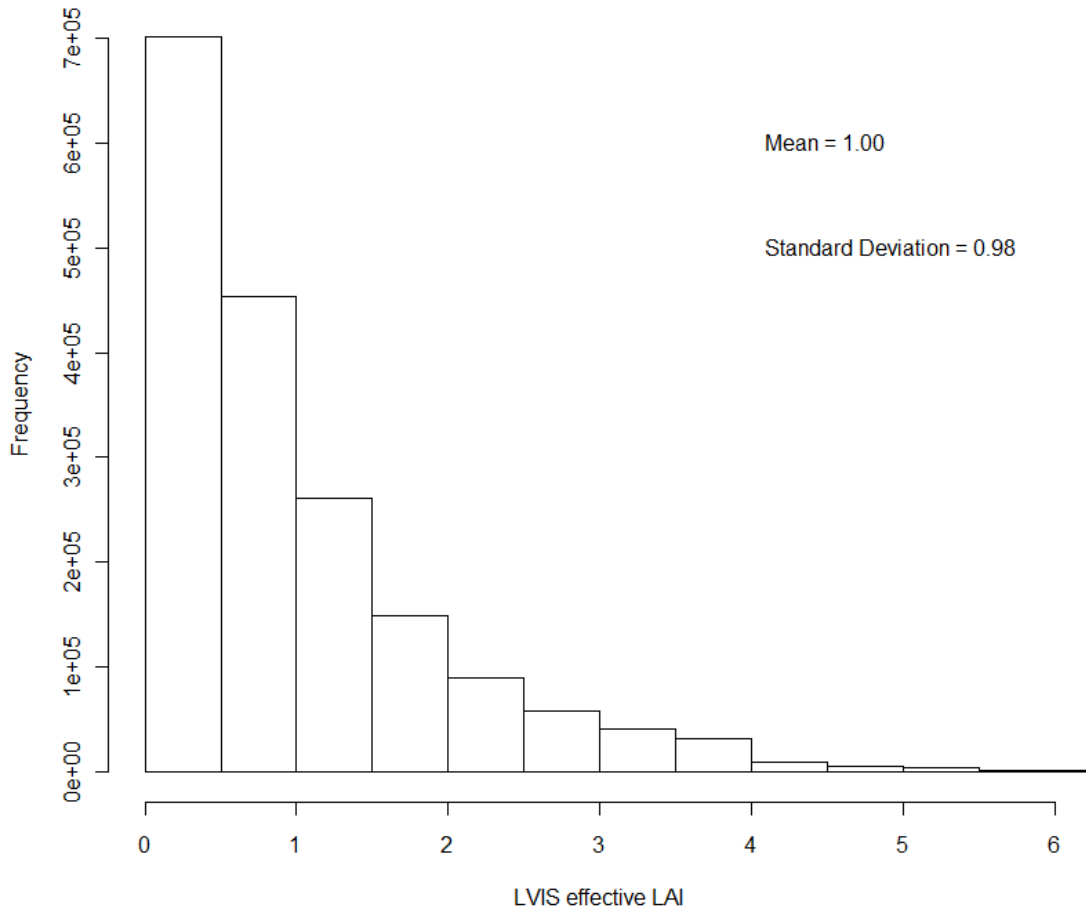


Fig. 3-4 Frequency distribution of effective LAI from LVIS data over the entire Sierra National Forest area.

3.4.2 LVIS LAI vs. Ground Based LAI

LVIS LAI was next compared to the three ground based sources of LAI (Fig. 3-5). Averaged LVIS derived LAI was highly correlated with data from hemispherical photographs ($r^2 = 0.80$), LAI-2000 ($r^2 = 0.85$), and Echidna LAI for which both regression LAI ($r^2 = 0.76$), and hinge LAI ($r^2 = 0.77$) were calculated. Both

bias and root mean square error (RMSE) were low (bias = 0.46, RMSE = 0.55 for hemispherical photographs, and bias = 0.46, RMSE = 0.56 for LAI-2000). The regression analysis between Echidna LAI (regression and hinge) and LVIS LAI also shows low residual errors of 0.54 and 0.63, but LAI estimates from LVIS are consistently biased lower relative to the Echidna data (bias = 1.07, RMSE = 1.24 for regression Echidna, and bias = 1.39, RMSE = 1.58 for hinge Echidna).

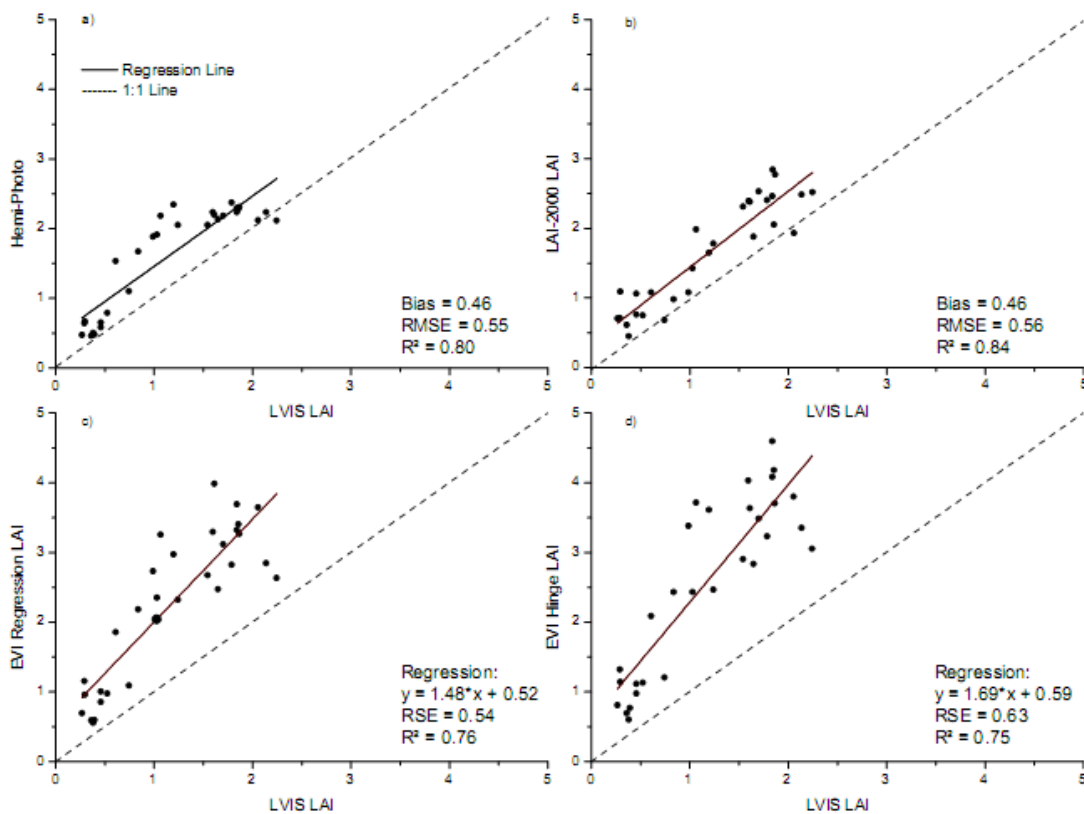


Fig. 3-5 Plot-level averaged LVIS effective LAI against plot-level LAI estimates from a) Hemispherical photos, b) LAI-2000, c) Echidna regression LAI and d) Echidna hinge angle LAI. While there are strong relationships, LVIS is biased low, especially with regards to Echidna.

3.4.3 LVIS LAI vs. GLAS LAI

There is a moderate agreement between averaged LVIS LAI and GLAS LAI for each GLAS footprint ($r^2=0.53$, bias = -0.09 and RMSE = 0.52) (Fig. 3-6). Most of the GLAS and averaged LVIS LAI data values fall within an LAI range of [0-1.5]. These lower values are expected given that the larger aggregation area includes more gaps. There are some areas of large disagreement and some heteroscedastic behavior, but little bias.

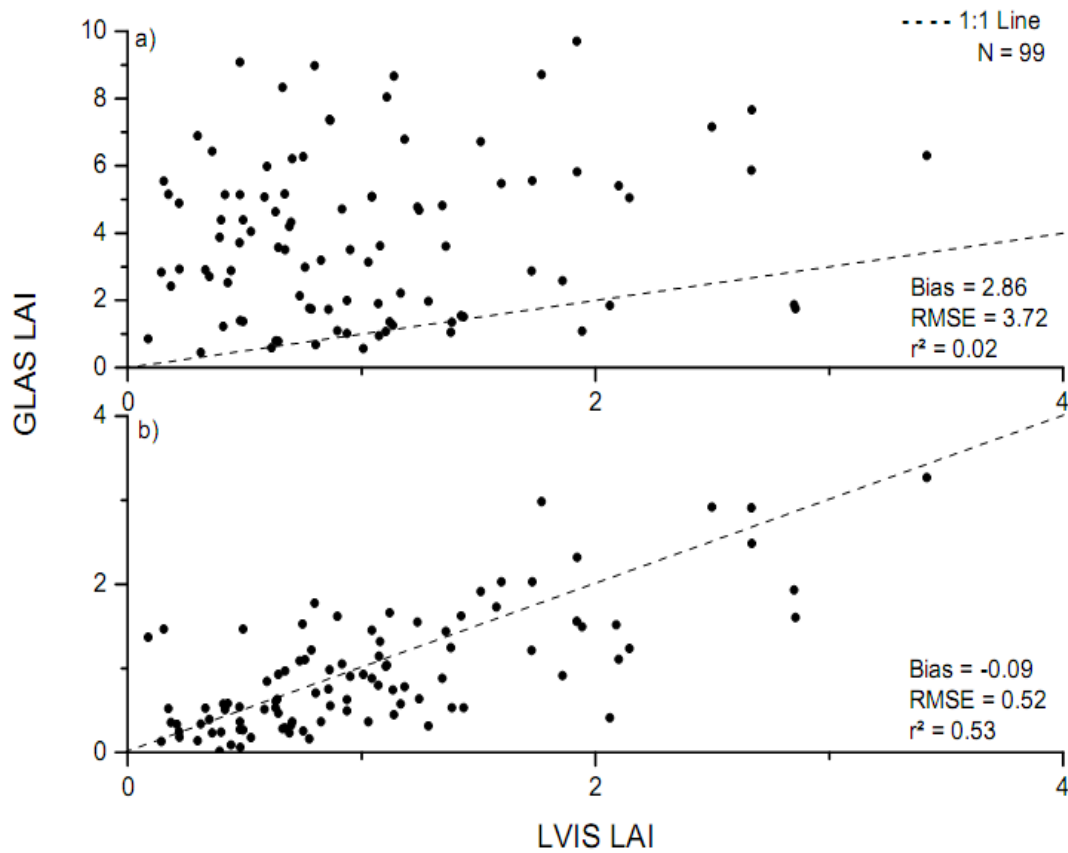


Fig. 3-6 a) GLAS LAI derived from non-recursive method; b) GLAS LAI derived from recursive method. The x-axis is averaged LVIS effective LAI and the y-axis is derived GLAS LAI.

Tang et al. (2012) performed a sensitivity analysis of LAI retrieval from waveform lidar that found slope to impact LAI retrieval accuracy. We examined both the RMSE and r^2 as functions of slope for each LVIS/GLAS comparison (Fig. 3-7). The RMSE remains low until a slope threshold value of $\alpha \approx 20^\circ$ before then rapidly rising. At approximately the same threshold value ($\alpha \approx 18^\circ$) the r^2 drops as expected. These data suggest an optimum slope threshold is located approximately about 20° . When comparisons are limited to slopes less than this r^2 and RMSE values are comparable to those seen between LVIS and the ground-based LAI values

To minimize slope-induced error, GLAS footprints were filtered with a cutoff slope threshold of 20, reducing the total number of GLAS footprints from 99 to 39. Through this process the comparative result between LVIS and GLAS was improved significantly, as shown in Fig. 3-8, with an increase in r^2 to 0.69 in comparison to the previous 0.53, evident prior to filtering (Fig. 3-6). The filtered data displays a bias = -0.05 and RMSE = 0.33. Apart from a few outlying results underestimating the GLAS LAI data points, almost all data are closely distributed around the 1:1 line, indicating a good agreement between GLAS and LVIS LAI.

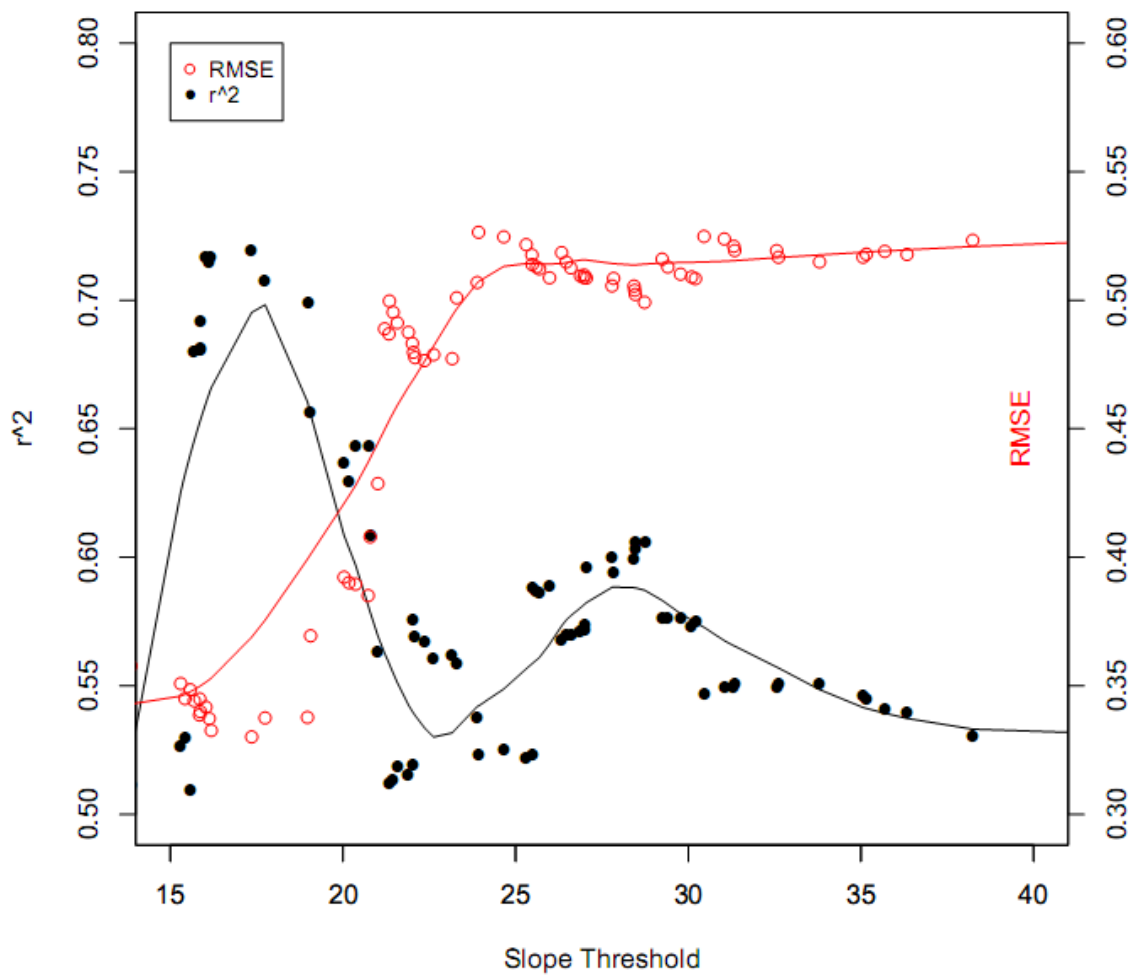


Fig. 3-7 Correlation statistics of RMSE and r^2 calculated upon comparison of all LVIS LAI and GLAS LAI values as a function of slope threshold (x). For a given slope threshold α , the y-axis represents the RMSE (or r^2) of all GLAS shots with slope $< \alpha$.

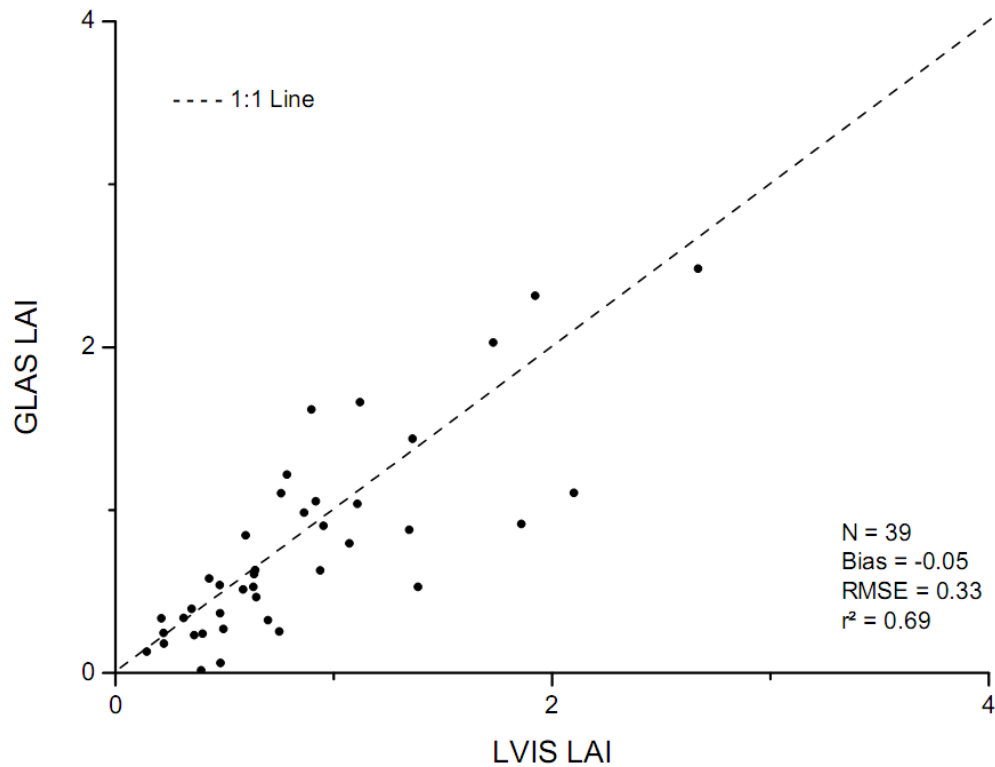


Fig. 3-8 Averaged LVIS effective LAI against GLAS LAI at the GLAS footprint level for GLAS shots with an average slope $< 20^\circ$.

3.4.4 LVIS LAI vs. MODIS LAI

Fig. 3-9 shows a weak relationship between the averaged LVIS LAI with MODIS 1 km pixels using the MODIS LAI 8-day composite product. LVIS derived total LAI was calculated from averaged effective LAI multiplied by a clumping index of 1.8 (Chen et al. 2005) at each MODIS pixel. Despite a low bias (-0.16) and low RMSE (0.67), the comparison between LVIS LAI and MODIS LAI has the lowest r^2

(0.20) among all comparison results (Table 3-2).

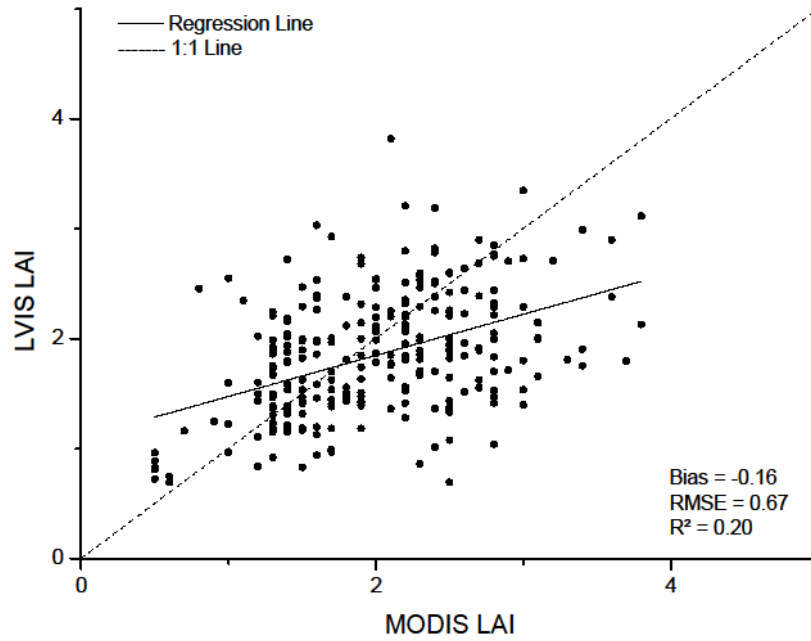


Fig. 3-9 Averaged LVIS total LAI against MODIS LAI at each MODIS 1 km pixel level.

Table 3-2 Summary of comparison results with LVIS LAI

	<i>Hemi- photo</i>	<i>EVI- regression</i>	<i>EVI- hinge</i>	<i>LAI- 2000</i>	<i>GLAS (all)</i>	<i>GLAS (low slope only)</i>	<i>MODIS</i>
r^2	0.80	0.76	0.75	0.85	0.53	0.69	0.20
RMSE	0.55	1.24	1.39	0.56	0.52	0.33	0.67
bias	0.46	1.07	1.58	0.46	-0.09	-0.05	-0.16

3.5 *Discussion*

This study demonstrates the feasibility of deriving LAI products from spaceborne waveform lidar and the potential to validate these products using ground validated airborne lidar data. This capability is examined using comparative LAI values obtained from ground based, airborne and spaceborne measurements with airborne lidar acting as the control dataset. Agreements are good between LVIS and all other LAI products studied in this work with the exception of MODIS (as shown in Table 3-2).

Ground-based LAI estimates (hemispherical photo and LAI-2000) are observed to show the most agreement with LVIS LAI data, specifically the highest r^2 and lowest RMSE. However, a consistent positive bias in the comparison indicates either an overestimate of ground-based LAI or an underestimate using LVIS. The main cause of this discrepancy is likely attributable to the use of different scanning angles: the nadir scanning of lidar observes more gaps within a canopy and hence produces relatively lower LAI values when compared with the ground hemispherical scanning method. In addition, this discrepancy can be exacerbated by the different viewing direction: satellites are downward looking, whereas ground measurements look up (Demarez et al. 2008). Without the gold standard of destructively sampled LAI data the validity of the approaches presented in this study remain unconfirmed and will require further investigation across multiple biomes to enable conclusive validation. In spite of this limitation the high coefficient of determination ($r^2 > 0.80$) exhibited between LVIS and ground-based measurements suggests that a feasible

correction of systematic biases is possible which may allow interchangeable LAI data sets for the purpose of validation.

Despite the high r^2 (~0.75) values, Echidna overestimates LAI in comparison to LVIS as well as other ground measurements (LAI-2000 and hemispherical photos). This occurrence is observed as a result of the effects of spectral scanning differences (near-infrared for Echidna vs. blue band for hemi), lower image sampling resolution (640 pixels for Echidna vs. 1520 pixels for hemi) and a mismatch in gap threshold setting (Zhao et al. 2012). A new generation Dual-Wavelength Echidna Lidar (DWEL) is proposed to extend and improve the ability of the current Echidna version to retrieve forest structural parameters, and hence help address this overestimation (Douglas et al. 2012).

MODIS LAI is observed to have the least agreement with LVIS LAI. The relatively low r^2 value indicates that MODIS LAI could have a large uncertainty within a 1 km pixel with this uncertainty likely due to the following two reasons. Principally, MODIS cannot describe the spatial structural heterogeneity of the forest within a 1 km pixel. LVIS, on the other hand, can fully capture the LAI spatial variability at ~ 30 m resolution. It may be the case that MODIS is able to provide similar estimates as LVIS over more homogenous forests but less accurate over forests of high heterogeneity. Secondly, MODIS LAI does not represent true LAI, but rather the mathematical expectation of LAI over an estimated LAI distribution function (Knyazikhin et al. 1998c). The default algorithm calculates the LAI distribution function by measuring probabilities of various LAI values given the spectral bands of a certain pixel. The probability-based LAI prediction can describe

the general trend but does not appear accurate at pixel level. These limitations explain the low r^2 but also the low bias as seen through our comparisons.

Our results also indicate that LAI can be accurately derived from GLAS data but only under desirable topographic conditions. The detrimental effect of slope is believed to be threefold. Slope may serve to increase the data variance, lower the signal amplitude of the ground Gaussian fit, and blur the separation between ground and canopy energy in a waveform signal. Such slope effects, coupled with low emitting laser energy and multiple scattering effects, comprise the major measurement errors existing in canopy height and LAI calculations using lidar remote sensing (Lefsky et al. 2005; Tang et al. 2012). For large footprint sizes the slope effect becomes more significant as the complexity and heterogeneity of topography increases relative to the mean footprint scale, as shown in Fig. 3-6 and Fig. 3-7. As a result, GLAS may not be suited to predicting LAI values over mountainous areas with large slopes.

When using GLAS for deriving LAI, the recursive method shows significant improvement compared with the non-recursive. As discussed in section 3.3, large LAI prediction errors occur when using the first Gaussian fit only (Fig. 3-6a). The recursive method can partially correct for slope and multiple-scattering effects but requires a priori information. This information is usually available from external and independent sources and need not be extremely accurate. For the case described in this study we used maximum summer MODIS LAI. As MODIS LAI serves as the upper limit constraint, its value is expected to be consistently greater than GLAS LAI (before clumping correction). However, the a priori guess may occasionally be

incorrect and MODIS at times may underestimate LAI (at GLAS scale, not the entire 1km MODIS pixel), particularly over mixed land cover types. This would lead to an underestimated prediction of GLAS LAI. As an example consider a MODIS 1 km pixel ($LAI = 2$) consisting of savannas ($LAI = 0.5$) and forests ($LAI = 4$). If the GLAS footprint were to fall over the savannas, the recursive algorithm works seamlessly. However, if the footprint falls over forests, the algorithm will set the LAI upper limit to 2 and not the actual maximum of 4. To minimize such an effect, accurate land classification maps or finer resolution LAI maps (e.g. from Landsat) will be helpful. Further work is planned to address this problem. Although the efficacy of such an algorithm remains largely untested, results in Sierra National Forest increase our confidence of deriving LAI products from GLAS.

Our GLAS LAI algorithm also benefits from additional environmental information, namely the leaf/soil reflectance ratio. The leaf/soil reflectance ratio is primarily applied to normalize the laser waveform energy between the canopy and ground components. Failure to incorporate the ratio into the LAI model increases the error and uncertainty, particularly over high LAI areas. Previous studies have used constant values obtained from either empirical or field sources (Lefsky 1999b; Tang et al. 2012). Armston et al. (2013) improved a model originally published by Ni-Meister (2010) to estimate the ratio value using waveform lidar. Their results suggest the possibility of retrieving robust leaf/soil ratio estimates at site level. This method has the potential to refine GLAS LAI products over large areas but will require additional developmental efforts.

Results of the inter-comparison of LAI values with respect to LVIS derived

values provide encouragement for the wider use of the outlined validation approach and indicate that 1) LVIS can be used to derive high accuracy effective LAI maps at ~20 m resolution as validated by all ground measurements (hemispherical photo/LAI-2000/Echidna) at plot scale, and 2) LVIS can be used to validate LAI products from spaceborne remote sensing (e.g. GLAS and MODIS). Our results highlight the feasibility of using airborne lidar as a validation intermediary between ground based field and spaceborne LAI measurements but it is expected that a direct comparison between field and spaceborne measurements may remain problematic due to differences in spatial coverage, ground heterogeneity and sampling density, in addition to sensor and algorithm complexity. The lack of coincident field plots with the footprints of GLAS data makes this an even more difficult achievement. As a consequence it is beneficial to facilitate validation and calibration activities at multiple scales when analyzing such varied data. This includes analysis of the varying ground based techniques featured in this study. Such consideration will help address the necessity to satisfy the accepted Global Terrestrial Observing System LAI mapping requirement of $\pm 15\%$ uncertainty at the pixel scale (Abuelgasim et al. 2006).

In the near future, our work will focus on improving the current method presented in this study, principally by incorporating more testing across the large gradient of biomes found in North America. We also intend to assess the accuracy of GLAS derived LAI profiles, potentially validated by LVIS and Echidna. Ultimately, these studies are intended to aid in the derivation of a continental scale LAI profile product using GLAS data linked to ground-based measurements, and aircraft and spaceborne observations through a similar validation framework to that presented in

this study. This will be one of the first attempts to investigate forest structural information on this large scale, and is of great importance in deepening our understanding of forest dynamics and terrestrial carbon flux.

3.6 Conclusion

This study has shown that LVIS airborne lidar can accurately estimate the spatial variability of total LAI exhibited in ground measurements. This has been shown for data collected at the Sierra National Forest. Direct comparison of results between LVIS LAI and ground measurements (bias ≈ 0.50 and RMSE ≈ 0.50 for hemispherical photographs/LAI-2000 and a significant overestimate in both statistics for Echidna) indicate the existence of a systematic bias in ground measurements of total LAI in comparison to LVIS data. This is mainly due to existing differences in scanning mechanism and data processing methods. However, the high coefficient of determination ($r^2 \approx 0.80$) exhibited between those datasets suggests that a feasible correction of the systematic bias is feasible and can be applied to create interchangeable data. Due to known flaws in ground based LAI acquisition and evidence from previous LVIS LAI studies, involving destructive sampling, it is reasonable to assume that LVIS may present a more accurate representation of true LAI. Significantly this allows a similar or greater confidence to be placed on the data obtained from airborne systems, and allows robust LAI maps to be constructed on a much greater scale and at a faster rate than currently possible.

Where LVIS data is available the high level of correlation acts as a validation for its use in providing an independent LAI dataset, offering an alternative product

with a high level of potential. This correlation between LVIS and ground measurements also suggests that LVIS data can be used as an intermediary link between ground and spaceborne measurements, bridging the gap between the vastly different spatial scales at which LAI data is available. This approach to GLAS validation fills a gap existing in the capability of spaceborne lidar interpretation as presently insufficient ground-based measurements are available for this purpose. Hence the vast global GLAS dataset is significantly underutilized.

GLAS LAI products should be viewed as a complementary source of LAI estimation to passive optical sources such as MODIS, which can also provide LAI data on a global scale. It is emphasized that GLAS LAI estimation offers several advantages and disadvantages in comparison to MODIS and the prospective use of the data together in some form of data fusion is bound to be beneficial to future studies. The advantages offered by GLAS not only include the relatively higher observed correlation with LVIS waveform data, but more significantly the potential to estimate vertical distribution of LAI, previously shown for LVIS waveform data. This of course suggests a more accurate link between the spatial extremes offered by ground and spaceborne measurements. It is believed that successful development of the large GLAS dataset independently or in fusion with passive optical methods has potentially huge ramifications for ecosystem modeling. In light of this the provision of a mid-scale validation method to maintain a direct link between large scale remote sensing and the plot level forest inventory is seen as a vital component to unlocking the full potential of GLAS data and the continued success of MODIS products. The evidence presented here acknowledges the efficacy of fulfilling this role with LVIS

LAI data and ultimately of improving global LAI coverage.

It is likely in the next decade that more active systems will be launched into space including ICESAT2. Future systems will potentially offer swath mapping lidar, and similar technological advances. The results of this study then hold the future promise of retrieving robust global estimations of leaf area index profiles with even greater coverage and accuracy than predicted here. This would create a remarkable dataset that could be used to revolutionize models that predict energy and mass exchange between the atmosphere and biosphere.

Acknowledgements

This work was funded by NASA under grant NNX08AP55G and Earth and Space Science graduate fellowship NNX12AN43H. The ground based measurements were supported by NASA under grant NNG06GI92G and NNX08AE94A and NSF under grant 0923389. We thank Yong Pang for original GLAS waveform processing, Ross Nelson for providing useful advice on GLAS data processing, Michelle Hofton for advice regarding LVIS processing and Tao He for his help in processing MODIS data. We also thank people in NSIDC (National Snow & Ice Data Center) User Services for the help on data acquisition.

Chapter 4 Large-scale Retrieval of Leaf Area Index and Vertical Foliage Profile from the Spaceborne Waveform Lidar (GLAS/ICESat)

4.1 Introduction

Leaf Area Index (LAI) and vertical foliage profile (VFP, or foliage height profile) are important biophysical variables in terrestrial ecosystems (Aber 1979; Gower and Norman 1991; Parker et al. 2001; Stark et al. 2012). Recent studies have reviewed the importance and potential applications of LAI and VFP derived from large footprint waveform lidar (Tang et al. 2014; Tang et al. 2012) and have shown the efficacy of a physical model to derive these profiles from waveform lidar data when compared to destructively sampled profiles in a tropical rain forest (Tang et al. 2012). This model was then transferred to the montane forests of the Sierra Nevada using GLAS sensor on board of ICESat. The comparison between GLAS-derived LAI data and airborne lidar data ($r^2 = 0.69$, bias = -0.05 and RMSE = 0.33) demonstrated the more general capability of our algorithm to provide total LAI and LAI profiles across biomes (Tang et al. 2014). The logical extension of these efforts is a further application of our methods over much larger areas, and is the goal of our work presented here.

Large scale derivation of GLAS LAI and VFP products have the potential to serve as a source of validation data for passive optical data sets, as well as providing needed canopy information that may be used within ecosystem and other models.

While observations from airborne lidar sensors have been used to derive both LAI and VFP, these data are limited spatially. Demonstration of the viability of using space-based retrievals of these from lidar over large areas opens the possibility of enhanced descriptions of the vertical organization of canopy elements that play large roles in the transfer of energy and mass between the surface and atmosphere in ecosystem models. For example, there currently exists no regional data set of the LAI profiles, let alone for areas as large as states and beyond. Providing such data would improve our understanding of LAI structure and dynamics, its role in terrestrial gross primary production (GPP) (Kotchenova et al. 2004), and global carbon cycling (Houghton 2007). Furthermore, foliar profiles have long been postulated to have an impact on habitat quality, species richness and abundance (Goetz et al. 2007). A global data set of such profiles would be exceptionally useful for clarifying the roles of LAI and VFP in these areas, as well as providing the means to explore the impact of climatic, edaphic, and human impacts on their magnitudes and variability.

The overall goal of this paper is to demonstrate large-scale LAI and VFP retrievals using GLAS data for the entire state of California. First, we describe the utilized inputs, including data from GLAS, MODIS and Landsat. We next briefly review details of our algorithm for deriving LAI and VFP from GLAS, initially presented in Tang et al. (2012) and implement our method to create footprint level LAI and VFP estimates from GLAS data over California. Our results include statistical analysis of GLAS LAI across environmental gradients (e.g. land cover type and elevation) and comparative analysis of GLAS and Landsat LAI retrievals for California.

4.2 *Data and Methods*

4.2.1 GLAS

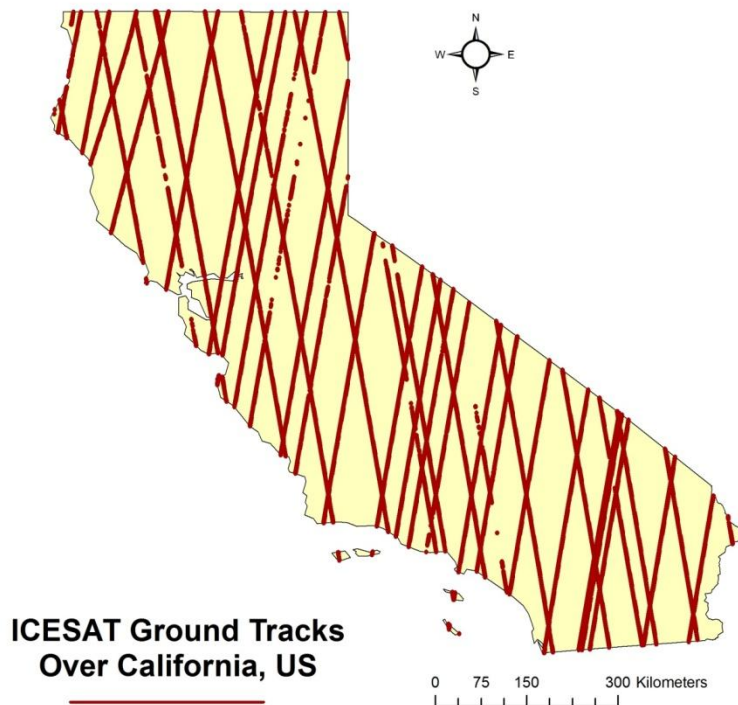


Fig. 4-1 Location of ICESat ground tracks over California, USA. ICESat did not provide a wall-to-wall coverage but rather data along transects separated by relatively long distances across track at mid-latitudes.

To this day GLAS has been one of the few operational spaceborne lidar instruments intended for global observations of the Earth. The GLAS system was developed for the ICESat mission and operated between 2003 and 2009. The primary objective of GLAS was to measure polar ice-sheet dynamics with the mission scope then extended to measure the height of vegetation canopies (Harding 2005). The GLAS laser sensor emits energy with wavelength of 1064 nm at a frequency of 40

Hz, and records the returned waveform from a ~65 m footprint (Abshire et al. 2005). Rather than providing wall-to-wall observation, GLAS yields individual footprint data with a centroid separation distance of ~165 m (Neuenschwander et al. 2008). Considering that the ICESat satellite primarily targeted polar regions, data acquired over global terrestrial ecosystems are quite sparse with large distances across track at equatorial and mid-latitudes. The GLAS data have been used to produce several global canopy height products (Lefsky 2010; Los et al. 2012; Simard et al. 2011).

The GLA01 and GLA14 data campaigns within the entire state of California from 2003 to 2007 were used in this study. GLA01 typically includes a 544-bin recorded waveform at a vertical resolution of 1 ns (15 cm) for land surface products. GLA14 products are accurate fits of the GLA01 waveform using up to 6 Gaussian peaks to represent the data, in addition to providing surface elevation and footprint centroid coordinates (Harding 2005). We did not use data associated with the campaigns Laser 1A or 2A due to an acknowledged signal truncation problem (Harding 2005). Low energy shots (waveform peak energy < 0.5 Volt) were filtered from the studied data to ensure the best retrieval quality.

4.2.2 Ancillary Input Data

In our retrieval approach terrestrial vegetation (excluding grasslands and croplands) was classified into nine types based on the MODIS Land Cover Type product (MCD12Q1) at 500 m resolution. The nine types were evergreen needleleaf forest, evergreen broadleaf forest, deciduous needleleaf forest, deciduous broadleaf forest, mixed forest, closed shrubland, open shrubland, woody savanna, and savanna.

This categorization followed the IGBP scheme of the MODIS land-cover map (MCD12). The overall accuracy of MODIS Collection 5 Global Land-cover data classification was estimated to be about 75% globally (Friedl et al. 2010).

Effective LAI derived from single angle looking remote sensing, such as from GLAS, should be corrected to true LAI using vegetation foliage clumping information. Such clumping effects could be ecologically significant and can be quantified using a biophysical parameter known as clumping index (Chen and Black 1992). The lidar-derived effective LAI can then be corrected into true LAI by dividing by the clumping index. We built a clumping look-up table by assigning each land cover class an average clumping index from multi-angular satellite POLDER (Chen et al. 2005).

For the retrieval procedure presented in this study, MODIS LAI (Myneni et al. 2002) was used as a filter to refine our GLAS LAI estimates by assessing the validity of each GLAS LAI retrieval (more details can be found in Section 2.4 and in Tang et al. 2014). The MODIS data used for this purpose were obtained from the MCD15A2 Collection 5 data set acquired during summer (July and August) from 2004 to 2007 and excluded cloud contaminated or low quality pixels based on associated QA data (Zhao et al. 2005). The maximum values of the temporal LAI series at each 1 km pixel were then calculated to represent the potential maximum LAI thresholds. Since MODIS LAI data may not represent the true maximum value (at GLAS footprint scale) within a 1 km pixel, pixels with maximum LAI values less than 1 were assigned the mean LAI value of its vegetation type (according to the MCD12 land cover map). Pixels with a LAI value greater than 6 were also re-assigned a value of

12 to correct the MODIS saturation domain (Myneni et al. 2002). These processes will ensure a proper upper boundary to filter GLAS LAI estimates.

4.2.3 LAI Derived from Landsat

We used a 30 m Landsat LAI map over California as a comparative data set. This map was produced from Landsat surface reflectance data based on canopy spectral invariants theory (Ganguly et al. 2012). The orthorectified Landsat data were acquired from the Global Land Survey (GLS) 2005 with core acquisition dates from 2005 to 2006 (Gutman et al. 2008). Surface reflectance data were then generated through the Landsat Ecosystem Disturbance Adaptive Processing System (LEDAPS) after applying radiance calibration and atmospheric correction (Masek et al. 2006). LAI at each 30 m pixel was retrieved based on a look-up table method, in accordance with MODIS LAI algorithms (Ganguly et al. 2008; Myneni et al. 2002; Yang et al. 2006). A comparison of Landsat-derived LAI with MODIS LAI showed reasonable agreement (Ganguly et al. 2012).

4.2.4 LAI Retrieval Algorithm

LAI and VFP can be derived from the vertical gap probability distribution as a function of height based on the MacArthur-Horn method (Chen et al. 1997; MacArthur and Horn 1969; Nilson 1971). This technique is essentially the optical point-quadrat sampling and computes vertical distribution of Leaf Area Density (LAD, unit: m^2/m^3), which is the density of foliage at discrete height layers within the canopy. The vertical arrangement of LAD constitutes VFP and an integration of LAD at all canopy layers gives the total leaf area, or total LAI.

Note that we do not specifically distinguish between PAI (Plant Area Index) and LAI here for several reasons. First, differences between LAI and PAI are generally small. For example, as shown in our previous work over a tropical forest in Costa Rica (Tang et al. 2012), destructively sampled stem-area was vastly smaller than leaf-area, with LAI comprising 93% of total Plant Area index and LAI derived from LVIS waveforms agreed well with these profiles. Additionally, our comparison with ground-based methods of LAI derivation in the Sierra Nevada, California, such as terrestrial scanning lidar and optical methods, again showed good agreement (Tang et al. 2014). Lastly, we expect the great majority of reflected laser energy from near-nadir looking NIR lidar comes from leaves, not branches, and Monte-Carlo simulation results support this contention (Hancock et al. 2012).

We estimated the vertical gap probability from lidar waveforms using the Geometric Optical and Radiative Transfer (GORT) model (Ni-Meister et al. 2001; Tang et al. 2012). This method was successfully implemented at multiple sites to derive landscape level LAI and VFP data using the airborne lidar system LVIS (Laser Vegetation Imaging Sensor) (Blair et al. 1999; Tang et al. 2012). Comparisons using different ground measurements (including destructively sampled data, hemispherical photos, LAI-2000 and terrestrial lidar) demonstrated that waveform lidar can provide accurate LAI and VFP estimates even in the presence of high LAI levels such as those expected in tropical rain forests (Tang et al. 2012; Zhao et al. 2011). Efforts were also made using similar methods to derive LAI from GLAS data. When using these models satisfactory results were achieved when comparing LAI-2000 or LAI estimates with those obtained from airborne lidar (Garcia et al. 2012; Luo et al.

2013). However these studies were limited to small and flat study areas featuring no significant topographic variation, which was found to have a significant impact on the accuracy of GLAS measurement (Pang et al. 2006; Simard et al. 2011).

In this study, we incorporated a 3-step recursive method developed by Tang et al. (2014) to retrieve LAI and VFP from GLAS data. This method was specifically designed to facilitate the separation of canopy and ground energy in GLAS waveforms. By incorporating prior knowledge of the LAI distribution (e.g. maximum potential LAI value of certain biomes), initial GLAS LAI estimates obtained from the GORT model can be refined. Pre-processed MODIS LAI was applied as the maximum potential LAI threshold. The method begins with the identification of the first Gaussian fit, assumed to be the ground return and used to calculate LAI and VFP. This estimate is then judged to be valid or invalid using the available prior knowledge. If considered invalid, the method iterates using the next feasible Gaussian fit until threshold conditions are met.

Canopy height predicted by the lidar waveform was calculated as the distance between the beginning of the waveform signal, the first return above the noise threshold ($3.5 \times$ standard deviation of identified noise), and the center of the chosen Gaussian fit. Our previous work showed that using this recursive method, GLAS could provide accurate LAI estimates under favorable topographic conditions, while a moderate level of accuracy could be achieved even over steep slopes (Tang et al., 2014). We extended this method by doubling the number of Gaussian fits to the GLAS waveform associated with the GLA14 data to 12 through a Gaussian decomposition method (Hofton et al. 2000). The default 6-Gaussian-curve fit, in

certain instances, could fail to capture the true ground position in the presence of complex topography or highly vegetated areas (Duncanson et al. 2010).

Within the outlined methodology an additional model was included to improve GLAS LAI estimates through accounting for spatial variability in the soil/leaf reflectance ratio. This ratio value, a required input parameter in the GORT model, was primarily applied to normalize the reflected canopy return and ground components in a GLAS waveform. Lefsky (1999) initially suggested a constant value of 2.0 for such a ratio while Ni-Meister et al. (2010) developed a method to estimate its value directly using waveform lidar data. The latter method was based on the assumption that this value did not change at local scales. Armston et al. (2013) further improved Ni-Meister's model by building a simple linear regression model between canopy energy and ground return with the slope of the regression taking on the value of the leaf/soil reflectance ratio. In this study we applied Armston's method at quarter-degree scale (~20 km) to calculate this parameter and its variability, assuming that the ratio value did not vary significantly over a homogenous forest or over similar land cover types. In keeping with Lefsky (1999) a default value of 2.0 was assigned to quarter-degree cells with different land cover types or those with poor regression estimates ($r^2 < 0.2$ and $N < 10$).

Finally, we performed three other analyses. First, estimates of true LAI at the footprint scale were derived from the effective GLAS LAI values using the clumping-biome look-up table, noting that true LAI should be consistently greater than effective LAI (Chen et al. 2005). Secondly, we compared total LAI values derived from GLAS with Landsat LAI data. This was not a validation, per se, but rather a means to

explore how the magnitude and variability of lidar-derived LAI compared with a commonly used passive optical product at fine scales. Lastly, much of California is mountainous. It was therefore of interest to explore if differences in GLAS vs. Landsat LAI were a function of topography as derived from the void-filled 90 m resolution SRTM DEM data (Reuter et al. 2007), as both products would be affected by topography, but in different ways.

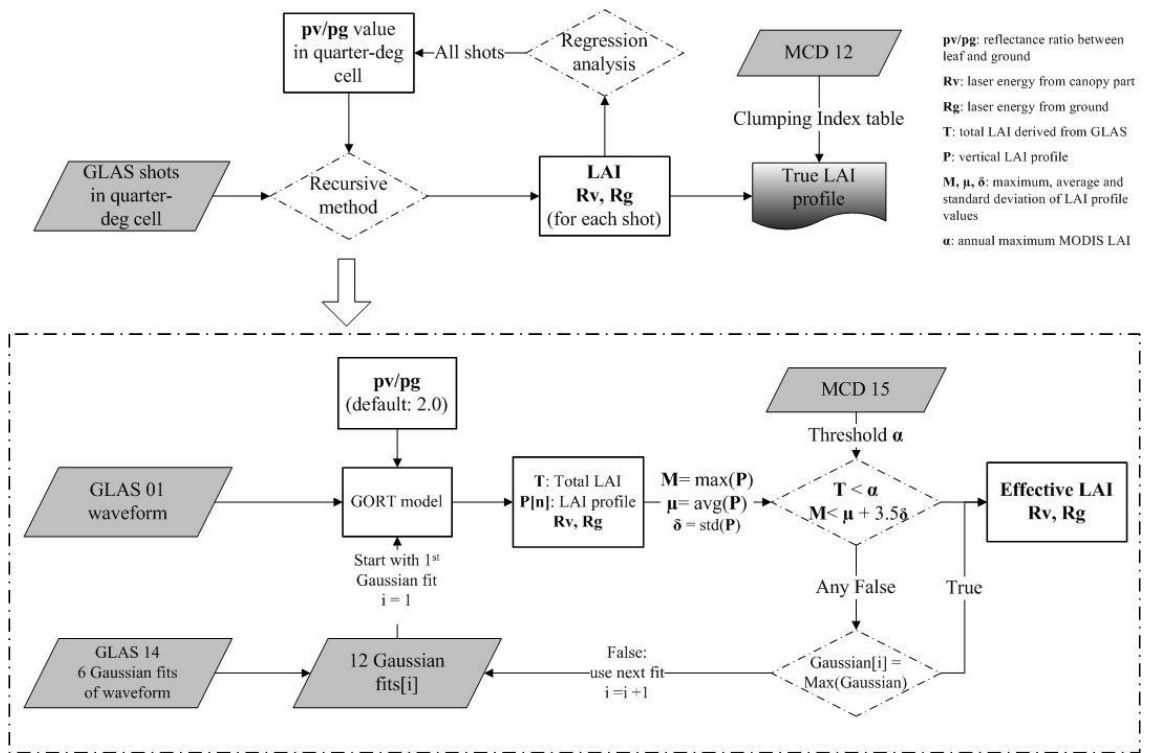


Fig. 4-2 Algorithm flowchart of retrieving LAI and VFP from GLAS data. Parallelograms are input data sets. The recursive method part (within the dash-dotted rectangle) is adapted from Tang et al. (2014).

4.3 Results

We derived a total of 16529 GLAS LAI and VFP observations. Using the

method of Armston et al. (2013), 42% of the GLAS footprints had a derived soil/leaf reflectance ratio different from the default of 2.0 (58%).

4.3.1 GLAS LAI

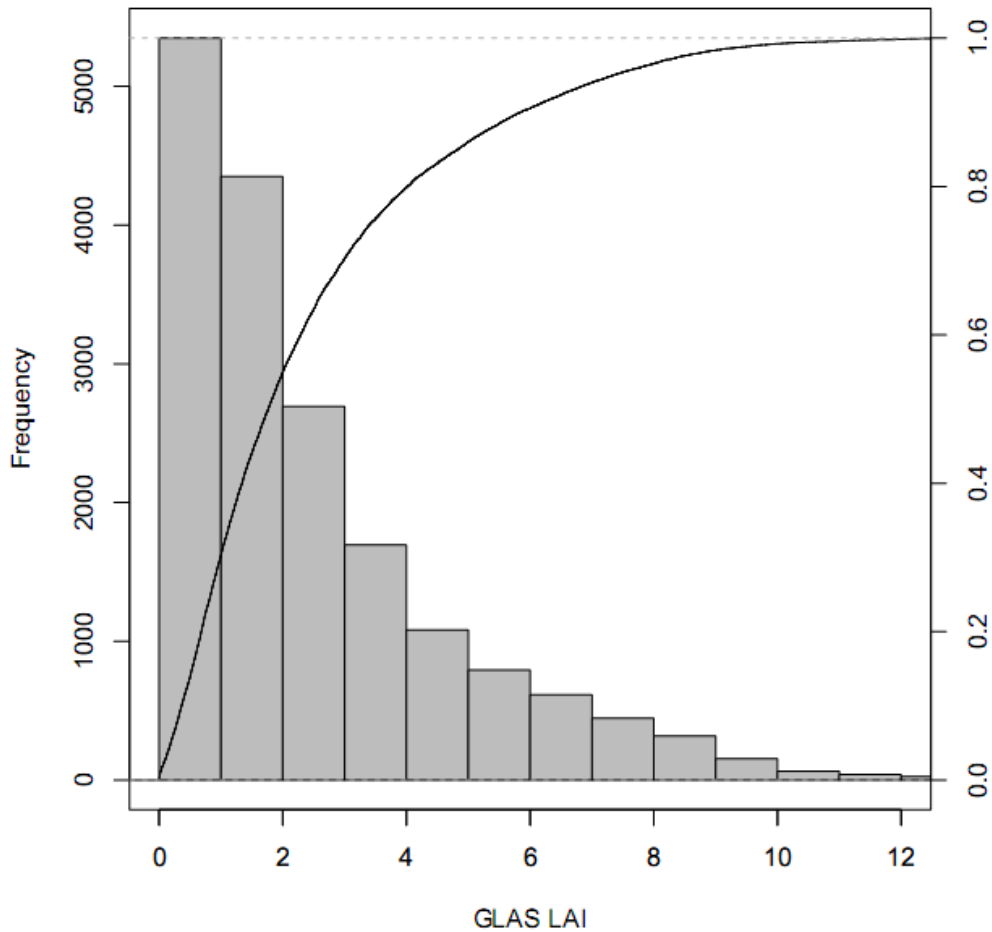


Fig. 4-3 GLAS LAI estimates over California. The majority of GLAS footprints had a LAI value less than 2 but there were also footprints with values greater than 8. The solid line shows the cumulative frequency.

The distribution of GLAS LAI over California (Fig. 4-3) was highly skewed towards lower values of LAI with more than 50% of the footprints less than 2 (the

median value was 1.76). This result was reasonable given that there were a large number of GLAS footprints occurring over land cover with expected low LAI values, such as savanna and shrubland.

The GLAS LAI values were grouped by land cover type according to our biome map (Fig. 4-4). Evergreen needle leaf forest and woody savanna comprised the highest frequency of GLAS observation numbers. Mixed forest showed the highest median LAI value (3.20) against all other biomes, followed by evergreen needle leaf forest (2.62). Woody savanna was observed to have a higher LAI value (1.23) than shrubland (1.05 for closed and 0.75 for open) and savanna (0.91) (and these differences were significant at $P < 0.001$). Evergreen broadleaf forest, deciduous needleleaf forest and deciduous broadleaf forest did not have sufficient observation numbers to perform a robust statistic analysis (results of all paired T-tests are given in Supplementary Table 1).

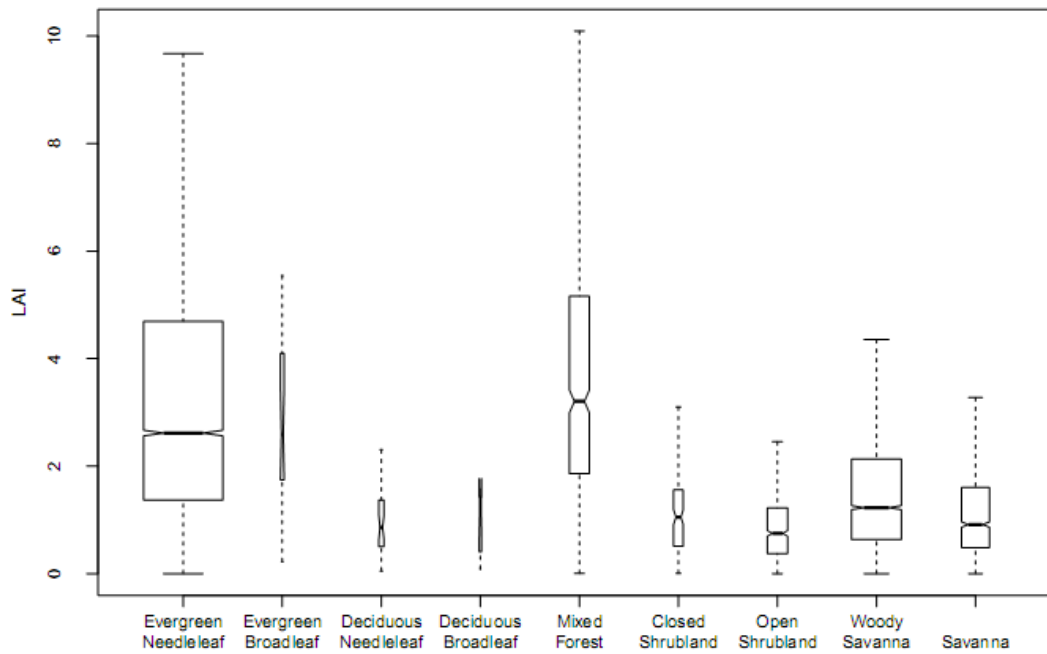


Fig. 4-4 GLAS LAI as a function of land-cover type. The width of the boxes is proportional to the number of observations for each type. Forest LAI (both evergreen needleleaf and mixed forest) are significantly larger than any other type. Note that difference between Evergreen needleleaf forest and mixed forest is also significant ($P < 0.001$).

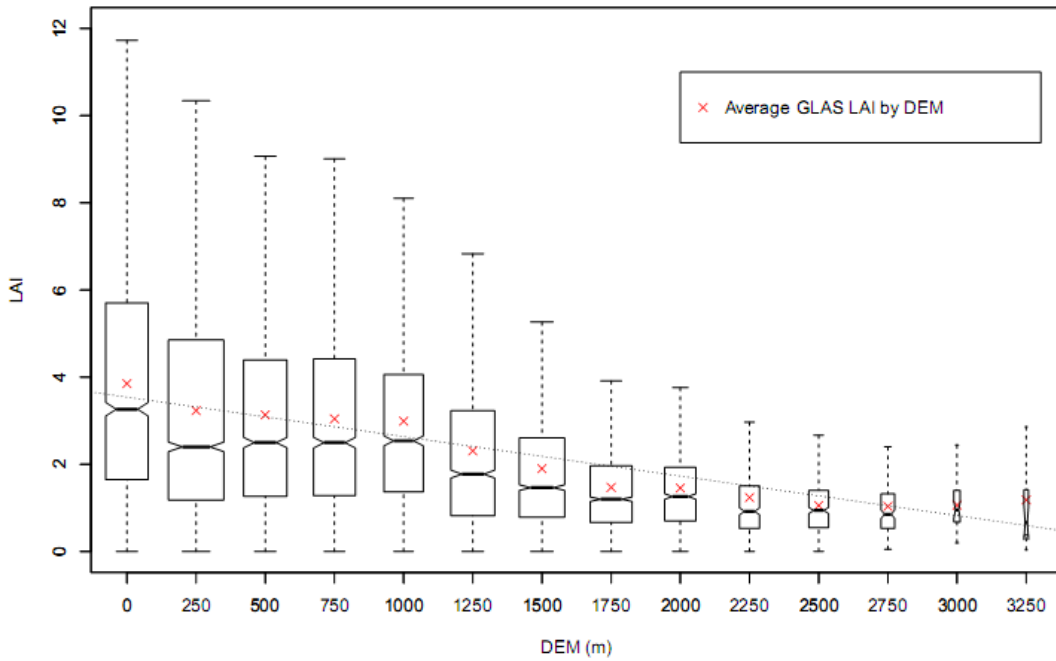


Fig. 4-5 Boxplot of GLAS LAI distribution as a function of elevation stratification groups. A linear regression analysis (dotted line) of LAI values averaged by elevation groups (red cross) shows a decreasing trend ($r^2 = 0.91$, $P < 0.001$).

GLAS LAI was also stratified by elevation (Fig. 4-5). The LAI values did not differ significantly in lower elevation groups (from 250 m to 1000 m) (all $P > 0.1$). A linear regression analysis showed that increasing altitude led to a significant ($r^2 = 0.91$, $P < 0.001$) but slow decrease in LAI values ($\Delta\text{LAI} = 0.91$ per km elevation change) accompanied by a general reduction in frequency (results of paired T-test in Supplementary Table 2).

4.3.2 GLAS Vertical Foliage Profiles (VFP)

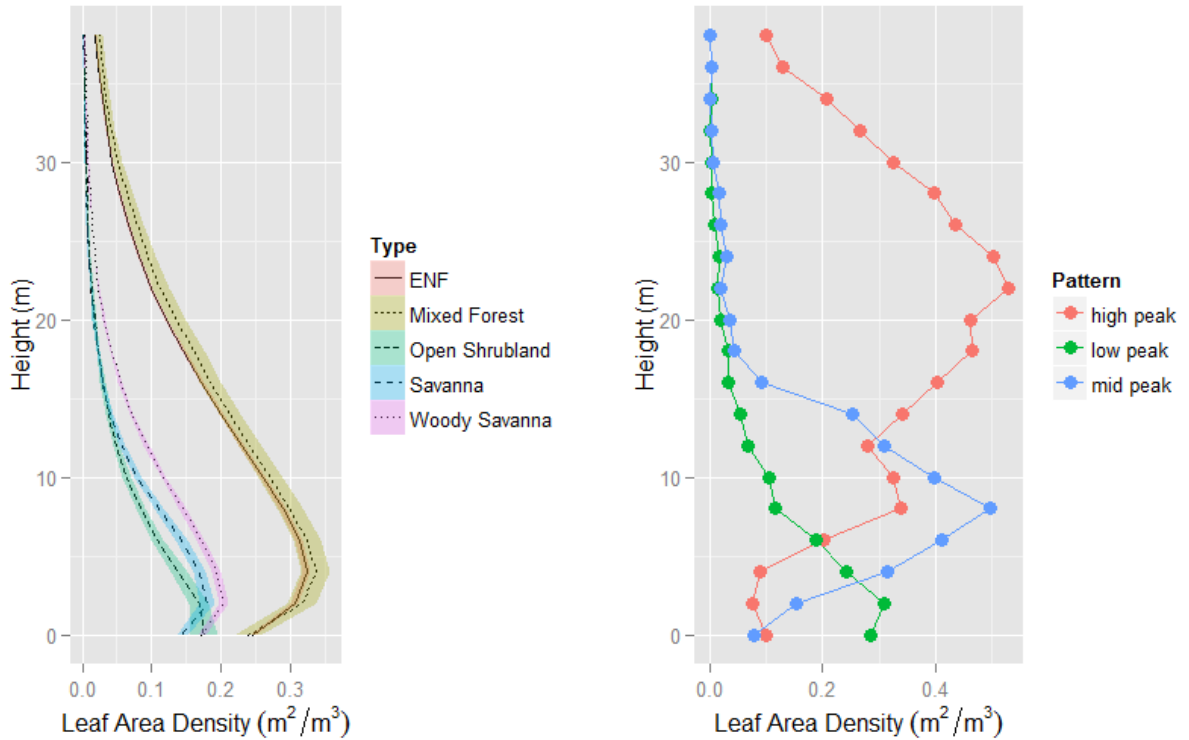


Fig. 4-6 Left: VFP (vertical resolution of 2 m) averaged for all GLAS shots over California for different land cover types. Each profile represents a single land cover type. Mean values are central lines within the color-filled 95% CI envelope. Note the low height of peak LAD is because of the averaging process over the land cover type. Individual profiles have much more variable shapes (see Right). Right: individual VFP examples with foliage density peak occurring at understory (<5 m), middle-story (~ 10 m) and up-story (>20 m).

Vertical foliage profiles were created by averaging GLAS shots for each different land cover type (Fig. 4-6). Here VFP were expressed as the vertical distribution of Leaf Area Density (LAD). These averaged profiles exhibited a peak of foliage density at approximately 5 m height for forest and values closer to ground level (2 m or lower) for savanna and shrubland. Foliage density of savanna and shrubland diminished quickly above heights of 10 m and dropped to almost 0 when reaching about 20 m on average. In the mid-story range (5 m ~ 10 m) differences between open shrubland, savanna and woody savanna were significant ($P < 0.01$).

Evergreen needleleaf and mixed forests had a similar vertical foliage distribution as would be expected if the mixed forest was heavily comprised of evergreen needleleaf (paired T-test results in Supplementary Table 3).

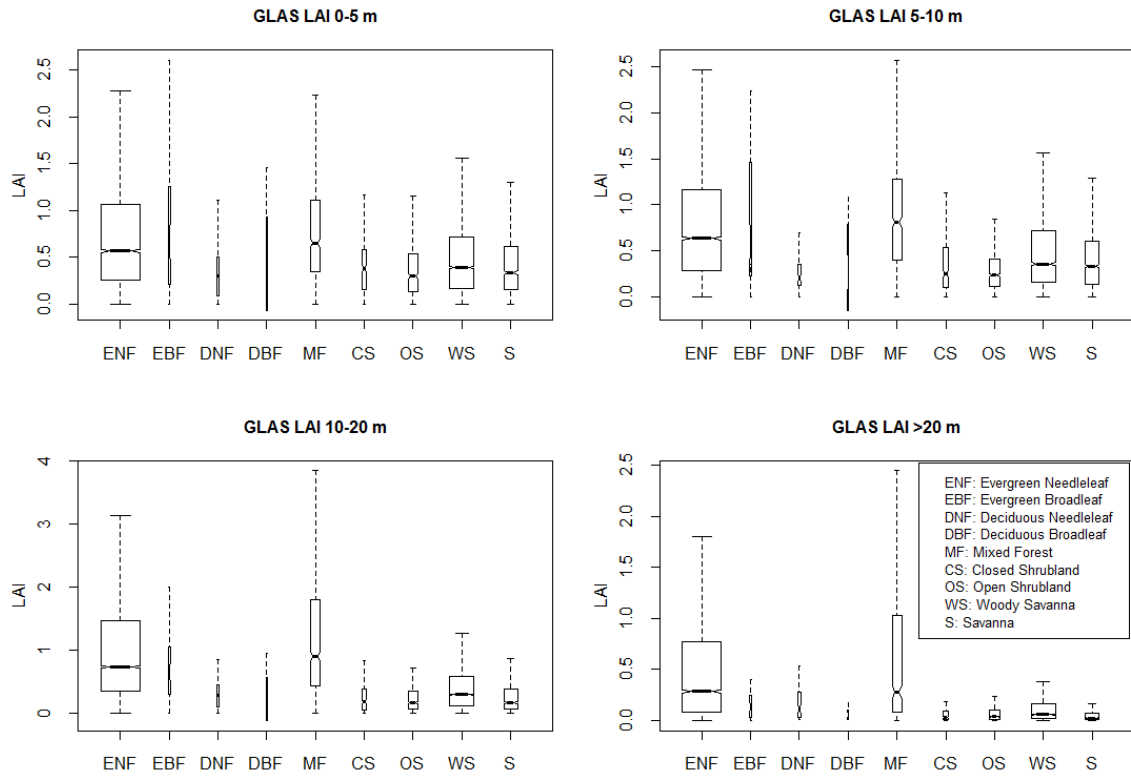


Fig. 4-7 GLAS LAI stratified by canopy position. Note that differences between needleleaf forest and mixed forest were only significant at the 10~20 m layer and > 20 m layer ($P = 0.003$ and $P < 0.001$ respectively). Note differing y-axis scales.

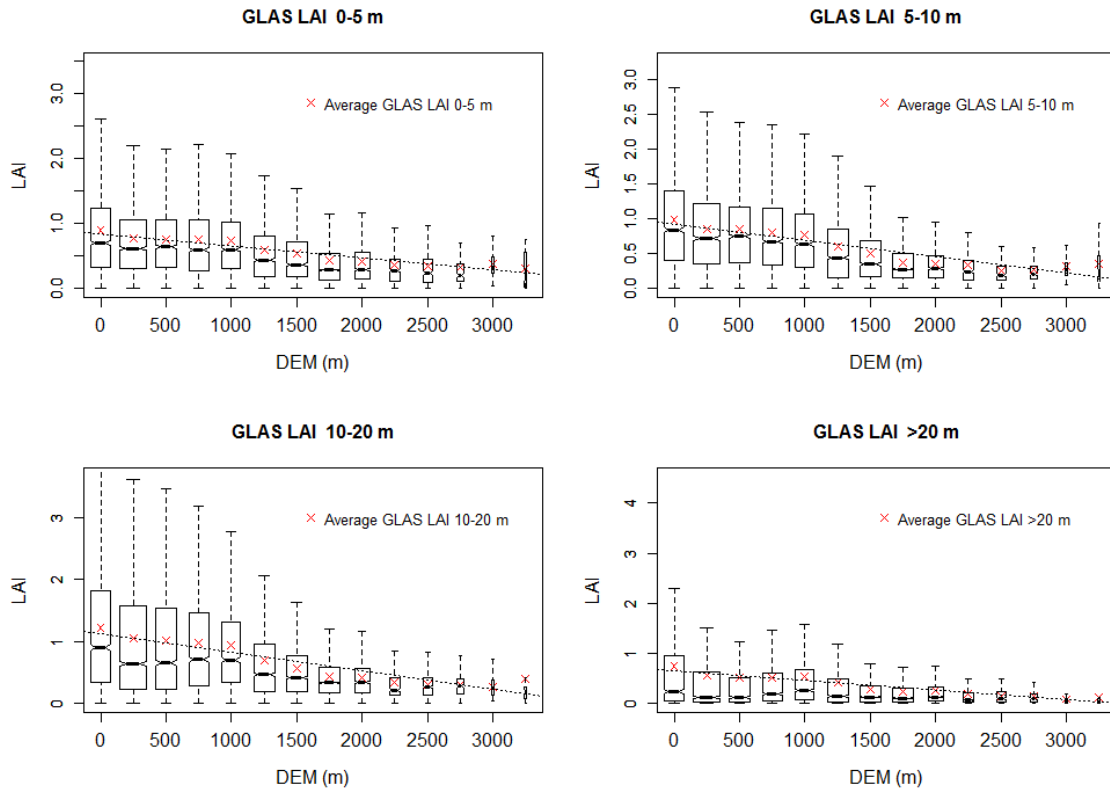


Fig. 4-8 Variability of GLAS LAI strata as a function of elevation for different canopy positions. The decreasing patterns were consistent in the 0-5 m, 5-10 m, 10-20 m and >20 m groups with slightly different rates. Note differing y-axis scales.

Forest vertical strata were produced from the original GLAS VFP data (0.15 m vertical resolution) through classification into four height groups: 0-5 m for understory, 5-10 m for lower mid-story, 10-20 m for upper mid-story, and > 20 m for upper-story (Table 4-1). Similar analysis to that shown in Section 3.1 was then performed on the forest strata to examine LAI variability as a function of land cover (Fig. 4-7). Differences between forest (needleleaf or mixed forest) and shrub (or savanna) were significant across all forest strata (all $P < 0.001$). There were also significant differences at the layer at 10-20 m ($P = 0.01$) and that above 20 m ($P < 0.001$) between needleleaf forest and mixed forest. However, we could not identify

any significant difference in understory (0 m - 5m) or lower mid-story (5 m - 10 m) between those two forest types ($P = 1.0$ and $P = 0.14$ respectively).

Canopy layers displayed a consistent decreasing trend of total LAI with elevation (Fig. 4-8), although the overall decreasing rates were slightly different for each layer ($\Delta\text{LAI} = 0.19, 0.23, 0.30$ and 0.19 per 1 km elevation change respectively). Despite the general decreasing trend, median values of upper-storey LAI appeared to reach maximum values at an altitude of ~ 1000 m. However, the differences among this layer and those of the adjacent elevation strata (groups of 250, 500, 750 and 1000 m) were not significant ($P > 0.05$ for all six comparisons. See Supplementary Table 4).

Table 4-1 Statistics of GLAS LAI and LAI strata by biome type (ENF = Evergreen Needle Forest, EBF = Evergreen Broadleaf Forest, DNF = Deciduous Needleleaf Forest, DBF = Deciduous Broadleaf Forest).

Biome Type	N	Total LAI Mean (\pm SD)	LAI 0- 5m Mean	LAI 5- 10m Mean	LAI 10- 20m Mean	LAI >20m Mean
ENF	9899	3.28 \pm 2.46	0.76	0.83	1.07	0.64
EBF	22	2.94 \pm 1.58	0.97	0.91	0.76	0.31
DNF	40	1.13 \pm 1.06	0.32	0.31	0.31	0.19
DBF	8	1.33 \pm 1.41	0.48	0.41	0.33	0.11
Mixed forest	615	3.66 \pm 2.38	0.80	0.90	1.19	0.78
Closed shrub	147	1.26 \pm 1.03	0.47	0.39	0.31	0.09
Open shrub	649	0.92 \pm 0.82	0.35	0.28	0.21	0.07
Woody savanna	3921	1.51 \pm 1.21	0.49	0.46	0.42	0.14
Savanna	1228	1.14 \pm 0.89	0.43	0.39	0.26	0.06

4.3.3 GLAS vs. Landsat

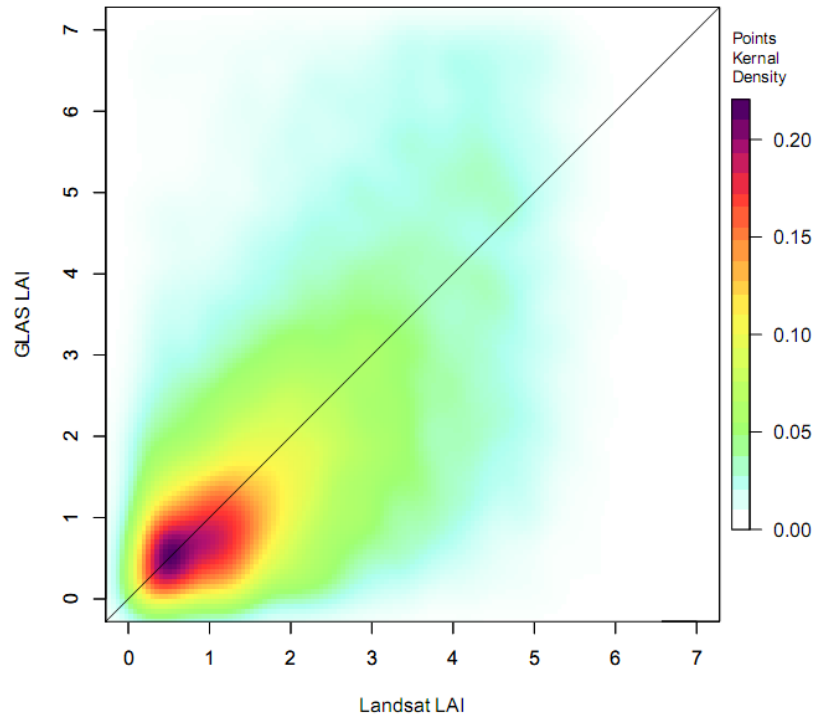


Fig. 4-9 Density scatter plot of Landsat LAI and GLAS LAI over California. The comparison reveals a fair agreement between the two data sets, but Landsat appears to saturate at about LAI = 5, and overestimates lower values relative to GLAS. Kernel density color bar refers to the distribution of LAI pairs with darker color indicating more clustered footprints.

There was a fair agreement between GLAS LAI and Landsat LAI at the GLAS footprint scale (Fig. 4-9), with $r^2 = 0.34$, bias = 0.26, and a RMSD (Root Mean Square Difference) = 1.85. Compared with GLAS, Landsat LAI was larger at lower values of LAI (< 2) but then saturated quickly at around LAI = 5. The histogram of differences (Fig. 4-10) between GLAS and Landsat is skewed because of large positive differences at high LAI (a long tail to the right), but there is also a large number of overestimates of Landsat relative to GLAS in the lower LAI regions.

While the overall bias is small, this was mostly a serendipitous cancelling out of systematic overestimates and underestimates (saturation) (as opposed to random variations). An example of the fine scale variability of along-track GLAS LAI estimates and Landsat is shown in Fig. 4-11.

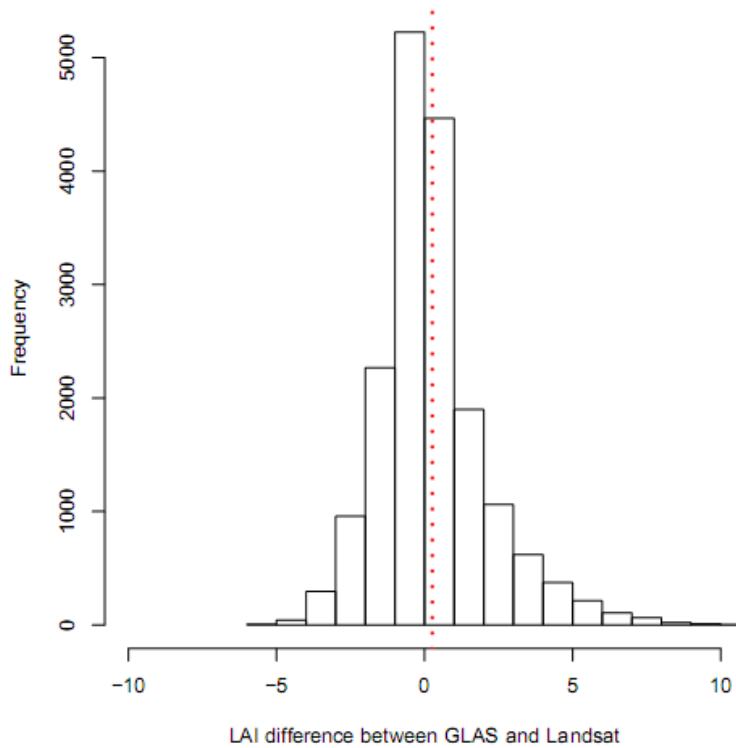


Fig. 4-10 Histogram of LAI difference between GLAS and Landsat. The red dashed line gives the bias (0.26). However, this low bias does not reflect the systematic differences apparent in Fig. 4-9.

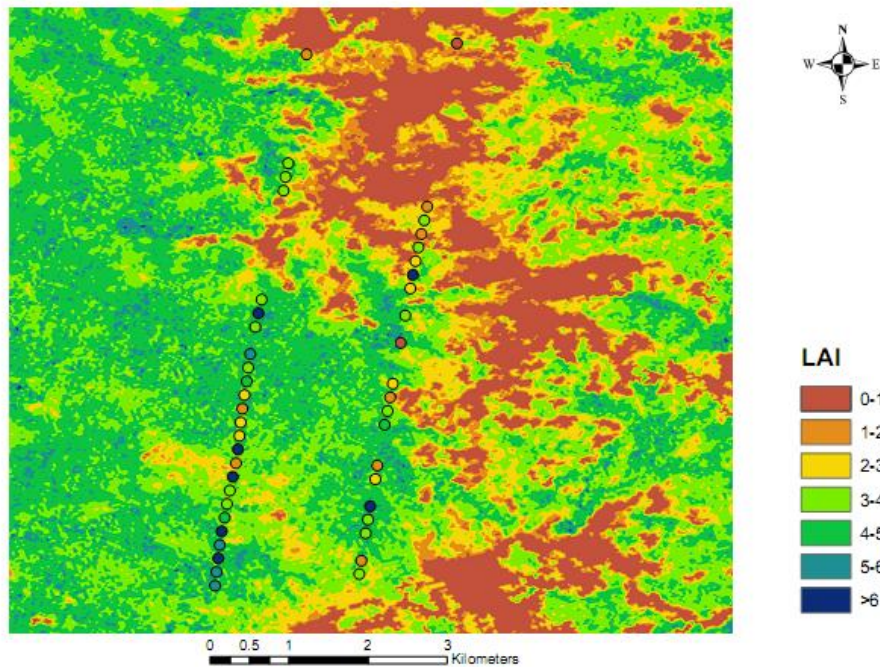


Fig. 4-11 An example of GLAS LAI and Landsat LAI at small scale. Overlaid GLAS LAI data is given by circles showing the sensor footprint to actual scale.

4.3.4 Slope Analysis

There are well-documented impacts of slope on large footprint lidar waveforms (Pang et al. 2006; Simard et al. 2011). We therefore analyzed the LAI differences between GLAS and Landsat as a function of slope to see what role, if any, slope might play in explaining them. We applied a linear regression model where $\Delta\text{LAI} = f(\text{slope})$ but found no relationship ($r^2 = 0.01$ and standard error (RSE) = 1.76):

$$\Delta\text{LAI} = 0.02 * \text{Slope} - 0.2$$

We also grouped LAI differences into eight different slope ranges from 0 ~ 40° with a 5° interval to examine the agreement of Landsat and GLAS LAI. The r^2 and RMSD were calculated within each slope range (Fig. 4-12). The r^2 generally

decreased from 0.3 to about 0.2 as the slope increased up to 40°. The RMSD doubled from about 1 to a maximum value over 2 at slopes greater than 20°.

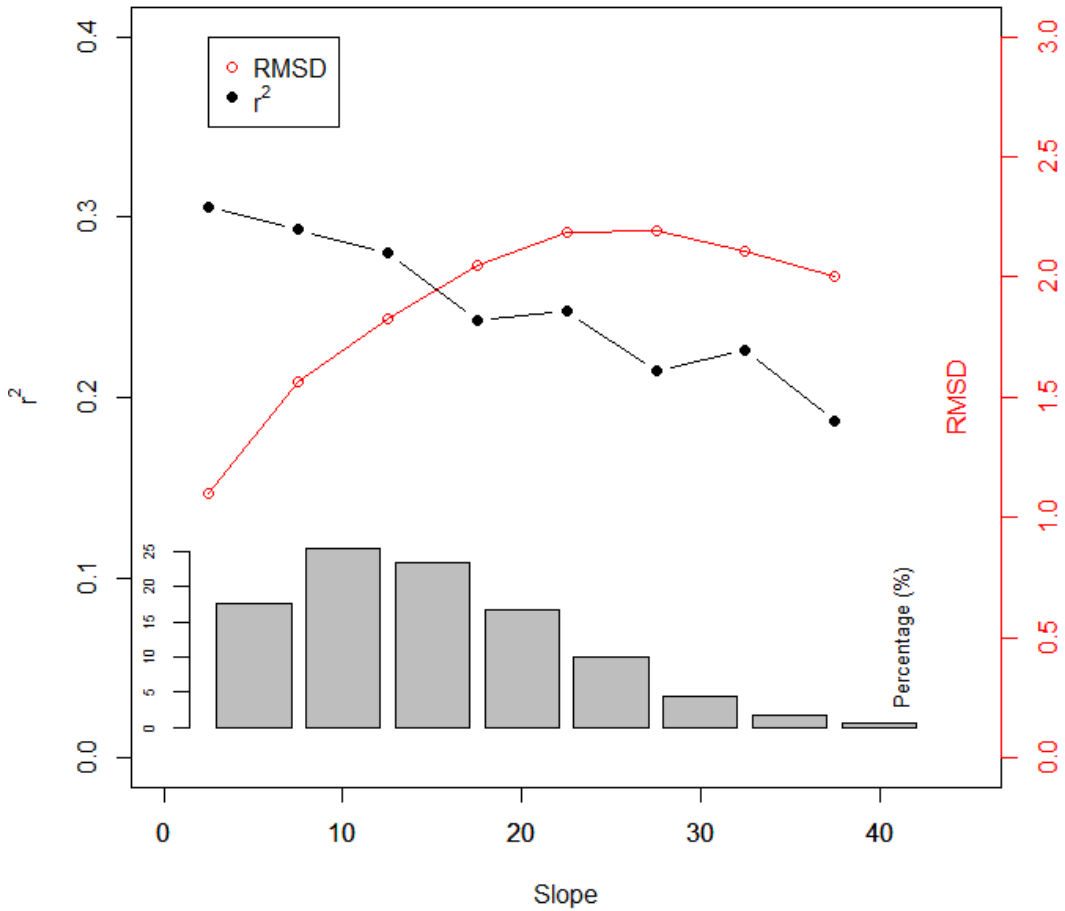


Fig. 4-12 Correlation statistics of r^2 and RMSD calculated upon comparison of GLAS LAI and Landsat LAI values by slope groups. Histogram gives distribution of slope groups. About 80% of the data had slopes less than 20°.

4.4 *Discussion*

Lidar technology has been proven to provide accurate measurements of many ecosystem structural parameters. Regional mappings of canopy height, LAI and forest strata have been deployed across all major biomes using airborne lidar data (Asner et al. 2012; Morsdorf et al. 2006; Tang et al. 2012; Wulder et al. 2007; Zhao and Popescu 2009). However, large-scale measurements of three-dimensional forest structure remain a major challenge, and this difficulty is mainly because of the limited availability of observations. One possible solution is to measure structure from space-based sensors. In this study we attempted to derive important biophysical structure in the form of LAI and VFP over a large region.

Our previous work has shown strong relationships between GLAS LAI and LAI derived from airborne waveform lidar (Tang et al. 2014) but was based on unique validation data (in the form of destructively sampled canopy profiles), or ground-based optical methods that are exceptionally limited spatially. These previous studies gave us confidence in the theoretical basis and efficacy of our models. For our work here, across an entire state, a comparable set of validation data for assessing our derivations do not exist. We therefore were limited to assessing differences in total LAI using passive optical data from Landsat. We found an overall fair agreement between derived GLAS LAI and 30 m Landsat LAI map. Despite their fundamental differences in sensor design and retrieval algorithms, this is quite an encouraging result. However, compared with GLAS data, Landsat was observed to both underestimate (saturate) LAI values for high LAI (Fig. 4-9) and overestimate LAI for

lower values. There are variations between the methods of observation that could lead to differences in total LAI such as system design (passive vs. active) and pixel size (30 m pixel vs. ~65 m eclipse for GLAS). Note there was also a temporal discrepancy between the two data sets (2005 only vs. 2003-2007).

Which is "correct", GLAS or Landsat? While we cannot answer this question definitively, saturation of LAI by passive optical sensors is well known (Shabanov et al. 2005; Yang et al. 2006). We further do not know of a plausible physical explanation that would lead us to suspect that GLAS observations for high LAI areas are overestimates. A plausible hypothesis could be passive optical sensor data do not detect energy from lower canopy portions or understory in dense forests. Progress in this area will depend on the availability of improved field data, coupled with terrestrial scanning and airborne lidar observations and radiative transfer simulation modeling.

Comparisons with Landsat aside, there are several potential sources of error in our GLAS LAI algorithm. In particular there are two major input parameters involved in the GLAS-LAI algorithm: a clumping index based on MODIS land cover classification and the leaf/ground reflectance ratio. The use of such ancillary data is the essence of data fusion, but the impacts of errors in the parameters on LAI variations need to be assessed. In our algorithm, MODIS land cover classification provides the clumping information required for converting GLAS effective LAI to total LAI values. For any given effective LAI value, error in true LAI varies linearly with clumping index. For example, a 10% error in clumping index would generally lead to a 10% error of true LAI value but does not change the effective LAI value.

Errors in clumping index, in turn, are caused by errors in land cover classification, the spatial variability of clumping index within land cover types, and the accuracy of the fundamental derivations of the index itself. Here we do not account the spatial variability of clumping index within biomes because the variation of clumping index for any given biome is small (Chen et al. 2005).

Leaf/ground ratio is the other important input parameter of our model. Methods have been developed to derive this value relying on lidar data themselves (Armston et al. 2013; Ni-Meister et al. 2010). However, this ratio cannot be obtained for all GLAS footprints because the mathematical solutions do not converge. In these cases we were left to assign a default value of 2.0. Sensitivity of LAI with respect to leaf/ground ratio value has been analyzed in our previous work (Tang et al. 2012). We found that the effect of the ratio on LAI is not large. For example, expected variations of the ratio would introduce an error of about ± 0.5 for $\text{LAI} \approx 4$, and this impact decreases as LAI gets smaller. Uncertainty introduced from the ratio should constitute roughly 10% or less of total LAI given an average LAI value of ~ 2 in California.

We discovered little relationship between LAI differences and slope with our regression analysis, while there was a trend of decreased r^2 (and increased RMSD) with steeper slope (). The relationship was not significant largely because of the distribution of GLAS-slope data: more than 80% of the data had a slope less than 20° . But when we grouped GLAS data by slope ranges, the slope effect on LAI difference is more evident. Steep slopes affect the lidar return by spreading the Gaussian ground return and blending canopy elements into the ground return. Thus, estimates of LAI

from GLAS near the ground (below 5 m) may sometimes be in error. Tang et al. (2014) showed that for the Sierra Nevada, differences between GLAS LAI and airborne waveform lidar LAI were minimized for slopes less than about 15°. This suggests that our iterative method of finding LAI overcomes impacts of slopes less than this magnitude, or effects of slope are overwhelmed by other sources of error or variation.

Our analysis also revealed GLAS data captures spatial LAI variability across different environmental gradients. For example, we found a significant relationship between GLAS LAI distribution and elevation groups (Fig. 4-5). An increase of 1 km elevation would typically lead to a decrease of ~0.9 LAI unit. This result agrees with published findings from previous studies of LAI and altitude gradients (Luo et al. 2004; Moser et al. 2007; Pfeifer et al. 2012). We also found a high variability of GLAS LAI values within and across different land cover types (Fig. 4-4).

One of the most exciting aspects of our work is the ability to derive LAI profiles at the landscape scale to develop a better understanding of their differences across land cover types. For example, we found foliage density peaks increase in both height location and maximum value, starting from shrubland, savanna, woody savanna and going to forest (Fig. 4-6). This finding is also supported by the distribution of LAI within forest vertical strata (0-5 m, 5-10 m, 10-20 m, and > 20 m, as shown in Fig. 4-7). In particular, we concluded that total LAI difference between needleleaf and mixed forest was due to their difference in upper-story rather than understory (Fig. 4-4 and Fig. 4-6). Moreover, we discovered that LAI strata contribute differently towards the total LAI change across elevation gradients (Fig.

4-8). Our results suggest that such data should improve our ability to evaluate the impacts of climatic and edaphic factors, as well as disturbance on spatial and vertical organization of canopies by revealing the existence of generalizable relationships between canopy structural information and these factors.

The availability of LAI profiles across large scales should be valuable for both the initialization and validation of ecological models by providing more robust and realistic representations of canopy structure. Previous studies suggest an underestimate of more than 50% of GPP when neglecting vertical foliage stratification (Aber 1979; Kotchenova et al. 2004; Sprintsin et al. 2012). A new canopy radiative transfer model (ISBA-A-gs) then recommends a minimum of 10 canopy layers to better estimate FAPAR and GPP (Carrer et al. 2013). A fully derived and validated continental or global scale VFP product from GLAS, using a similar process to those developed in this study would therefore be of great interest.

There is one note of caution considering the initialization of such models with lidar-derived profiles. If the models are run at a coarse modeling scale, e.g. say 50 km x 50 km as is typical of many carbon models, the use of an average profile for a land cover type would be misleading. As shown in Fig. 4-6, the average profiles show peaks very close to the ground partially due to the artifact of sampling. Hurtt et al. (2010) have shown that impact of spatial scale, either in the data through averaging, or in the model through coarse grid size cells, can have dramatic impacts on estimates of carbon flux, among others, between the canopy and the atmosphere when compared to the scale individual trees. Care must be taken to adequately represent the true vertical and spatial variability of the LAI profiles, either through shifts to finer

model resolutions or sub-grid scale parameterizations of LAI. For example, individual-based ecosystem models, such as the Ecosystem Demography model (Hurtt et al. 2010), have now been implemented at 1 ha spatial resolution. Furthermore, at coarser modeling scales, ED can potentially ingest the actual probability distribution (PDF) of LAI profiles for a grid scale, as observed from lidar. Thus, the great power of a remote sensing approach to LAI profile derivation is that it captures this PDF directly. If applied globally to GLAS data, our algorithm would provide the first data set of LAI profiles across biomes for use in modeling efforts.

Similarly, such profiles also have the potential to help quantify habitat heterogeneity, a fundamental component of biodiversity studies. Relationship between habitat heterogeneity and vegetation structure from airborne lidar have been explored at local scales (Ferber et al. 2014; Goetz et al. 2007; Swatantran et al. 2012). Analyses using continental scale data sets, such as the Breeding Bird Survey (BBS) (Sauer et al. 2008), may be facilitated by the inclusion of GLAS LAI profiles in models of species richness and diversity (Culbert et al. 2013; Goetz et al. 2014).

4.5 Conclusion

In this study we have demonstrated the feasibility of deriving LAI and VFP from spaceborne waveform lidar over large areas. The state-level GLAS LAI product showed a fair correspondence with 30 m Landsat LAI maps produced over California, but also highlighted potential issues with the latter: namely, saturation at high LAI values relative to GLAS. This suggests that further analyses should be conducted to validate both data sets using other data, and from these, refinement of algorithms for

both active and passive optical remote sensing.

While our previous validation studies have been limited to tropical and coniferous forests, our work here spanned a range of biomes, land cover types and environmental gradients. Because our modeling is based on physical principles, we are optimistic that future validation studies in different biomes will provide further support of the accuracy of our methods. Independent of these activities, our results here provide a unique and valuable data set on two key environmental variables that has been previously been unavailable over large areas, and thus provides the basis for a continental and global LAI data set from GLAS. It is our belief that such datasets, once available, will be of a great importance in deepening our understanding of the role spatial and vertical canopy structure plays in ecosystem processes, and the factors which impact that structure through time.

Acknowledgements

This work was funded by NASA under grant NNX12AK07G (Dubayah) and an Earth and Space Science graduate fellowship NNX12AN43H (Dubayah/Tang). We thank Maosheng Zhao and Qing Ying for their help in processing MODIS data. We also thank the NSIDC (National Snow & Ice Data Center) User Services for the help on data acquisition and NASA Earth Exchange (NEX) for computing resources.

Chapter 5 Characterizing Leaf Area Index (LAI) and Vertical Foliage Profile (VFP) across the United States

5.1 Introduction

Accurate measurements of three-dimensional canopy structure and function play a key role in our understanding of global carbon dynamics, climate feedbacks as well as biodiversity studies (Cramer et al. 2001; Heimann and Reichstein 2008; Loreau et al. 2001; Schimel et al. 2001). Spatial variations of ecosystem structural information largely constitute the geographical patterns of ecological processes as well as species richness (Cramer et al. 2001; Goetz et al. 2007; Turner et al. 2003). These structural variables, including canopy height, leaf area index (LAI) and vertical foliage profile (VFP), have been identified as essential climate variables (ECV), essential biodiversity variables (EBV) or both (Aber 1979; Baret et al. 2013; Gower and Norman 1991; Pereira et al. 2013). Yet measurements of these canopy structural data are often limited at field sites, and their spatial distributions over broader geographical areas still remain under characterization due to heterogeneity of natural vegetation and inexact measuring techniques (Asner et al. 2013; Clark and Kellner 2012). A spatially explicit characterization of LAI and VFP at large scale is therefore of great importance and interest to help reduce current measurement uncertainty in global carbon cycling and habitat heterogeneity (Houghton 2007; Sauer et al. 2008).

Remote sensing offers global observations of terrestrial ecosystems, and the science community has produced several LAI products at continental or global scale

using passive remote sensing techniques (Baret et al. 2007; Deng et al. 2006; Ganguly et al. 2012; Myneni et al. 2002). Most of these techniques try to derive LAI through exploring the correlation between canopy foliage density and the total reflected intensity of electromagnetic radiation at multiple wavelengths. Applications of these LAI products have achieved great success with significant improvements in current observations of global terrestrial ecosystem dynamics and its interactions with atmosphere (Mu et al. 2007; Randerson et al. 2009; Zhao et al. 2005). However overall accuracy of these products still cannot fully satisfy the requirement of Global Terrestrial Observing System, and the most profound problem is the saturation of spectral signal over dense forests with high canopy covers (Abuelgasim et al. 2006; Shabanov et al. 2005; Yang et al. 2006). This is because solar radiation decreases exponentially as penetrating through canopy of high foliage density, and the majority of recorded signal comes from the upper canopy in the form of direct reflectance and multiple scattering. Such effect greatly limits their observation capabilities over vertical aspects of forest structure and leads to an underestimate of LAI values over high canopy cover areas as well. As a result, traditional methods have limited measurement capability of forest structural data and new technologies are required in expanding current studies of carbon cycle science and biodiversity change.

Recent advance in Light Detection and Ranging (LiDAR), an active remote sensing technology, has proven as an effective measuring method of three-dimensional canopy structural information (Lefsky et al. 2002). Lidar measures the distance between a target and the sensor by the roundtrip traveling time of an emitted laser pulse. It would then be able to determine the accurate 3-D position of canopy

structural components, including foliage, branch and trunk. Forest structural data, including canopy height and biomass, have been increasingly explored from regional to global scales with terrestrial, airborne and spaceborne lidar sensors (Asner et al. 2012; Baccini et al. 2012; Drake 2002a; Lefsky 2010; Los et al. 2012; Saatchi et al. 2011; Simard et al. 2011; Strahler et al. 2008). Some Studies explored the capability of deriving LAI and VFP from lidar data but only at limited regional areas (Morsdorf et al. 2006; Tang et al. 2012; Zhao et al. 2013). There have been fewer efforts of trying to demonstrate the possibility of deriving LAI and VFP data across different landscapes from Geoscience Laser Altimeter System (GLAS) on board of Ice, Cloud and land Elevation Satellite (ICESat) (Garcia et al. 2012; Luo et al. 2013). These studies derived LAI and VFP from lidar waveforms based on biophysical and statistical models and their comparison results with field based measurements are very encouraging, suggesting the potential of further developing LAI and VFP product from GLAS.

Tang et al. (2014a) demonstrated the capability of deriving LAI and VFP data from GLAS data using a physically based model rather than an empirical method. Further improvement of the model led to a GLAS LAI and VFP product over the entire state of California, USA (Tang et al. 2014b). However, there is still a need to further examine the relationship between vertical foliage distribution and lidar waveforms over even broader areas. Assessment of their relationship across different forest types and environmental gradients will not only strengthen our confidence in acquiring a potential global LAI and VFP measurement, but also provide important implications on design and science definition of future lidar missions such as the

Global Ecosystem Dynamics Investigation (GEDI). These global LAI and VFP products, once available, would revolutionize our current observing dimension of terrestrial ecosystems in together with all terrestrial and airborne lidar data.

The objective of this study was to demonstrate the measurement capability of forest structure using GLAS data at near-continental scale. To achieve this goal, we quantified and analyzed LAI and VFP distributions throughout the Contiguous United States (CONUS). First, we implemented our algorithm at GLAS footprint level and compared the derived data with LAI and VFP products from existing airborne lidar at different forest types. Next we mapped the aggregated LAI and VFP product according to different ecoregions and land cover types over CONUS. Finally we analyzed the distribution of GLAS LAI across different environmental factors, including elevation and precipitation.

5.2 *Methods*

5.2.1 GLAS Data

GLAS is a spaceborne waveform sampling lidar sensor with the working wavelength at near-infrared band (1064 nm). It emits laser pulses at a frequency of 40 Hz and records the energy reflected from both the ground surface and canopy in an approximately 65 m footprint (Abshire et al. 2005). GLAS samples the Earth surface in transects with individual footprints separated by ~165 m from each other, and hence cannot provide a wall-to-wall observation of forests. Its spatial allocation of laser footprints cannot be appropriately labeled as either random or systematic sampling scheme, and would be better defined as a pseudo-systematic sampling or

cluster sampling strategy (Healey et al. 2012; Stahl et al. 2011). To obtain a spatially continuous estimate of LAI at continental scale, it is recommended either to extrapolate those lidar footprints with passive remote sensing images (Dubayah et al. 2008; Lefsky 2010), or to upscale them to the spatially explicit ecoregions using statistical analysis.

5.2.2 Retrieval of GLAS LAI and VFP

We collected a total of 1,100,498 cloud-free GLA01 and GLA14 data over Contiguous United States from 2003 to 2007. GLA01 included the complete recorded waveform at a vertical resolution of 15 cm for land surface products and GLA14 products were comprised of geographical information and various parameters calculated from the waveform (Harding 2005). Low energy shots (peak energy < 0.5 Volt) were excluded from data process for retrieval quality control because those waveforms were susceptible to noise contamination. Shots during leaf-off season (Nov. to Mar.) were also filtered out over deciduous forests and mixed forests. LAI and its profiles (0.15 m at vertical resolution) were calculated at GLAS footprint level using a recursive method (Tang et al. 2014a) based on a Geometric Optical and Radiative Transfer (GORT) model (Ni-Meister et al. 2001). Canopy VFP were calculated from integration of footprint level LAI profiles at height intervals of 0 - 5 m, 5- 10 m, 10 - 15 m and 15 - 20 m.

5.2.3 Comparison Data Set

Here we chose LAI and VFP data sets from an airborne lidar system LVIS to validate GLAS products. LVIS is an airborne medium footprint (~ 25 m) waveform

scanning lidar system designed by NASA Goddard Space Flight Center (GSFC) (Blair et al. 1999). It can sample the terrestrial surface across a 2 km wide swath with more than 100 beams, and has been highly useful in mapping different forest structural parameters (e.g. canopy height, VFP and LAI) at regional scale (Drake 2002a; Swatantran et al. 2012; Tang et al. 2012). We calculated both total LAI and VFP at 5 m height interval from existing LVIS campaigns using a well established LVIS-LAI model, which has previously been examined by field destructively sampling, LAI-2000 and hemispherical photos (Tang et al. 2014a; Tang et al. 2012; Zhao et al. 2013). LVIS data applied in this study included major forest types from eastern, central and western US, including Maine Forest (2003), Sierra National Forest in California (2008), mixed forests along Baltimore/Washington corridor (2003) and White River National Wildlife Refuge in Arkansas (2006). All these LVIS data were collected during leaf-on season.

We also included a 30 m resolution Landsat LAI map to examine the spatial distribution of GLAS LAI. Landsat has the longest earth observation history at moderate resolution (30 m), and for decades, it has provided a consistent and unique measurement of terrestrial ecosystems. The applied Landsat LAI map was produced at NASA AMES using Global Land Survey (GLS) 2005 orthorectified Landsat data based on the canopy spectral invariants theory (Ganguly et al. 2012).

5.2.4 Analysis

The comparison between LVIS and GLAS was performed at GLAS footprint level. LVIS shots falling within a 32.5 m radius from GLAS shot center were

selected. We excluded GLAS footprints with LVIS intersection numbers less than 3 to ensure the validity of comparison. Both LAI and the 5 m interval VFP of selected LVIS shots were averaged onto each coincident GLAS footprint for comparison. We also made a footprint level comparison between GLAS LAI and the Landsat LAI map. A 3×3 window was applied to each GLAS footprint center to extract the averaged Landsat LAI pixels. Pixels with invalid values (e.g. retrieval failure or non-vegetation pixel) were excluded in the comparison.

Next, we aggregated the footprint level GLAS data up to terrestrial ecoregions based on the WWF ecoregion map (Olson et al. 2001). Statistical analysis of total LAI and LAI strata (VFP aggregated at every 10 m height interval) was performed subsequently at each ecoregion. We also analyzed the GLAS LAI and VFP distribution across different environmental gradients throughout CONUS. Each GLAS footprint was classified according to different environmental factors, including vegetation type, topographic data and annual precipitation measurement. The vegetation map was derived from the MODIS Land Cover Type product (MCD12Q1) at 500 m resolution following the IGBP scheme (Friedl et al. 2010). Elevation data was extracted from the void-filled 90 m resolution SRTM (Shuttle Radar Topography Mission) DEM data (Reuter et al. 2007). Precipitation information originated from the 800 m resolution 30-yr annual normal precipitation data developed by the PRISM Climate Group (PRISM 2013). All these data were combined to footprint level LAI and VFP data based on the geolocation coordinates of GLA14.

5.3 Results

5.3.1 GLAS LAI and VFP Comparisons with LVIS and Landsat

The footprint level comparison between GLAS LAI and LVIS LAI level led to an overall r^2 of 0.60, bias of -0.23, and RMSE (Root Mean Square Error) of 0.82 (**Error! Reference source not found.**). Except for some outliers at the lower range of LAI, most of the comparison points were distributed along the 1:1 line suggesting no systematic difference between the two data sets. No significant bias was found across individual sites either. Overall, there was a good agreement between LVIS and GLAS derived LAI data.

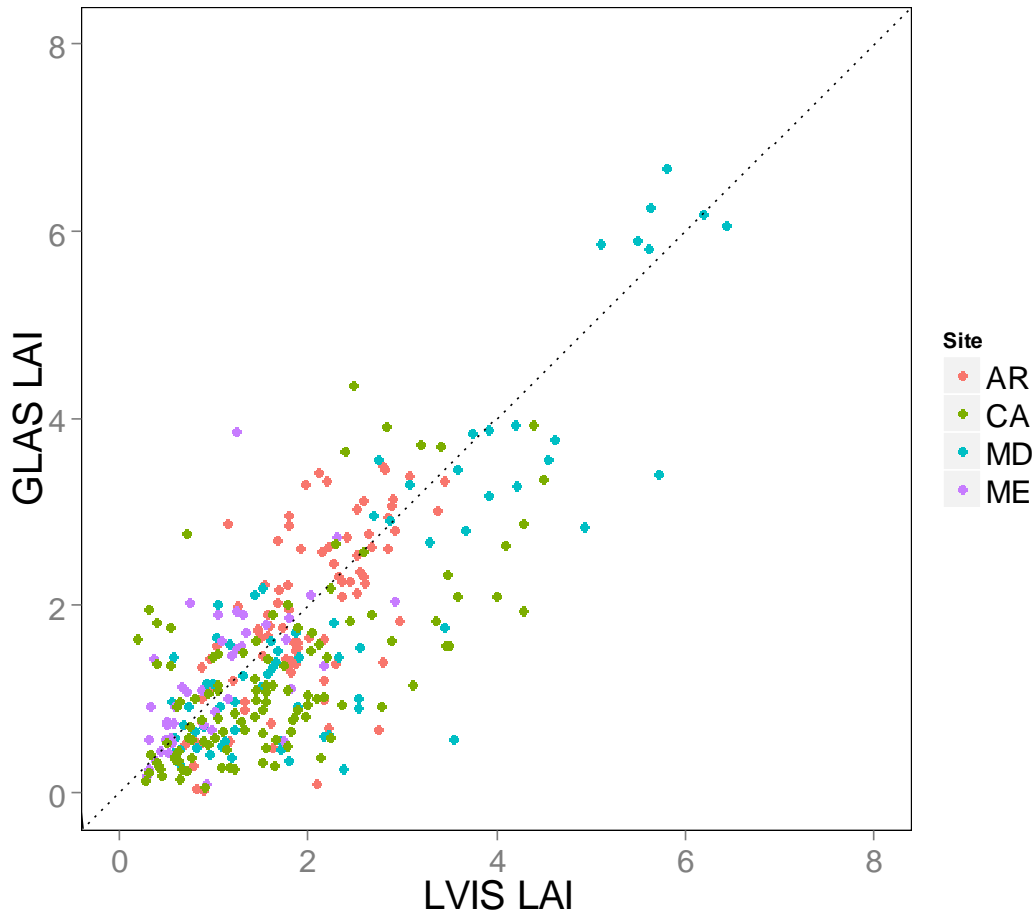


Fig. 5-1 Comparison between LVIS LAI and GLAS LAI at different sites across US (N = 318). Each point represents a comparison at GLAS footprint while different colors indicate different sites. The comparison result ($r^2 = 0.60$, bias = -0.23, and RMSE = 0.82) reveals a good agreement between the two data sets.

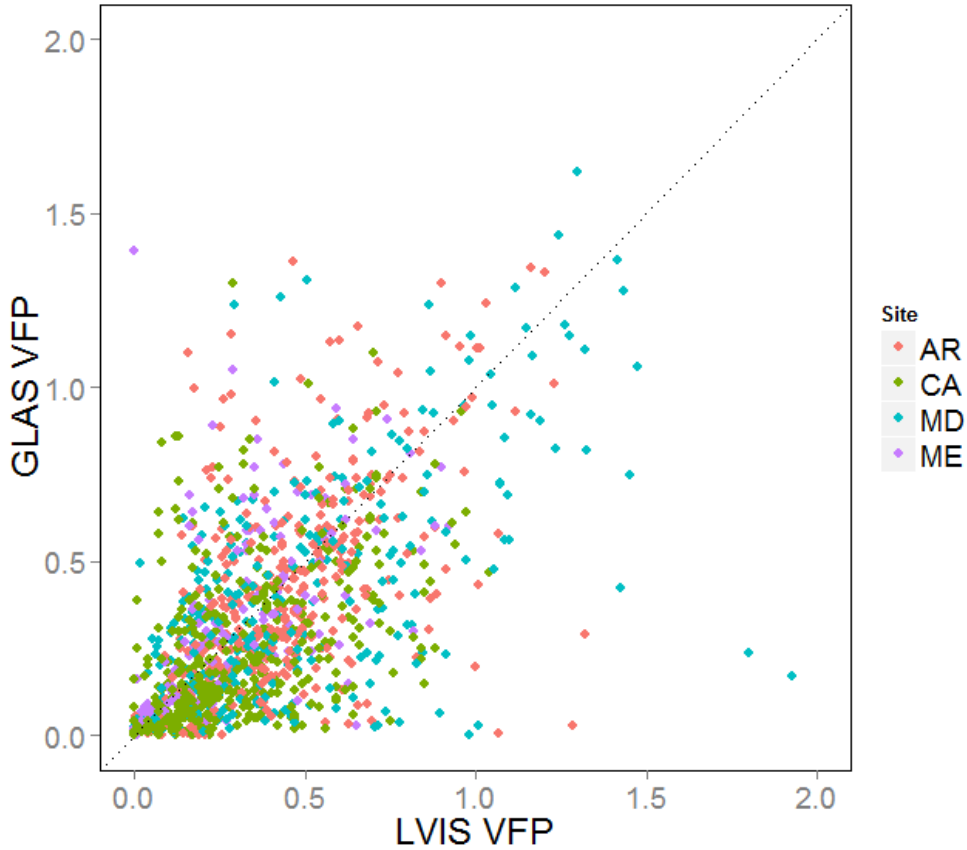


Fig. 5-2 Comparison between LVIS VFP and GLAS VFP integrated at 5 m height interval over different sites in CONUS (N = 1272). The comparison result ($r^2 = 0.36$, bias = -0.043, and RMSE = 0.26) has a relatively lower agreement than that of LAI.

The agreement of 5 m height interval VFP distribution between the two data sets was somehow lower than that of total LAI (Fig. 5-2). While most of the comparison points were distributed close to the 1:1 line, there were a few outliers well off the line. The comparison led to an r^2 of 0.36 with a bias of -0.04 and RMSE of 0.26. Although there was no systematic bias observed across all sites either,

however, it was found that GLAS had a slight overestimate of understory LAI against LVIS (Fig. 5-3). It was also found that agreements of VFP at different height levels varied: agreement between LVIS and GLAS was lowest in the understory part (0 - 5 m, $r^2 = 0.04$, bias = 0.09, RMSE = 0.31), and increased significantly towards the middle canopy layers (5 - 10 m, $r^2 = 0.33$, bias = -0.13, RMSE = 0.29; and 10 - 15 m, $r^2 = 0.53$, bias = -0.08, RMSE = 0.22), and reached the maximum and equivalent accuracy level of total LAI at upper-story (15 - 20 m, $r^2 = 0.66$, bias = -0.05, RMSE = 0.20).

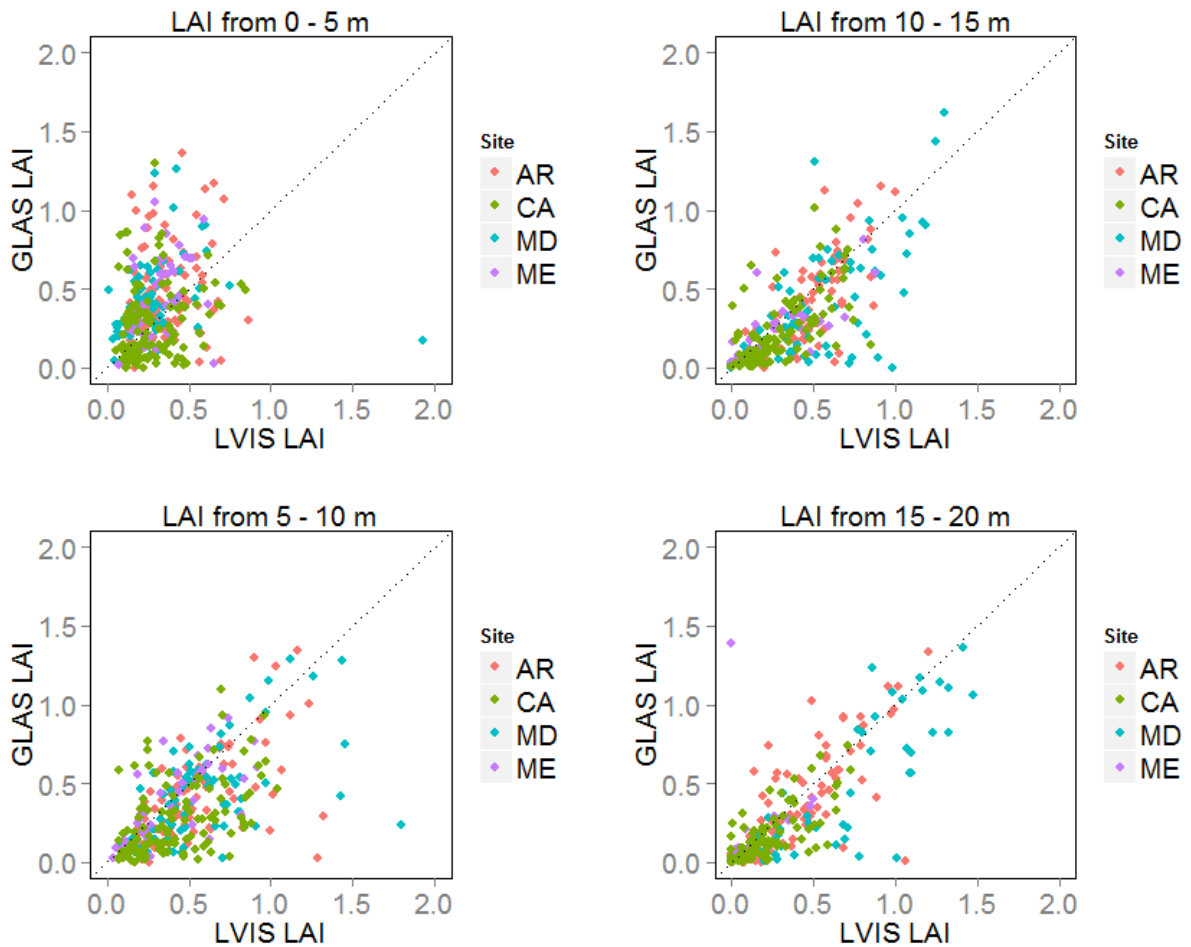


Fig. 5-3 Comparison between LVIS and GLAS LAI density integrated at every 5 m height interval. Their agreements increase as the height interval moving upward: 1) 0

- 5 m: $r^2 = 0.04$, bias = 0.09, RMSE = 0.31; 2) 5 - 10 m: $r^2 = 0.33$, bias = -0.13, RMSE = 0.29; 3) 10 - 15 m: $r^2 = 0.53$, bias = -0.08, RMSE = 0.22; 4) 15 - 20 m, $r^2 = 0.66$, bias = -0.05, RMSE = 0.20.

The comparison between Landsat LAI and GLAS LAI had a much lower agreement than that of LVIS with a r^2 of 0.18, bias of 0.18 and RMSE of 2.02 (Fig. 5-4). Even though the two data sets agreed well and exhibited the same distribution pattern at lower LAI values, Landsat overestimates LAI at the middle range (from 1 to 3) and then appeared to saturate above a threshold of 4 against GLAS data.

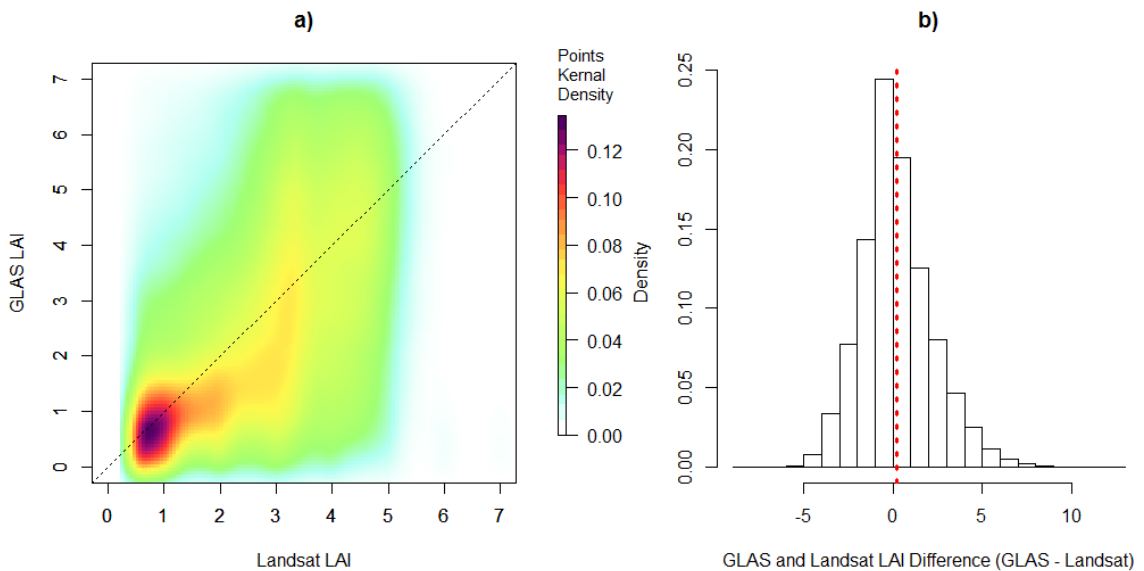


Fig. 5-4 Comparison between Landsat LAI and GLAS LAI over Contiguous US: a) density scatter plot of Landsat and GLAS LAI; b) histogram of LAI difference between Landsat and GLAS. Darker kernel density color refers to more clustered distribution of LAI pairs. Despite a low bias value of 0.18 (red dot-line in b), the comparison ($r^2= 0.18$, RMSE = 2.02) reveals a relatively low level agreement between the two data sets. In particular, Landsat appears to saturate at about LAI = 4 relative to GLAS.

5.3.2 Aggregated GLAS LAI and VFP at Ecoregions

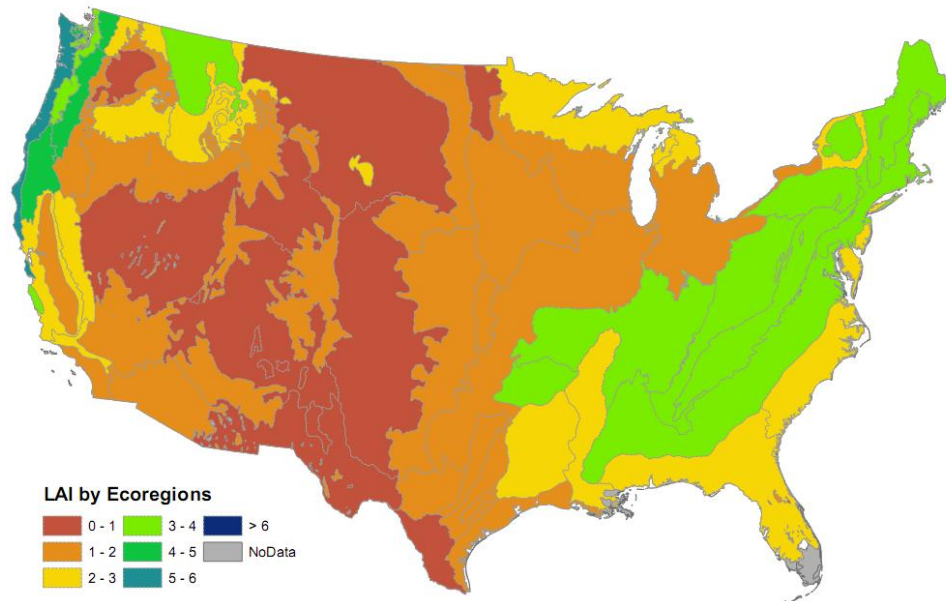


Fig. 5-5 GLAS LAI distributions by WWF ecoregions. LAI values decrease from eastern (or western) coast towards inner land.

Ecoregion-level GLAS LAI was mapped across CONUS and showed that GLAS LAI values decreased from both eastern and western coastal areas towards central plains (Fig. 5-5). Highest LAI values were found along northern Pacific Coast while lowest values occurred around Rocky Mountain areas and the majority of Nevada. In particular, Northern California coastal forests were found to have the highest mean LAI value of 5.24. In the east, Appalachian-Blue Ridge forests had the highest value of 3.95 while other ecoregions around north-south direction of Appalachian Mountains had similar LAI values around 3 ~ 4 (Table 1).

Table 5-1 Ecoregions with highest total LAI values

Ecoregions	Total LAI Mean(\pmSD)	LAI 0-10m Mean(\pmSD)	LAI 10-20m Mean(\pmSD)	LAI >20m Mean(\pmSD)
Northern California coastal forests	5.24 \pm 2.11	2.06 \pm 1.32	1.67 \pm 1.09	1.08 \pm 1.15
Central Pacific coastal forests	5.00 \pm 2.14	1.52 \pm 1.61	1.10 \pm 1.16	0.84 \pm 1.25
British Columbia mainland coastal forests	4.74 \pm 2.26	1.48 \pm 1.31	1.23 \pm 1.08	1.13 \pm 1.13
Central and Southern Cascades forests	4.31 \pm 2.34	1.06 \pm 1.35	0.79 \pm 1.02	0.64 \pm 1.07
Klamath-Siskiyou forests	4.31 \pm 2.31	1.26 \pm 1.30	0.99 \pm 1.07	0.73 \pm 0.99
Willamette Valley forests	3.99 \pm 2.24	0.73 \pm 1.09	0.60 \pm 0.89	0.75 \pm 1.31
Appalachian-Blue Ridge forests	3.95 \pm 2.03	1.04 \pm 1.27	0.82 \pm 0.99	0.47 \pm 0.82
Puget lowland forests	3.91 \pm 2.25	0.98 \pm 1.39	0.71 \pm 1.08	0.40 \pm 0.81
Appalachian mixed mesophytic forests	3.86 \pm 2.04	1.06 \pm 1.29	0.77 \pm 0.93	0.48 \pm 0.83
North Central Rockies forests	3.67 \pm 2.27	1.61 \pm 1.55	0.84 \pm 0.89	0.47 \pm 0.72

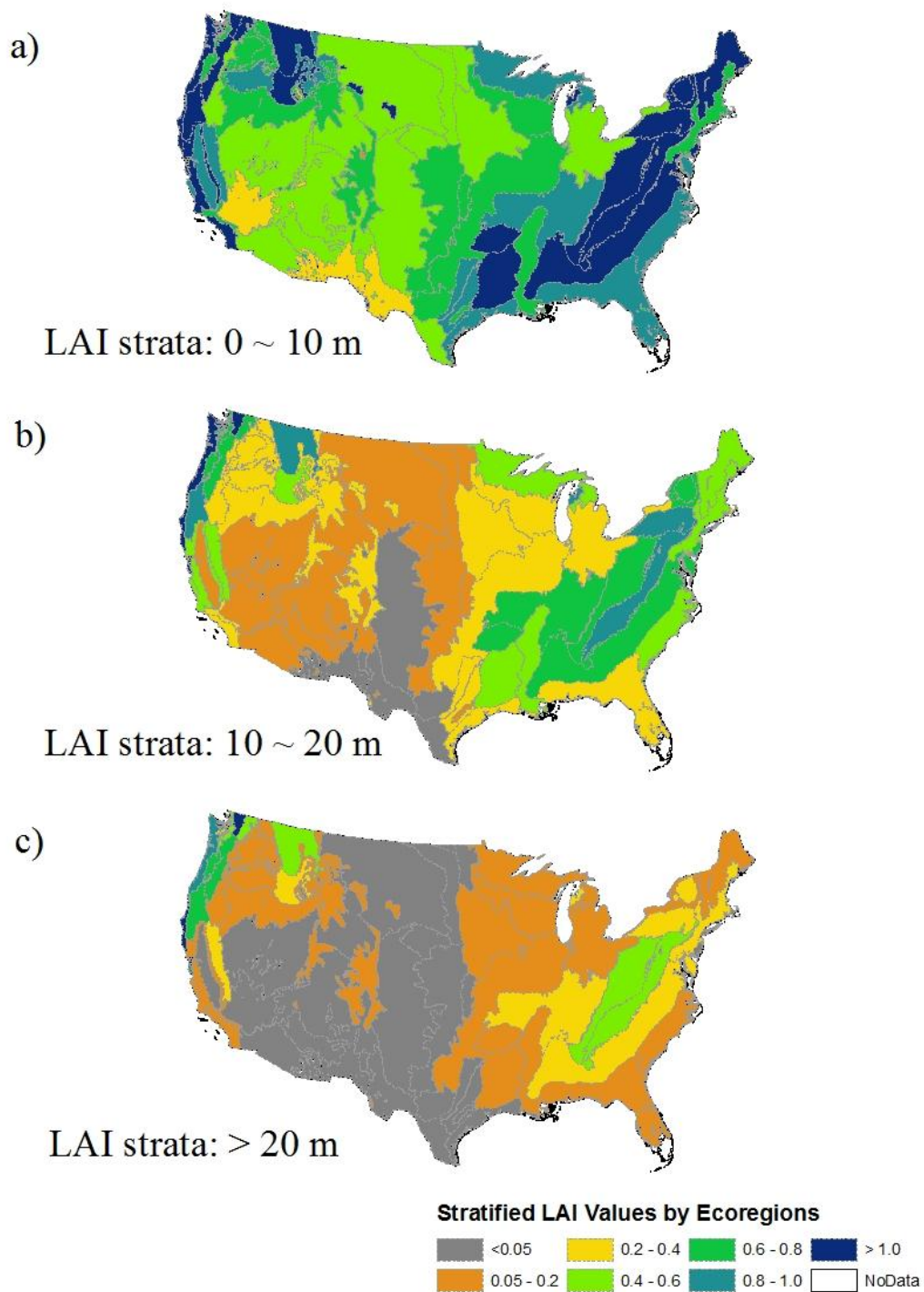


Fig. 5-6 LAI strata distributions by WWF ecoregions. Despite similar total LAI values, the southeastern forests show different LAI values at stratified height intervals.

LAI strata formed by VFP at each 10 m height interval were also averaged and mapped across CONUS at ecoregions (Fig. 5-6). Each strata exhibited similar spatial pattern as that of total LAI with the decreasing trend from coast to inner land, but the exact pattern of each LAI strata differed significantly. In general, northwestern forests were observed to have the highest total LAI values as well as LAI strata values. Northern California coastal forests exhibited the largest total LAI value as well as highest foliage density under 20 m height. However, British Columbia mainland coastal forests were found to exceed its foliage density in the upper canopy part (higher than 20 m).

The distribution of GLAS total LAI and profiles were examined across different land cover types (Fig. 5-7 and Fig. 5-8). Deciduous broadleaf forests had the highest value of total LAI (mean value = 4.03) as well as that of middle and upper LAI strata (height > 10 m). Open shrubland showed the lowest total LAI values of 0.77, followed by closed shrubland (mean value = 1.00). Vertical distribution of non-forest vegetation had highly similar pattern, where foliage density was concentrated near the ground. Their peak values increased following the order of open shrubland, closed shrubland, savanna and woody savanna. All forest types had consistently larger LAI values than those of non-forest types. In particular, evergreen broadleaf forest had the highest understory VFP values approaching 0.6 m²/m³ unit. Evergreen needleleaf, evergreen broadleaf, and deciduous needleleaf forests showed a similar foliage distribution pattern of non-forest vegetation. Deciduous broadleaf forest exhibited a slightly different canopy mode — most of leaves were distributed at

middle-story level with a peak height at about 8 m and VFP values did not decrease significantly until reaching a height of 15 m. Mixed forest showed somehow a combined pattern of deciduous broadleaf forests and the other types as we expected.

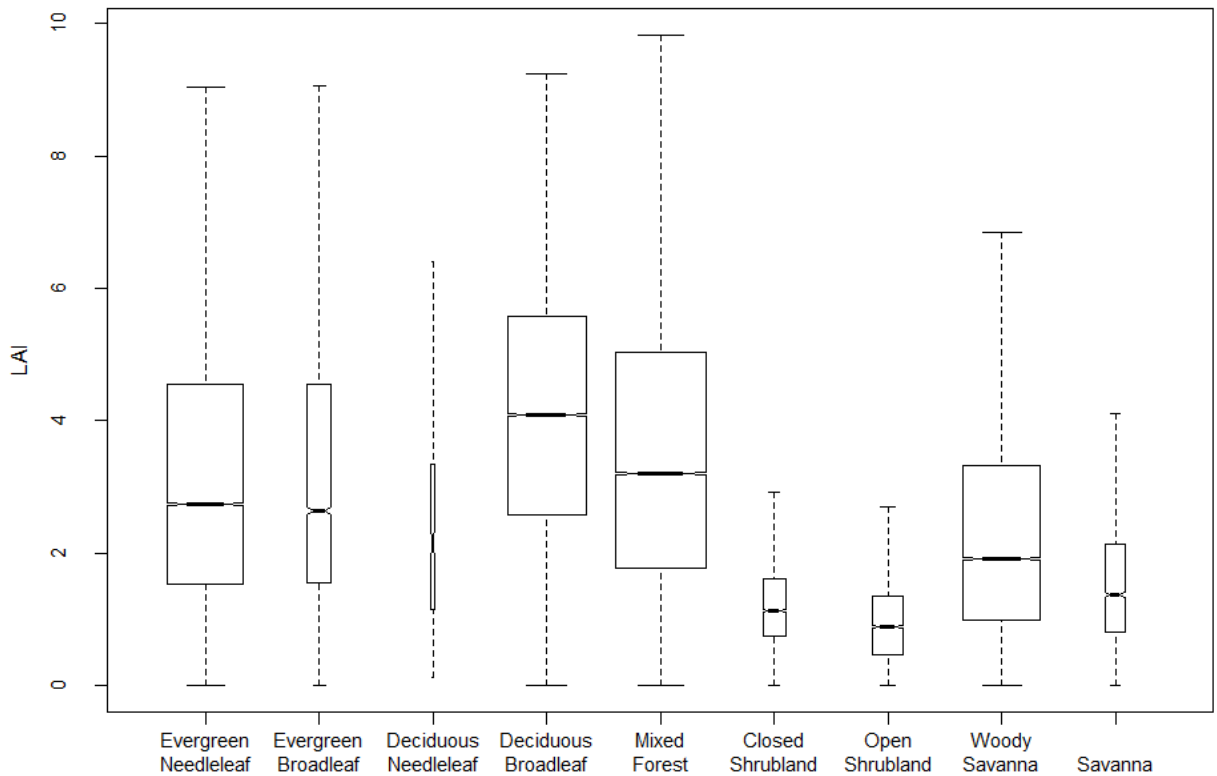


Fig. 5-7 Distribution of total LAI across different land cover types. The width of the boxes is proportional to the number of observations for each type. Notches show the 95% confidence interval of median values.

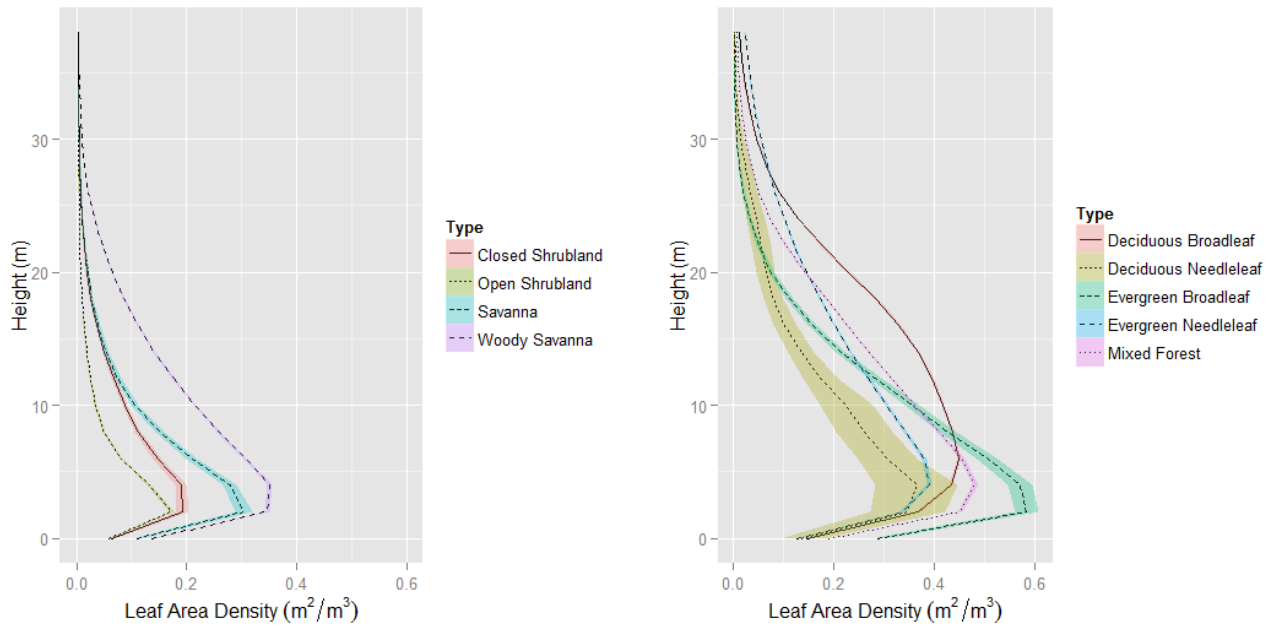


Fig. 5-8 Averaged GLAS VFP for different land cover types across US: non-forest vegetation types (left) and forest types (right). Mean values are central lines within the color-filled 95% CI envelope.

5.3.3 GLAS LAI Distributions by Environmental Factors

A linear regression analysis between GLAS LAI and SRTM DEM showed that increasing altitude would lead to an overall reduction in LAI values ($r^2 = 0.59$, $P < 0.01$). However, we found that GLAS LAI did not exactly follow the decreasing trend with elevated topography (Fig. 5-9). GLAS LAI values increased with DEM at the elevation range from 0 to 750 m and 2000 to 3000 m. The variation in LAI-DEM relationship agreed well ($r^2 = 0.45$, $P < 0.01$) with forest ratio of GLAS footprints, defined as the percentage of footprints classified as forests in total GLAS shots (forests and non-forest). A multiple linear regression analysis indicated the about 87% of total variance could be explained by a simple combination of elevation groups and forest ratio values:

$$\text{LAI} = 2.59 \times \text{Forest Ratio} - 0.595 \times \text{Elevation (km)} + 1.58$$

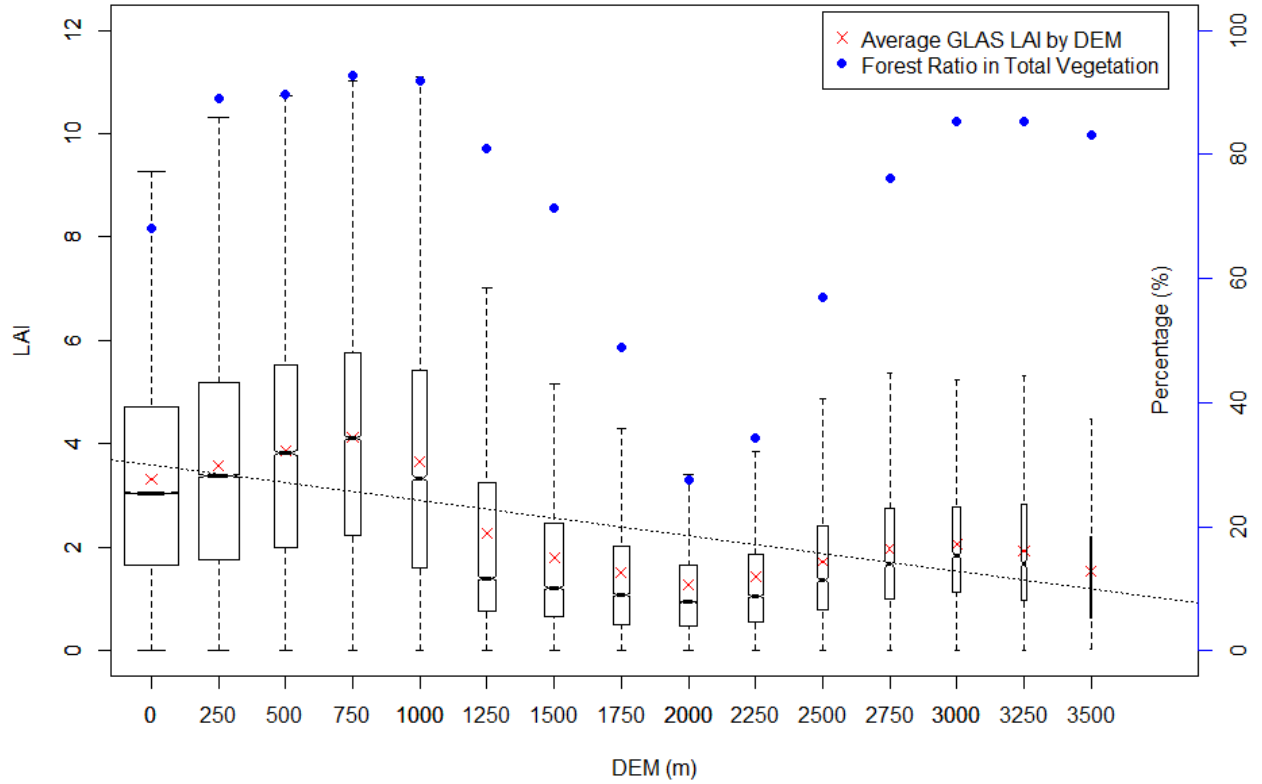


Fig. 5-9 Distribution of GLAS LAI and forest ratio (GLAS shots over forest divided by total shot numbers) as a function of elevation stratification groups. Overall, there is a decreasing trend of LAI values as elevation increases ($r^2 = 0.59$, $adj\text{-}r^2 = 0.56$, $P < 0.01$) despite an observed variation. Such variation pattern of total LAI coincides with the distribution of forest ratio at elevation groups ($r^2 = 0.45$, $adj\text{-}r^2 = 0.40$, $P < 0.01$).

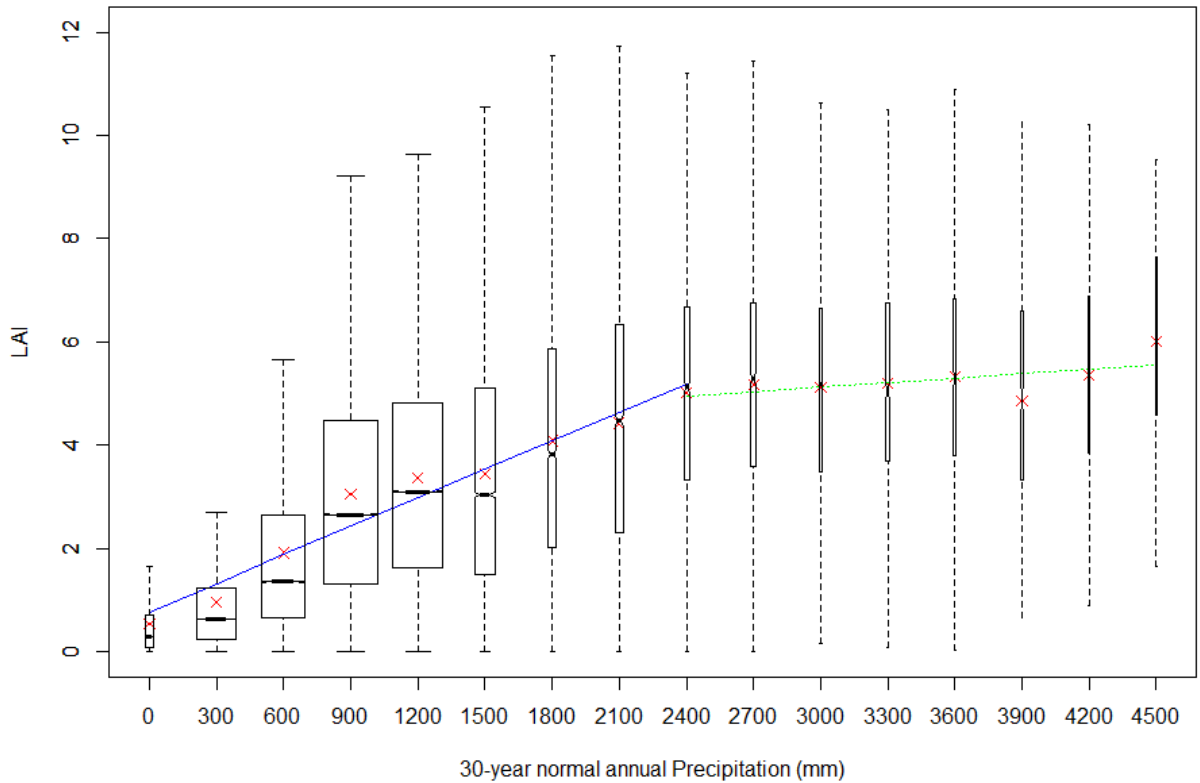


Fig. 5-10 Distribution of GLAS LAI as a function of precipitation stratification groups. A linear regression analysis of LAI values averaged by precipitation groups shows a very significant increasing trend (1.84 unit per 1000 mm, $r^2 = 0.96$, $adj-r^2 = 0.95$, $P < 0.001$) at areas with annual precipitation less than 2400 mm but almost no increase above that.

We also stratified and analyzed GLAS LAI by 30-year normal annual precipitation data using linear regression models (Fig. 5-10). It was observed that increasing precipitation significantly increased LAI values ($\Delta LAI = 1.84$ per 1000 mm precipitation increase) but only at low precipitation levels (< 2400 mm). It contributed little when exceeding that threshold, as we found no significant LAI increase among groups greater than 2400 mm using a bonferroni adjusted t-test.

$$LAI = 1.84 \times \text{precipitation (mm)} \times 1e-3 + 0.774 \quad (r^2 = 0.96, adj-r^2 = 0.95)$$

An example of combined environmental effects on distribution of LAI and VFP in northwestern US was shown in Fig. 5-11. Three parallel GLAS transects were selected from Western Cascade, Eastern Cascade and northern Rocky Mountain forests with averaged LAI values of 4.90, 2.75 and 3.99. Western Cascade forests exhibited the highest stands density followed by northern Rocky Mountain forests. Western Cascade forests had a variety of foliage density distribution patterns, while those in northern Rocky Mountain forests were mostly similar with foliage density peak concentrated close to the ground. For the three transects, the average precipitation values were 2360, 980, and 970 mm and the average elevation values were 570, 1080 and 1340 m respectively. The highest LAI forests, Western Cascade forests, had the lowest elevation and highest precipitation values. Northern Rocky Mountain forests, despite a lower precipitation and higher elevation value, were found to have a higher LAI value compared with Eastern Cascade forests.

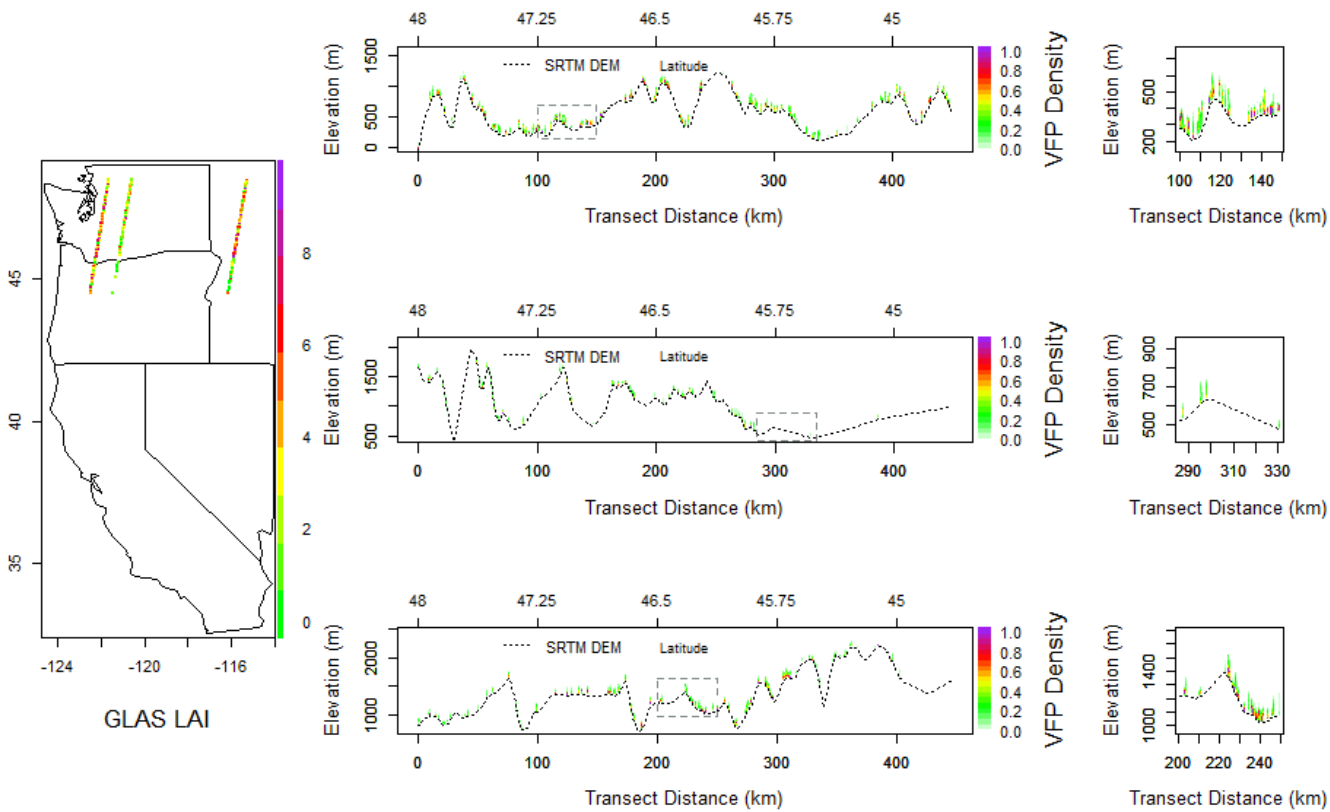


Fig. 5-11 Example of a combined environmental effect on GLAS total LAI and VFP. GLAS transects selected from Western Cascade, Eastern Cascade and northern Rocky Mountain areas have averaged LAI values of 4.90, 2.75 and 3.99. Heights in the second and third rows are multiplied by 10 to show foliage distribution within canopy.

5.4 Discussion

In this study we did not include any field data in recognition of two major difficulties in the direct footprint level comparison between GLAS and field data: 1) there was hardly any coincidence between the two, and 2) most field work did not measure VFP. Instead we adapted a bottom-up validation approach and chose those highly accurate LAI and VFP maps derived from various airborne systems as an alternative validation tool (Morissette et al. 2006; Tang et al. 2014a). LVIS is such a

good example for validation purposes which has demonstrated its excellence in LAI and VFP estimates as examined by destructively-sampled data in a dense tropical rainforest (Tang et al. 2012). Examination from LVIS at different forest types across CONUS shows that GLAS generally provides accurate LAI and VFP estimates at footprint level. Consider the temporal and spatial allocation differences between LVIS and GLAS, their overall agreements on LAI and VFP are reasonable ($r^2 = 0.60$, bias = -0.23, and RMSE = 0.82; and $r^2 = 0.36$, bias = -0.043, and RMSE = 0.26). We find no significant or systematic estimate bias across all LVIS campaigns. Comparison results further demonstrate the efficacy of our retrieval method at a much boarder scale, regardless of the variation of forest types and environmental factors.

Although the overall measurement of GLAS VFP was accurate, we found its VFP measurement accuracy appeared to decrease when penetrating down to the understory part. The r^2 decreased from a peak value of 0.66 at upper-story (15 - 20 m) to 0.33 at middle-story (5 - 10 m), and bottomed at understory with a value of 0.04 (0 - 5m). There could be multiple factors contributing to such trends. First, a slope effect could greatly reduce the LAI measurement accuracy of GLAS (Tang et al. 2014a). Despite efforts from different methods, this effect can still not be fully mitigated especially over steep slopes, and would consequently introduce errors and uncertainties into VFP estimates as well. Additionally, topographical effects can lead to the misalignment of VFP between LVIS and GLAS. GLAS measures the terrestrial surface at a much larger footprint with higher topographical variations, and a direct average of LVIS VFP can possibly result in a mismatch of vertical foliage distribution up to several meters. A vertical integration of VFP at longer height

interval could partially mitigate such effect but not fully, and this explains the higher agreement in total LAI comparison. Moreover, measurement of near-ground understory vegetation is approaching the observation limits of GLAS data. By default GLAS waveforms are processed by a Gaussian decomposition method to get an approximate fit comprised of a series of Gaussian functions where the last one usually represents the ground (Hofton et al. 2000). The upper tail of ground Gaussian peak could be mixed with signals from lower understory, and it is almost impossible to separate them given the specification of GLAS pulse width and scanning frequency. All these factors, plus the nature of high complexity and heterogeneity in canopy understory, lead to the lower agreement on understory VFP between LVIS and GLAS.

Comparison between GLAS and Landsat displayed a much lower agreement than that of LVIS. The r^2 (0.18) was lower with a much larger RMSE (1.99) and a higher bias (0.33). We also observed a saturation trend of Landsat LAI relative to GLAS when exceeding a value around 4. On the low end of LAI spectrum, GLAS was found to have underestimated values against Landsat. It is because GLAS may not be able to adequately capture LAI values of short grassland with no discernible vertical structure, whereas Landsat could measure both tree and grass LAI based on their total spectral response. This difference would lead to an underestimated observation of GLAS LAI at low canopy cover levels. There are also other factors leading to their difference in LAI estimates such as sensor design (active vs. passive), observation scale (65 m vs. 30 m) and misclassifications of land cover types. But the overall low bias value still suggests a possible data fusion strategy between GLAS

and Landsat on forests with LAI less than 4.

Analysis of GLAS LAI and VFP across ecoregions displayed a reasonable geographical distribution and similar pattern when compared with existing LAI product (Deng et al. 2006; Myneni et al. 2002). More importantly, the LAI strata maps exhibited vertical canopy stratification of US terrestrial ecosystems for the first time. With these data it is possible to track not only the horizontal distribution of canopy structure but its vertical variations as well. In specific, one could identify the foliage concentration at understory, middle-story or up-story part at either fine resolution or ecoregions (Fig. 5-5, Fig. 5-6 and Table 1). Such large scale VFP data could possibly be the clue leading to stories hidden by the "Big-leaf" model, and would be a huge contribution towards continental scale ecological and biological studies of forest structure and dynamics.

LAI and VFP also varied across different landscapes represented by various land cover types. For example, we found both total LAI and maximum value of foliage density peaks significantly increase following the gradient of shrubland, savanna, woody savanna towards forests (Fig. 5-7 and Fig. 5-8). In particular, we found deciduous broadleaf forest showing a different pattern with its foliage more evenly distributed in understory and middle-story when compared with all other forests. Our results not only confirm the existence of canopy layers in concept, but more importantly, highlight the feasibility of quantifying those layers across landscapes. Once further developed and validated, these data would provide full 3-dimensional measurement of terrestrial ecosystems and help update our knowledge about spatial distribution of vegetation structure over different forest species and

types. Such new knowledge would then be possibly adapted to help refine current empirical assumptions about vegetation structure of different land cover types in current LAI inversion algorithm (e.g. MODIS).

Different environmental factors were found to have a significant impact on LAI at different levels. For example, we found an increase of 1 km in elevation would generally cause a decrease of about 0.5 unit in GLAS LAI ($r^2 = 0.59$, $P < 0.01$) (Fig. 5-9). This decreasing trend is consistent with previous studies across different scales (Luo et al. 2004; Moser et al. 2007; Pfeifer et al. 2012). The variation of the overall trend could be largely explained by the vegetation type composition along the elevation gradient. A simple classification of GLAS shots between forest and non-forest vegetation explained about 50% of the variation. A combination of the two factors (elevation groups and forest ratio) explained almost 90% variance of average LAI distribution. We also found a significant but nonlinear relationship between GLAS LAI and annual precipitation (Fig. 5-10). At relatively drier areas (annual precipitation $< \sim 2000$ mm), an increase of 1000 mm in annual precipitation would lead to a significant LAI increase of about 1.84 unit ($r^2 = 0.96$, $P < 0.001$). The increasing trend diminished when annual precipitation reached a value of about 2400 mm. This non-linear relationship agrees well with previous studies in the tropics (Pfeifer et al. 2014; Spracklen et al. 2012). Examples in Fig. 5-11 showed a combined environmental effect of elevation and precipitation on distributions of LAI values.

As a direct quantification of 3-D foliage distribution, GLAS LAI profiles are so far the best representations of terrestrial ecosystem structure over broad geographical areas. Further ecological applications of these profiles could be

important. First, they could refine current large-scale measurements of plant respiration and photosynthesis and consequently help identify the "missing carbon"(Houghton 2007). Previous studies reported a potential 50% underestimate of GPP values with no consideration of vertical foliage stratification (Kotchenova et al. 2004; Sprintsin et al. 2012). A successful integration strategy may reduce current carbon uncertainty in biospheres. This could be achieved by either improving initialization of ecological models (Hurtt et al. 2004), or establishing the relationship with Gross Primary Production (GPP) in together with passive remote sensing data (Turner et al. 2006). Second, these profiles could also help describe species richness and habitat heterogeneity in biodiversity studies. Many studies have confirmed the general relationship between species richness, habitat heterogeneity and forest structural complexity across different landscapes (Ferber et al. 2014; Goetz et al. 2010; Schut et al. 2014; Swatantran et al. 2012). The inclusion of LAI profiles provides spatially explicit vegetation structure data and may potentially improve current observations of species distribution at continental scale, such as the North American Breeding Bird Survey (Culbert et al. 2013; Sauer et al. 2008).

5.5 Conclusion

Lidar technology allows 3-D observations of forest structure but most of relevant studies only focus on regional or landscape scale. In this study we presented a demonstration of GLAS LAI and VFP product over Contiguous United States. This product shows reasonable footprint-level agreement with existing airborne lidar LAI and VFP data sets except for lower understory across different landscapes. The

comparison with 30 m Landsat data highlights the potential limits of passive optical remote sensing but also the power of fusion approaches. The derived GLAS LAI and VFP product may improve current climate and ecological models through more accurate parameterization of canopy structure. A similar but global-scale data set, once available, will be of a great interest in help better understanding of terrestrial ecosystem dynamics and global biodiversity hotspots.

Chapter 6 Conclusion

This dissertation aimed at developing approaches to retrieve leaf area index and its vertical stratification through canopy using waveform lidar. My research demonstrated the accuracy of lidar on LAI measurements over dense canopy cover forests when compared with passive optical methods. The methods for deriving LAI and VFP developed in this dissertation are innovative and the products are among the best available representations of these attributes at continental scale, across the US. Methods developed in this study are not site-specific and are applicable in future lidar missions (e.g. ICESat-2 and GEDI) with a potential measurement of global LAI and VFP within every 500 m cell.

The main findings of this dissertation are chapter specific and have been summarized in a compilation of different themes as follows. First, my research demonstrated a novel pathway of measuring LAI profiles directly without building statistical relationships between field-based LAI data and sensor signals. This was one of the few attempts to derive LAI and VFP from lidar data based on a Geometric Optical and Radiative Transfer (GORT) model retrieval rather than through empirical methods. I applied the GORT model to produce LAI and VFP directly from airborne lidar (LVIS) waveforms in Chapter 2 and Chapter 3. I also derived LAI and VFP from spaceborne GLAS data based on the same model in Chapter 3 to Chapter 5. These applications suggested that the relationship between vertical foliage distribution and lidar signals were not site-specific but universally applicable across vegetation types and lidar platforms.

Secondly, lidar based estimates of LAI and VFP were highly accurate when compared with different field measurements. By comparing modeled results with destructively sampled LAI measurements, I showed that large footprint waveform lidar can provide accurate estimates of LAI and vertical foliage stratification in a tropical rainforest, even under conditions of high canopy cover (> 95%). This finding was significant and proved that lidar based estimates do not saturate even when LAI values reaching a unit of 10, a range far exceeding current observation limits (around 6 unit) of passive remote sensing. I also discovered good measuring agreements between LVIS and other widely accepted methods including hemispherical photo, LAI-2000 and terrestrial scanning lidar.

Thirdly, identifications and corrections of spatial difference were of great importance in the validation process of lidar derived LAI and VFP. In Chapter 2, I found an improved agreement between LVIS and field LAI measurements after a scale adjustment. I also found a significant improvement after filtering LVIS footprints with center non-coincident to tower centers. In Chapter 3, I bridged the spatial mismatch between field and spaceborne measurements using LAI maps from airborne lidar. In Chapter 6, this multiple scale approach played an important role in validating GLAS LAI and VFP product across US given the sparse spatial allocation of GLAS footprints. My research suggests the ever-increasing number of regional airborne lidar campaigns should be integrated to build a national validation network for continental scale products of spaceborne lidar.

In addition, the slope effect of large footprint lidar can be partially corrected in LAI retrievals. My initial experiments showed that algorithms developed for

medium footprint airborne lidar could not be directly applied to GLAS data as there were large errors during the execution. This was mainly because the LVIS algorithm failed to correctly separate vegetation information from the ground energy in the presence of complex topography. I therefore developed a recursive analysis method to facilitate the separation and found significant improvements in the results. Despite these improvements, the recursive methods could not fully mitigate the slope effect produced LAI with lower accuracy confidence over large slope areas with high heterogeneous vegetation distribution especially. I found an optimal slope threshold of about 20° for highest LAI retrieval quality, below which this r^2 and RMSE values were comparable to those seen between LVIS and the ground-based measurements.

Lastly, spaceborne lidar systems can well characterize horizontal and vertical canopy structure across broad geographical areas. Implementation of GORT model and recursive method led to the production of GLAS LAI and VFP over Contiguous US. Comparisons between GLAS and LVIS over different forest types suggested GLAS was able to provide accurate near continental scale measurements of both total LAI and vertical canopy stratification as well. The derived GLAS LAI and VFP product provided a first ever overview of both horizontal and vertical canopy structure distribution of North American ecosystems, and thereby set up a quantitative baseline for future monitoring.

Despite the general success, limitations still exist, and there are three problems that need further work. The first is the topographic or slope effect. All results indicate that LAI can be accurately derived from GLAS data but only under desirable topographic conditions, namely with a slope of 20° or less. Existence of

high slopes can significantly decrease data quality and lower the confidence of retrieval accuracy when coupled with low incident laser energy, multiple scattering effect and geolocation error. It is more evident for larger footprint size lidar (GLAS in this case) considering the fact that complexity and heterogeneity of both topography and canopy structure increase significantly with enlarged scale. Although efforts have been made to mitigate such effect, it cannot be eradicated completely. A possible remedy relies on calibrations from external data sources, including DEMs from SRTM or Tandem-X. Prior knowledge of topographic information would be of huge help in modeling and correcting slope effect on individual waveform and hence can improve the accuracy of LAI and VFP estimates. Fortunately, future spaceborne lidar missions may be less affected by slope effect in ecosystem observations. The ATLAS sensor on board of ICESat-2 mission is a new generation photon-counting lidar system, which will collect photons at each 10 m radius footprint with an increment of 70 cm along track. The GEDI instrument will collect waveforms at diameter of only 15 - 20 m, similar to LVIS. More accurate LAI and VFP products can be expected with a minimized slope effect from these future lidar datasets.

The second problem is because of the interchangeable use of terms of LAI and Plant Area Index (PAI) in lidar observation. Strictly speaking, products derived from lidar waveform are actually PAI rather than LAI. The term of LAI is still preferred for several reasons: 1) the difference between LAI and PAI is small. Our study in La Selva with destructive sampled field data indicates that LAI covers 93% of total PAI with only 7% coming from stems and trunks in vertical projection. 2) Most of the reflected energy towards the sensor comes from the leaves for downward looking

lidar systems (including both airborne and spaceborne). Results from Monte Carlo Simulation (Hancock et al. 2012) have shown when seeing the canopy from the top, the viewed leaf area will be much larger than woody components. 3) Our long-term goal aims to apply these data onto initializations of ecosystem models, and "LAI" is the term commonly used by the ecological and remote sensing community. The passive optical products from Landsat or MODIS are also referred to as "LAI even though they include branches. There is no real difference between the lidar nadir observation and observation of LAI with the sun in the hotspot on these systems. At some point, we need to reconsider the definition and use of PAI and LAI and better understand the differences of products derived from active and passive remote sensing at a more fundamental theoretical level.

Lastly, GLAS cannot directly provide a spatially continuous observation of forests. Unlike traditional passive remote sensing, spaceborne lidar systems sample the Earth in transects formed by a series of individual waveform footprints. It is fundamentally impossible for GLAS to provide a wall-to-wall observation, and greatly limits its broader ecological application particularly at landscape scale. A common solution to this problem relies on the extrapolation of footprint level lidar data in together with other remote sensing images, such as MODIS or Landsat. It basically applies machine learning algorithm to train spectral bands data with lidar observations and then to predict the rest areas. There have been several global and continental scale canopy height and aboveground biomass maps produced using this method (Baccini et al. 2012; Lefsky 2010; Simard et al. 2011). Another solution is based on sampling theory and spatial statistics. It is essentially an aggregation

strategy of upscaling footprint observations into tessellations with no spatial overlaps or gaps (Healey et al. 2012). A more promising method is to the fusion between lidar and InSAR data. Lidar and InSAR are both equipped with 3D observation capability and provide independent measurements of vertical canopy structure. Canopy height measurements from lidar data are mostly accurate and straightforward, and will be applied in calibrating InSAR estimates to obtain a broader observation scale. This technique has not yet been fully understood but its potential application is huge, given the overlapping timeline of future lidar and SAR missions deployed by NASA and ESA.

Ultimately, what will greatly improve current climate and ecological models is the most realistic parameterization of foliage profile and leaf area distribution. This would require spatially continuous global estimates of LAI and VFP. Such products will also help achieve a better understanding of energy and mass exchange at the boundary layer between biosphere and atmosphere. Developing these maps would be a next step in this research. Deriving LAI and VFP at large scales using lidar is relatively new compared to efforts with passive remote sensing data. Despite encouraging results, progress has been limited because of the lack of continental/global lidar data and lack of efficient processing algorithms. This dissertation is among the pioneering efforts in deriving and validating large scale LAI and VFP from spaceborne lidar missions, both theoretically and practically. Applications of the study are not limited to GLAS products but also allow the generation and validation of products from future lidar missions such as ICESat-2 and GEDI. A full collection of these LAI products, once available and validated

appropriately, will be of a great importance in deepening our understanding of forest dynamics and better quantifying the magnitude of terrestrial carbon stock and flux. I hope that my research has provided useful algorithms and approaches towards this goal

Appendices

Supplementary Table 1 p-values of pairwise T-test on total GLAS LAI by elevation

<i>Elevation</i>	<i>0</i>	<i>250</i>	<i>500</i>	<i>750</i>	<i>1000</i>	<i>1250</i>	<i>1500</i>
250	0	-	-	-	-	-	-
500	0	1	-	-	-	-	-
750	0	1	1	-	-	-	-
1000	0	0.05	0.06	1	-	-	-
1250	<1e-9	<1e-9	<1e-9	<1e-9	0	-	-
1500	<1e-9	<1e-9	<1e-9	<1e-9	<1e-9	0	-
1750	<1e-9	<1e-9	<1e-9	<1e-9	<1e-9	0	0.003
2000	<1e-9	<1e-9	<1e-9	<1e-9	<1e-9	0	0.675
2250	<1e-9	<1e-9	<1e-9	<1e-9	<1e-9	0	0
2500	<1e-9	<1e-9	<1e-9	<1e-9	<1e-9	0	0
2750	<1e-9	<1e-9	<1e-9	<1e-9	<1e-9	0	0.001
3000	0	0	0	0	0	0.022	0.533
3250	0	0.002	0.001	0.005	0.013	0.961	1

*Continue of Supplementary Table 1

<i>Elevation</i>	<i>1750</i>	<i>2000</i>	<i>2250</i>	<i>2500</i>	<i>2750</i>	<i>3000</i>
250	-	-	-	-	-	-
500	-	-	-	-	-	-
750	-	-	-	-	-	-
1000	-	-	-	-	-	-
1250	-	-	-	-	-	-
1500	-	-	-	-	-	-
1750	-	-	-	-	-	-
2000	1	-	-	-	-	-
2250	0.101	0.035	-	-	-	-
2500	0.199	0.069	1	-	-	-
2750	0.696	0.289	1	1	-	-
3000	1	1	1	1	1	-
3250	1	1	1	1	1	1

Supplementary Table 2 p-values of pairwise T-test on total GLAS LAI by land cover types

	<i>ENF</i>	<i>EBF</i>	<i>DNF</i>	<i>DBF</i>	<i>Mixed forest</i>	<i>Closed shrubland</i>	<i>Open shrubland</i>	<i>Woody savanna</i>
EBF	1.0	-	-	-	-	-	-	-
DNF	0.0	0.032	-	-	-	-	-	-
DBF	0.176	1.0	1.0	-	-	-	-	-
Mixed forest	<1e-3	1.0	0.0	0.031	-	-	-	-
Closed shrubland	<1e-9	0.013	1.0	1.0	<1e-9	-	-	-
Open Shrubland	<1e-9	<1e-3	1.0	1.0	<1e-9	1.0	-	-
Woody savanna	<1e-9	0.040	1.0	1.0	<1e-9	1.0	0.0	-
Savanna	<1e-9	0.002	1.0	1.0	<1e-9	1.0	1.0	0.0

Supplementary Table 3 p-values of pairwise T-test on GLAS LAI strata by land cover types

0-5m	<i>ENF</i>	<i>EBF</i>	<i>DNF</i>	<i>DBF</i>	<i>Mixed forest</i>	<i>Closed shrubland</i>	<i>Open shrubland</i>	<i>Woody savanna</i>
EBF	1.0	-	-	-	-	-	-	-
DNF	0.001	0.027	-	-	-	-	-	-
DBF	1.0	1.0	1.0	-	-	-	-	-
Mixed forest	<u>1.0</u>	1.0	0.0	1.0	-	-	-	-
Closed shrubland	0.0	0.154	1.0	1.0	0.0	-	-	-

Open shrubland	<1e-9	0.018	1.0	1.0	0.0	1.0	-	-
Woody savanna	<1e-9	0.328	1.0	1.0	0.0	1.0	0.0	-
Savanna	<1e-9	0.028	1.0	1.0	0.0	1.0	1.0	0.0
5-10m	ENF	EBF	DNF	DBF	Mixed forest	Closed shrubland	Open shrubland	Woody savanna
EBF	1.0	-	-	-	-	-	-	-
DNF	0.0	0.163	-	-	-	-	-	-
DBF	1.0	1.0	1.0	-	-	-	-	-
Mixed forest	<u>0.107</u>	1.0	0.0	0.420	-	-	-	-
Closed shrubland	<1e-9	0.188	1.0	1.0	0.0	-	-	-
Open shrubland	<1e-9	0.011	1.0	1.0	0.0	1.0	-	-
Woody savanna	<1e-9	1.0	1.0	1.0	0.0	0.590	0.0	-
Savanna	<1e-9	0.132	1.0	1.0	0.0	1.0	0.039	0.0
10-20m	ENF	EBF	DNF	DBF	Mixed forest	Closed shrubland	Open shrubland	Woody savanna
EBF	0.952	-	-	-	-	-	-	-
DNF	0.0	1.0	-	-	-	-	-	-
DBF	0.308	1.0	1.0	-	-	-	-	-
Mixed forest	<u>0.003</u>	0.119	0.0	0.076	-	-	-	-
Closed shrubland	<1e-9	1.0	1.0	1.0	0.0	-	-	-
Open shrubland	<1e-9	0.363	1.0	1.0	0.0	1.0	-	-
Woody savanna	<1e-9	1.0	1.0	1.0	0.0	1.0	0.0	-
Savanna	<1e-9	0.647	1.0	1.0	0.0	1.0	1.0	0.0
> 20m	ENF	EBF	DNF	DBF	Mixed forest	Closed shrubland	Open shrubland	Woody savanna
EBF	1.0	-	-	-	-	-	-	-
DNF	0.005	1.0	-	-	-	-	-	-
DBF	1.0	1.0	1.0	-	-	-	-	-
Mixed forest	<u>0.0</u>	0.896	0.0	0.332	-	-	-	-
Closed shrubland	<1e-9	1.0	1.0	1.0	0.0	-	-	-
Open shrubland	<1e-9	1.0	1.0	1.0	0.0	1.0	-	-
Woody savanna	<1e-9	1.0	1.0	1.0	0.0	1.0	0.229	-
Savanna	<1e-9	1.0	1.0	1.0	0.0	1.0	1.0	0.032

ENF: Evergreen Needleleaf Forest

EBF: Evergreen Broadleaf Forest

DNF: Deciduous Broadleaf Forest

DBF: Deciduous Broadleaf Forest

Bibliography

Abdalati, W., Zwally, H.J., Bindschadler, R., Csatho, B., Farrell, S.L., Fricker, H.A., Harding, D., Kwok, R., Lefsky, M., Markus, T., Marshak, A., Neumann, T., Palm, S., Schutz, B., Smith, B., Spinhirne, J., & Webb, C. (2009). The ICESat-2 Laser Altimetry Mission. *Proceedings of the IEEE*, 98, 735-751

Aber, J.D. (1979). Foliage-Height Profiles and Succession in Northern Hardwood Forests. *Ecology*, 60, 18-23

Abshire, J.B., Sun, X., Riris, H., Sirota, J.M., McGarry, J.F., Palm, S., Yi, D., & Liiva, P. (2005). Geoscience Laser Altimeter System (GLAS) on the ICESat Mission: On-orbit measurement performance. *Geophysical Research Letters*, 32

Abuelgasim, A.A., Fernandes, R.A., & Leblanc, S.G. (2006). Evaluation of national and global LAI products derived from optical remote sensing instruments over Canada. *IEEE Transactions on Geoscience and Remote Sensing*, 44, 1872-1884

Adams, W.M., Aveling, R., Brockington, D., Dickson, B., Elliott, J., Hutton, J., Roe, D., Vira, B., & Wolmer, W. (2004). Biodiversity conservation and the eradication of poverty. *Science*, 306, 1146-1149

Armston, J., Disney, M., Lewis, P., Scarth, P., Phinn, S., Lucas, R., Bunting, P., & Goodwin, N. (2013). Direct retrieval of canopy gap probability using airborne waveform lidar. *Remote Sensing of Environment*, 134, 24-38

Arora, V.K., & Boer, G.J. (2005). A parameterization of leaf phenology for the terrestrial ecosystem component of climate models. *Global Change Biology*, 11, 39-59

Asner, G.P. (2005). Selective Logging in the Brazilian Amazon. *Science*, 310, 480-482

Asner, G.P., Elmore, A.J., Hughes, R.F., Warner, A.S., & Vitousek, P.M. (2005). Ecosystem structure along bioclimatic gradients in Hawaii from imaging spectroscopy. *Remote Sensing of Environment*, 96, 497-508

Asner, G.P., Knapp, D.E., Boardman, J., Green, R.O., Kennedy-Bowdoin, T., Eastwood, M., Martin, R.E., Anderson, C., & Field, C.B. (2012). Carnegie Airborne Observatory-2: Increasing science data dimensionality via high-fidelity multi-sensor fusion. *Remote Sensing of Environment*, 124, 454-465

Asner, G.P., Mascaro, J., Anderson, C., Knapp, D.E., Martin, R.E., Kennedy-Bowdoin, T., van Breugel, M., Davies, S., Hall, J.S., Muller-Landau, H.C., Potvin, C., Sousa, W., Wright, J., & Bermingham, E. (2013). High-fidelity national carbon mapping for resource management and REDD+. *Carbon Balance and Management*, 8

Assessment, M.E. (2005). Ecosystems and human well-being : synthesis / A report of Millennium Ecosystem Assessment. In. Washington D.C.

Baccini, A., Goetz, S.J., Walker, W.S., Laporte, N.T., Sun, M., Sulla-

- Menashe, D., Hackler, J., Beck, P.S.A., Dubayah, R., Friedl, M.A., Samanta, S., & Houghton, R.A. (2012). Estimated carbon dioxide emissions from tropical deforestation improved by carbon-density maps. *Nature Climate Change*, 2, 182-185
- Baret, F., Hagolle, O., Geiger, B., Bicheron, P., Miras, B., Huc, M., Berthelot, B., Nino, F., Weiss, M., Samain, O., Roujean, J.L., & Leroy, M. (2007). LAI, fAPAR and fCover CYCLOPES global products derived from VEGETATION - Part 1: Principles of the algorithm. *Remote Sensing of Environment*, 110, 275-286
- Baret, F., Weiss, M., Lacaze, R., Camacho, F., Makhmara, H., Pacholczyk, P., & Smets, B. (2013). GEOV1: LAI and FAPAR essential climate variables and FCOVER global time series capitalizing over existing products. Part 1: Principles of development and production. *Remote Sensing of Environment*, 137, 299-309
- Blair, J.B., & Hofton, M.A. (1999). Modeling laser altimeter return waveforms over complex vegetation using high resolution elevation data. *Geophysical Research Letters*, 26, 2509-2509
- Blair, J.B., Rabine, D.L., & Hofton, M.A. (1999). The Laser Vegetation Imaging Sensor (LVIS): A Medium-Altitude, Digitization-Only, Airborne Laser Altimeter for Mapping Vegetation and Topography. *ISPRS Journal of Photogrammetry and Remote Sensing*, 54, 115-122
- Bonan, G.B. (2008). Forests and climate change: Forcings, feedbacks, and the climate benefits of forests. *Science*, 320, 1444-1449
- Bradbury, R.B., Hill, R.A., Mason, D.C., Hinsley, S.A., Wilson, J.D., Balzter, H., Anderson, G.Q.A., Whittingham, M.J., Davenport, I.J., & Bellamy, P.E. (2005). Modelling relationships between birds and vegetation structure using airborne LiDAR data: a review with case studies from agricultural and woodland environments. *Ibis*, 147, 443-452
- Brodu, N., & Lague, D. (2012). 3D terrestrial lidar data classification of complex natural scenes using a multi-scale dimensionality criterion: Applications in geomorphology. *ISPRS Journal of Photogrammetry and Remote Sensing*, 68, 121-134
- Chen, J., Menges, C., & Leblanc, S. (2005). Global mapping of foliage clumping index using multi-angular satellite data. *Remote Sensing of Environment*, 97, 447-457
- Chen, J.M., & Cihlar, J. (1995). Plant canopy gap-size analysis theory for improving optical measurements of leaf-area index. *Applied Optics*, 34, 6211-6211
- Chen, J.M., Liu, J., Cihlar, J., & Goulden, M.L. (1999). Daily canopy photosynthesis model through temporal and spatial scaling for remote sensing applications. *Ecological Modelling*, 124, 99-119
- Chen, J.M., Rich, P.M., Gower, S.T., Norman, J.M., & Plummer, S. (1997). Leaf area index of boreal forests: Theory, techniques, and measurements. *Journal of Geophysical Research*, 102, 29429-29443
- Clark, D.A. (2004). Sources or sinks? The responses of tropical forests to

current and future climate and atmospheric composition. *Philosophical Transactions of the Royal Society of London Series B-Biological Sciences*, 359, 477-491

Clark, D.B., & Clark, D.A. (2000). Landscape-scale variation in forest structure and biomass in a tropical rain forest. *Forest Ecology and Management*, 137, 185-198

Clark, D.B., & Kellner, J.R. (2012). Tropical forest biomass estimation and the fallacy of misplaced concreteness. *Journal of Vegetation Science*, 23, 1191-1196

Clark, D.B., Olivas, P.C., Oberbauer, S.F., Clark, D.A., & Ryan, M.G. (2008). First direct landscape-scale measurement of tropical rain forest Leaf Area Index, a key driver of global primary productivity. *Ecology Letters*, 11, 163-172

Clark, M.L., Roberts, D.A., & Clark, D.B. (2005). Hyperspectral discrimination of tropical rain forest tree species at leaf to crown scales. *Remote Sensing of Environment*, 96, 375-398

Cohen, W.B., Maiersperger, T.K., Gower, S.T., & Turner, D.P. (2003). An improved strategy for regression of biophysical variables and Landsat ETM+ data. *Remote Sensing of Environment*, 84, 561-571

Cote, J.F., Widlowski, J.L., Fournier, R.A., & Verstraete, M.M. (2009). The structural and radiative consistency of three-dimensional tree reconstructions from terrestrial lidar. *Remote Sensing of Environment*, 113, 1067-1081

Cramer, W., Bondeau, A., Woodward, F.I., Prentice, I.C., Betts, R.A., Brovkin, V., Cox, P.M., Fisher, V., Foley, J.A., Friend, A.D., Kucharik, C., Lomas, M.R., Ramankutty, N., Sitch, S., Smith, B., White, A., & Young-Molling, C. (2001). Global response of terrestrial ecosystem structure and function to CO₂ and climate change: results from six dynamic global vegetation models. *Global Change Biology*, 7, 357-373

Culbert, P.D., Radeloff, V.C., Flather, C.H., Kellndorfer, J.M., Rittenhouse, C.D., & Pidgeon, A.M. (2013). The Influence of Vertical and Horizontal Habitat Structure on Nationwide Patterns of Avian Biodiversity. *Auk*, 130, 656-665

Dale, V.H., Joyce, L.A., McNulty, S., Neilson, R.P., Ayres, M.P., Flannigan, M.D., Hanson, P.J., Irland, L.C., Lugo, A.E., Peterson, C.J., Simberloff, D., Swanson, F.J., Stocks, B.J., & Wotton, B.M. (2001). Climate change and forest disturbances. *BioScience*, 51, 723-734

DeFries, R.S., Houghton, R.A., Hansen, M.C., Field, C.B., Skole, D., & Townshend, J. (2002). Carbon emissions from tropical deforestation and regrowth based on satellite observations for the 1980s and 1990s. *Proceedings of the National Academy of Sciences of the United States of America*, 99, 14256-14261

Demarez, V., Duthoit, S., Baret, F., Weiss, M., & Dedieu, G. (2008). Estimation of leaf area and clumping indexes of crops with hemispherical photographs. *Agricultural and Forest Meteorology*, 148, 644-655

Deng, F., Chen, J.M., Plummer, S., Chen, M.Z., & Pisek, J. (2006). Algorithm

for global leaf area index retrieval using satellite imagery. *IEEE Transactions on Geoscience and Remote Sensing*, 44, 2219-2229

Douglas, E.S., Strahler, A., Martel, J., Cook, T., Mendillo, C., Marshall, R., Chakrabarti, S., Schaaf, C., Woodcock, C., Li, Z., Yang, X., Culvenor, D., Jupp, D., Newnham, G., & Lovell, J. (2012). DWEL: A Dual-Wavelength Echidna Lidar for ground-based forest scanning. In (pp. 4998-5001): IEEE

Drake, J. (2002a). Estimation of tropical forest structural characteristics using large-footprint lidar. *Remote Sensing of Environment*, 79, 305-319

Drake, J. (2002b). Sensitivity of large-footprint lidar to canopy structure and biomass in a neotropical rainforest. *Remote Sensing of Environment*, 81, 378-392

Dubayah, R., Bergen, K., Hall, F., Hurtt, G., Houghton, R., Kellndorfer, J., Lefsky, M., Moorcroft, P., Nelson, R., & Saatchi, S. (2008). Global vegetation structure from NASA's DESDynI mission: An overview. In, *AGU Fall Meeting Abstracts* (p. 01)

Dubayah, R., Goetz, S., Blair, J.B., Fatoyinbo, T., Hansen, M., Healey, S., Hofton, M., Hurtt, G., Kellner, J.R., Luthcke, S.B., & Swatantran, A. (2014). The Global Ecosystem Dynamics Investigation. In, *American Geophysical Union, Fall Meeting 2014*. San Francisco: AGU

Dubayah, R.O., & Drake, J.B. (2000). Lidar remote sensing for forestry. *Journal of Forestry*, 98, 44-46

Dubayah, R.O., Sheldon, S.L., Clark, D.B., Hofton, M.A., Blair, J.B., Hurtt, G.C., & Chazdon, R.L. (2010). Estimation of tropical forest height and biomass dynamics using lidar remote sensing at La Selva, Costa Rica. *Journal of Geophysical Research*, 115

Duncanson, L.I., Niemann, K.O., & Wulder, M.A. (2010). Estimating forest canopy height and terrain relief from GLAS waveform metrics. *Remote Sensing of Environment*, 114, 138-154

Edwards, D.P., Fisher, B., & Boyd, E. (2010). Protecting degraded rainforests: enhancement of forest carbon stocks under REDD+. *Conservation Letters*, 3, 313-316

Ellsworth, D.S., & Reich, P.B. (1993). Canopy structure and vertical patterns of photosynthesis and related leaf traits in a deciduous forest. *Oecologia*, 96, 169-178

Fang, H.L., Jiang, C.Y., Li, W.J., Wei, S.S., Baret, F., Chen, J.M., Garcia-Haro, J., Liang, S.L., Liu, R.G., Myneni, R.B., Pinty, B., Xiao, Z.Q., & Zhu, Z.C. (2013). Characterization and intercomparison of global moderate resolution leaf area index (LAI) products: Analysis of climatologies and theoretical uncertainties. *Journal of Geophysical Research-Biogeosciences*, 118, 529-548

Fang, H.L., & Liang, S.L. (2003). Retrieving leaf area index with a neural network method: Simulation and validation. *IEEE Transactions on Geoscience and Remote Sensing*, 41, 2052-2062

Fang, H.L., Wei, S.S., Jiang, C.Y., & Scipal, K. (2012). Theoretical

uncertainty analysis of global MODIS, CYCLOPES, and GLOBCARBON LAI products using a triple collocation method. *Remote Sensing of Environment*, 124, 610-621

Farid, A., Goodrich, D.C., Bryant, R., & Sorooshian, S. (2008). Using airborne lidar to predict Leaf Area Index in cottonwood trees and refine riparian water-use estimates. *Journal of Arid Environments*, 72, 1-15

Ferger, S.W., Schleuning, M., Hemp, A., Howell, K.M., & Böhning-Gaese, K. (2014). Food resources and vegetation structure mediate climatic effects on species richness of birds. *Global Ecology and Biogeography*, 23, 541-549

Frazer, G.W., Magnussen, S., Wulder, M.A., & Niemann, K.O. (2010). Simulated impact of sample plot size and co-registration error on the accuracy and uncertainty of LiDAR-derived estimates of forest stand biomass. *Remote Sensing of Environment*, 115, 636-649

Friedl, M.A., Sulla-Menashe, D., Tan, B., Schneider, A., Ramankutty, N., Sibley, A., & Huang, X.M. (2010). MODIS Collection 5 global land cover: Algorithm refinements and characterization of new datasets. *Remote Sensing of Environment*, 114, 168-182

Ganguly, S., Nemani, R.R., Zhang, G., Hashimoto, H., Milesi, C., Michaelis, A., Wang, W.L., Votava, P., Samanta, A., Melton, F., Dungan, J.L., Vermote, E., Gao, F., Knyazikhin, Y., & Myneni, R.B. (2012). Generating global Leaf Area Index from Landsat: Algorithm formulation and demonstration. *Remote Sensing of Environment*, 122, 185-202

Ganguly, S., Schull, M.A., Samanta, A., Shabanov, N.V., Milesi, C., Nemani, R.R., Knyazikhin, Y., & Myneni, R.B. (2008). Generating vegetation leaf area index earth system data record from multiple sensors. Part 1: Theory. *Remote Sensing of Environment*, 112, 4333-4343

Garcia, M., Popescu, S., Riano, D., Zhao, K., Neuenschwander, A., Agca, M., & Chuvieco, E. (2012). Characterization of canopy fuels using ICESat/GLAS data. *Remote Sensing of Environment*, 123, 81-89

Garrigues, S., Lacaze, R., Baret, F., Morisette, J.T., Weiss, M., Nickeson, J.E., Fernandes, R., Plummer, S., Shabanov, N.V., Myneni, R.B., Knyazikhin, Y., & Yang, W. (2008). Validation and intercomparison of global Leaf Area Index products derived from remote sensing data. *Journal of Geophysical Research-Biogeosciences*, 113, -

Gobron, N., & Verstraete, M.M. (2009). ECV T11: Leaf Area Index. In G.T.O. System (Ed.), *Assessment of the status of the development of standards for the Terrestrial Essential Climate Variables*. Rome

Goetz, S., Steinberg, D., Dubayah, R., & Blair, B. (2007). Laser remote sensing of canopy habitat heterogeneity as a predictor of bird species richness in an eastern temperate forest, USA. *Remote Sensing of Environment*, 108, 254-263

Goetz, S.J., Steinberg, D., Betts, M.G., Holmes, R.T., Doran, P.J., Dubayah,

- R., & Hofton, M. (2010). Lidar remote sensing variables predict breeding habitat of a Neotropical migrant bird. *Ecology*, *91*, 1569-1576
- Gower, S.T., & Norman, J.M. (1991). Rapid Estimation of Leaf Area Index in Conifer and Broad-Leaf Plantations. *Ecology*, *72*, 1896-1900
- Hall, F., Saatchi, S., & Dubayah, R. (2011). PREFACE: DESDynI VEG-3D Special Issue. *Remote Sensing of Environment*, *115*, 2752-2752
- Harding, D.J. (2005). ICESat waveform measurements of within-footprint topographic relief and vegetation vertical structure. *Geophysical Research Letters*, *32*
- Healey, S.P., Patterson, P.L., Saatchi, S., Lefsky, M.A., Lister, A.J., & Freeman, E.A. (2012). A sample design for globally consistent biomass estimation using lidar data from the Geoscience Laser Altimeter System (GLAS). *Carbon Balance and Management*, *7*
- Heimann, M., & Reichstein, M. (2008). Terrestrial ecosystem carbon dynamics and climate feedbacks. *Nature*, *451*, 289-292
- Hofton, M. (2002). Validation of Vegetation Canopy Lidar sub-canopy topography measurements for a dense tropical forest. *Journal of Geodynamics*, *34*, 491-502
- Hofton, M.A., Minster, J.B., & Blair, J.B. (2000). Decomposition of laser altimeter waveforms. *IEEE Transactions on Geoscience and Remote Sensing*, *38*, 1989-1996
- Houghton, R.A. (2007). Balancing the global carbon budget. *Annual Review of Earth and Planetary Sciences*, *35*, 313-347
- Houghton, R.A., Davidson, E.A., & Woodwell, G.M. (1998). Missing sinks, feedbacks, and understanding the role of terrestrial ecosystems in the global carbon balance. *Global Biogeochemical Cycles*, *12*, 25-34
- Hunsaker, C., Boroski, B., & Steger, G. (2002). Relations between canopy cover and occurrence and productivity of California spotted owls, predicting species occurrences, issues of accuracy and scale. In J.M. Scott, P. Heglund & M.L. Morrison (Eds.), *Predicting Species Occurrences: Issues of Accuracy and Scale*. Covelo, CA Island Press
- Hurttt, G.C., Dubayah, R., Drake, J., Moorcroft, P.R., Pacala, S.W., Blair, J.B., & Fearon, M.G. (2004). Beyond potential vegetation: combining lidar data and a height-structured model for carbon studies. *Ecological Applications*, *14*, 873-883
- Hyde, P., Dubayah, R., Peterson, B., Blair, J., Hofton, M., Hunsaker, C., Knox, R., & Walker, W. (2005). Mapping forest structure for wildlife habitat analysis using waveform lidar: Validation of montane ecosystems. *Remote Sensing of Environment*, *96*, 427-437
- Hyde, P., Dubayah, R., Walker, W., Blair, J., Hofton, M., & Hunsaker, C. (2006). Mapping forest structure for wildlife habitat analysis using multi-sensor (LiDAR, SAR/InSAR, ETM+, Quickbird) synergy. *Remote Sensing of Environment*,

IPCC (2007). *Climate Change 2007 - The Physical Science Basis: Working Group I Contribution to the Fourth Assessment Report of the IPCC (Climate Change 2007)*

IPCC (2013). *Climate change 2013: the physical science basis. Intergovernmental Panel on Climate Change*

Jensen, J., Humes, K., Vierling, L., & Hudak, A. (2008). Discrete return lidar-based prediction of leaf area index in two conifer forests. *Remote Sensing of Environment, 112*, 3947-3957

Jonckheere, I., Fleck, S., Nackaerts, K., Muys, B., Coppin, P., Weiss, M., & Baret, F. (2004). Review of methods for in situ leaf area index determination - Part I. Theories, sensors and hemispherical photography. *Agricultural and Forest Meteorology, 121*, 19-35

Jupp, D.L.B., Culvenor, D.S., Lovell, J.L., Newnham, G.J., Strahler, A.H., & Woodcock, C.E. (2009). Estimating forest LAI profiles and structural parameters using a ground-based laser called 'Echidna (R)'. *Tree Physiology, 29*, 171-181

Kellndorfer, J., Walker, W., LaPoint, E., Bishop, J., Cormier, T., Fiske, G., Hoppus, M., Kirsch, K., & Westfall, J. (2012). NACP Aboveground Biomass and Carbon Baseline Data (NBCD 2000), U.S.A., 2000. In: ORNL DAAC, Oak Ridge, Tennessee, U.S.A

Kellner, J.R., Asner, G.P., Vitousek, P.M., Tweiten, M.A., Hotchkiss, S., & Chadwick, O.A. (2011). Dependence of Forest Structure and Dynamics on Substrate Age and Ecosystem Development. *Ecosystems, 14*, 1156-1167

Knyazikhin, Y., Kranigk, J., Myneni, R.B., Panfyorov, O., & Gravenhorst, G. (1998a). Influence of small-scale structure on radiative transfer and photosynthesis in vegetation canopies. *Journal of Geophysical Research-Atmospheres, 103*, 6133-6144

Knyazikhin, Y., Martonchik, J.V., Diner, D.J., Myneni, R.B., Verstraete, M., Pinty, B., & Gobron, N. (1998b). Estimation of vegetation canopy leaf area index and fraction of absorbed photosynthetically active radiation from atmosphere-corrected MISR data. *Journal of Geophysical Research-Atmospheres, 103*, 32239-32256

Knyazikhin, Y., Martonchik, J.V., Myneni, R.B., Diner, D.J., & Running, S.W. (1998c). Synergistic algorithm for estimating vegetation canopy leaf area index and fraction of absorbed photosynthetically active radiation from MODIS and MISR data. *Journal of Geophysical Research-Atmospheres, 103*, 32257-32275

Koetz, B., Baret, F., Poilve, H., & Hill, J. (2005). Use of coupled canopy structure dynamic and radiative transfer models to estimate biophysical canopy characteristics. *Remote Sensing of Environment, 95*, 115-124

Kotchenova, S.Y., Song, X.D., Shabanova, N.V., Potter, C.S., Knyazikhin, Y., & Myneni, R.B. (2004). Lidar remote sensing for modeling gross primary production of deciduous forests. *Remote Sensing of Environment, 92*, 158-172

- Leblanc, S.G., Chen, J.M., Fernandes, R., Deering, D.W., & Conley, A. (2005). Methodology comparison for canopy structure parameters extraction from digital hemispherical photography in boreal forests. *Agricultural and Forest Meteorology*, *129*, 187-207
- Lefsky, M. (1999a). Lidar Remote Sensing of the Canopy Structure and Biophysical Properties of Douglas-Fir Western Hemlock Forests. *Remote Sensing of Environment*, *70*, 339-361
- Lefsky, M. (1999b). Surface Lidar Remote Sensing of Basal Area and Biomass in Deciduous Forests of Eastern Maryland, USA. *Remote Sensing of Environment*, *67*, 83-98
- Lefsky, M.A. (2010). A global forest canopy height map from the Moderate Resolution Imaging Spectroradiometer and the Geoscience Laser Altimeter System. *Geophysical Research Letters*, *37*
- Lefsky, M.A., Cohen, W.B., Parker, G.G., & Harding, D.J. (2002). Lidar Remote Sensing for Ecosystem Studies. *BioScience*, *52*, 19-19
- Lefsky, M.A., Harding, D.J., Keller, M., Cohen, W.B., Carabajal, C.C., Del Bom Espirito-Santo, F., Hunter, M.O., & de Oliveira, R. (2005). Estimates of forest canopy height and aboveground biomass using ICESat. *Geophysical Research Letters*, *32*
- Lefsky, M.A., Keller, M., Pang, Y., De Camargo, P.B., & Hunter, M.O. (2007). Revised method for forest canopy height estimation from Geoscience Laser Altimeter System waveforms. *Journal of Applied Remote Sensing*, *1*, 013537-013537
- Lewis, S.L., Lopez-Gonzalez, G., Sonke, B., Affum-Baffoe, K., Baker, T.R., Ojo, L.O., Phillips, O.L., Reitsma, J.M., White, L., Comiskey, J.A., Djuikouo, M.N., Ewango, C.E.N., Feldpausch, T.R., Hamilton, A.C., Gloor, M., Hart, T., Hladik, A., Lloyd, J., Lovett, J.C., Makana, J.R., Malhi, Y., Mbago, F.M., Ndangalasi, H.J., Peacock, J., Peh, K.S.H., Sheil, D., Sunderland, T., Swaine, M.D., Taplin, J., Taylor, D., Thomas, S.C., Votere, R., & Woll, H. (2009). Increasing carbon storage in intact African tropical forests. *Nature*, *457*, 1003-U1003
- Lindner, M., Maroschek, M., Netherer, S., Kremer, A., Barbati, A., Garcia-Gonzalo, J., Seidl, R., Delzon, S., Corona, P., Kolstrom, M., Lexer, M.J., & Marchetti, M. (2010). Climate change impacts, adaptive capacity, and vulnerability of European forest ecosystems. *Forest Ecology and Management*, *259*, 698-709
- Loreau, M., Naeem, S., Inchausti, P., Bengtsson, J., Grime, J.P., Hector, A., Hooper, D.U., Huston, M.A., Raffaelli, D., Schmid, B., Tilman, D., & Wardle, D.A. (2001). Ecology - Biodiversity and ecosystem functioning: Current knowledge and future challenges. *Science*, *294*, 804-808
- Los, S.O., Rosette, J.A.B., Kljun, N., North, P.R.J., Chasmer, L., Suñez, J.C., Hopkinson, C., Hill, R.A., van Gorsel, E., Mahoney, C., & Berni, J.A.J. (2012). Vegetation height and cover fraction between 60° S and 60° N from ICESat GLAS data. *Geosci. Model Dev.*, *5*, 413-432

- Luo, S.Z., Wang, C., Li, G.C., & Xi, X.H. (2013). Retrieving leaf area index using ICESat/GLAS full-waveform data. *Remote Sensing Letters*, 4, 745-753
- Luo, T.X., Pan, Y.D., Ouyang, H., Shi, P.L., Luo, J., Yu, Z.L., & Lu, Q. (2004). Leaf area index and net primary productivity along subtropical to alpine gradients in the Tibetan Plateau. *Global Ecology and Biogeography*, 13, 345-358
- MacArthur, R.H., & Horn, H.S. (1969). Foliage profile by vertical measurements. *Ecology*, 50, 802-804
- Miller, J. (1967). A formula for average foliage density. *Australian Journal of Botany*, 15, 141-141
- Mittermeier, R.A., Myers, N., Thomsen, J.B., da Fonseca, G.A.B., & Olivieri, S. (1998). Biodiversity hotspots and major tropical wilderness areas: Approaches to setting conservation priorities. *Conservation Biology*, 12, 516-520
- Monsi, M., & Saeki, T. (1953). Uber den Lichtfaktor in den Pflanzengesellschaften und seine Bedeutung fur die Stoffproduktion. *Japanese Journal of Botany*, 14, 22-52
- Monteith, J.L., & Unsworth, M.H. (2008). *Principles of environmental physics*. Amsterdam ; Boston: Elsevier ;
- Morissette, J.T., Baret, F., Privette, J.L., Myneni, R.B., Nickeson, J.E., Garrigues, S., Shabanov, N.V., Weiss, M., Fernandes, R.A., Leblanc, S.G., Kalacska, M., Sanchez-Azofeifa, G.A., Chubey, M., Rivard, B., Stenberg, P., Rautiainen, M., Voipio, P., Manninen, T., Pilant, A.N., Lewis, T.E., Iames, J.S., Colombo, R., Meroni, M., Busetto, L., Cohen, W.B., Turner, D.P., Warner, E.D., Petersen, G.W., Seufert, G., & Cook, R. (2006). Validation of global moderate-resolution LAI products: A framework proposed within the CEOS Land Product Validation subgroup. *IEEE Transactions on Geoscience and Remote Sensing*, 44, 1804-1817
- Morsdorf, F., Kotz, B., Meier, E., Itten, K., & Allgower, B. (2006). Estimation of LAI and fractional cover from small footprint airborne laser scanning data based on gap fraction. *Remote Sensing of Environment*, 104, 50-61
- Moser, G., Hertel, D., & Leuschner, C. (2007). Altitudinal change in LAI and stand leaf biomass in tropical montane forests: a transect study in Ecuador and a pan-tropical meta-analysis. *Ecosystems*, 10, 924-935
- Mu, Q., Heinsch, F.A., Zhao, M., & Running, S.W. (2007). Development of a global evapotranspiration algorithm based on MODIS and global meteorology data. *Remote Sensing of Environment*, 111, 519-536
- Myneni, R.B. (2001). A large carbon sink in the woody biomass of Northern forests. *Proceedings of the National Academy of Sciences*, 98, 14784-14789
- Myneni, R.B., Hoffman, S., Knyazikhin, Y., Privette, J.L., Glassy, J., Tian, Y., Wang, Y., Song, X., Zhang, Y., Smith, G.R., Lotsch, A., Friedl, M., Morissette, J.T., Votava, P., Nemani, R.R., & Running, S.W. (2002). Global products of vegetation leaf area and fraction absorbed PAR from year one of MODIS data.

Remote Sensing of Environment, 83, 214-231

Naesset, E. (1997). Determination of mean tree height of forest stands using airborne laser scanner data. *ISPRS Journal of Photogrammetry and Remote Sensing*, 52, 49-56

Naesset, E. (2002). Predicting forest stand characteristics with airborne scanning laser using a practical two-stage procedure and field data. *Remote Sensing of Environment*, 80, 88-99

Nagendra, H. (2001). Using remote sensing to assess biodiversity. *International Journal of Remote Sensing*, 22, 2377-2400

Ni-Meister, W., Jupp, D.L.B., & Dubayah, R. (2001). Modeling lidar waveforms in heterogeneous and discrete canopies. *IEEE Transactions on Geoscience and Remote Sensing*, 39, 1943-1958

Ni-Meister, W., Lee, S.Y., Strahler, A.H., Woodcock, C.E., Schaaf, C., Yao, T.A., Ranson, K.J., Sun, G.Q., & Blair, J.B. (2010). Assessing general relationships between aboveground biomass and vegetation structure parameters for improved carbon estimate from lidar remote sensing. *Journal of Geophysical Research-Biogeosciences*, 115

Nilson, T. (1971). A theoretical analysis of the frequency of gaps in plant stands. *Agricultural Meteorology*, 8, 25-38

Nilson, T. (1999). Inversion of gap frequency data in forest stands. *Agricultural and Forest Meteorology*, 98-99, 437-448

Nilsson, M. (1996). Estimation of tree heights and stand volume using an airborne lidar system. *Remote Sensing of Environment*, 56, 1-7

NRC (2007). *Earth Science and Applications from Space: National Imperatives for the Next Decade and Beyond*: The National Academies Press

Olson, D.M., Dinerstein, E., Wikramanayake, E.D., Burgess, N.D., Powell, G.V.N., Underwood, E.C., D'amico, J.A., Itoua, I., Strand, H.E., Morrison, J.C., Loucks, C.J., Allnutt, T.F., Ricketts, T.H., Kura, Y., Lamoreux, J.F., Wettengel, W.W., Hedao, P., & Kassem, K.R. (2001). Terrestrial Ecoregions of the World: A New Map of Life on Earth: A new global map of terrestrial ecoregions provides an innovative tool for conserving biodiversity. *BioScience*, 51, 933-938

Pan, Y., Birdsey, R.A., Fang, J., Houghton, R., Kauppi, P.E., Kurz, W.A., Phillips, O.L., Shvidenko, A., Lewis, S.L., Canadell, J.G., Ciais, P., Jackson, R.B., Pacala, S.W., McGuire, A.D., Piao, S., Rautiainen, A., Sitch, S., & Hayes, D. (2011). A large and persistent carbon sink in the world's forests. *Science*, 333, 988-993

Pang, Y., Li, Z., Lefsky, M., Sun, G., & Yu, X. (2006). Model Based Terrain Effect Analyses on ICESat GLAS Waveforms. In: *Geoscience and Remote Sensing Symposium, 2006. IGARSS 2006. IEEE International Conference on*

Parker, G.G., Lefsky, M.A., & Harding, D.J. (2001). Light transmittance in forest canopies determined using airborne laser altimetry and in-canopy quantum

measurements. *Remote Sensing of Environment*, 76, 298-309

Pereira, H.M., Ferrier, S., Walters, M., Geller, G.N., Jongman, R.H.G., Scholes, R.J., Bruford, M.W., Brummitt, N., Butchart, S.H.M., Cardoso, A.C., Coops, N.C., Dulloo, E., Faith, D.P., Freyhof, J., Gregory, R.D., Heip, C., Hoft, R., Hurtt, G., Jetz, W., Karp, D.S., McGeoch, M.A., Obura, D., Onoda, Y., Pettorelli, N., Reyers, B., Sayre, R., Scharlemann, J.P.W., Stuart, S.N., Turak, E., Walpole, M., & Wegmann, M. (2013). Essential Biodiversity Variables. *Science*, 339, 277-278

Pfeifer, M., Gonsamo, A., Disney, M., Pellikka, P., & Marchant, R. (2012). Leaf area index for biomes of the Eastern Arc Mountains: Landsat and SPOT observations along precipitation and altitude gradients. *Remote Sensing of Environment*, 118, 103-115

Pfeifer, M., Lefebvre, V., Gonsamo, A., Pellikka, P., Marchant, R., Denu, D., & Platts, P. (2014). Validating and Linking the GIMMS Leaf Area Index (LAI3g) with Environmental Controls in Tropical Africa. *Remote Sensing*, 6, 1973-1990

Popescu, S.C. (2007). Estimating biomass of individual pine trees using airborne lidar. *Biomass & Bioenergy*, 31, 646-655

PRISM (2013). 30-yr Normal Precipitation: Annual. In, 1981-2010: PRISM Climate Group, Oregon State University

Randerson, J.T., Hoffman, F.M., Thornton, P.E., Mahowald, N.M., Lindsay, K., Lee, Y.H., Nevison, C.D., Doney, S.C., Bonan, G., Stockli, R., Covey, C., Running, S.W., & Fung, I.Y. (2009). Systematic assessment of terrestrial biogeochemistry in coupled climate-carbon models. *Global Change Biology*, 15, 2462-2484

Reuter, H.I., Nelson, A., & Jarvis, A. (2007). An evaluation of void-filling interpolation methods for SRTM data. *International Journal of Geographical Information Science*, 21, 983-1008

Riano, D. (2004). Estimation of leaf area index and covered ground from airborne laser scanner (Lidar) in two contrasting forests. *Agricultural and Forest Meteorology*, 124, 269-275

Richardson, J.J., Moskal, L.M., & Kim, S.-H. (2009). Modeling approaches to estimate effective leaf area index from aerial discrete-return LIDAR. *Agricultural and Forest Meteorology*, 149, 1152-1160

Running, S.W., Baldocchi, D.D., Turner, D.P., Gower, S.T., Bakwin, P.S., & Hibbard, K.A. (1999). A global terrestrial monitoring network integrating tower fluxes, flask sampling, ecosystem modeling and EOS satellite data. *Remote Sensing of Environment*, 70, 108-127

Saatchi, S.S., Harris, N.L., Brown, S., Lefsky, M., Mitchard, E.T.A., Salas, W., Zutta, B.R., Buermann, W., Lewis, S.L., Hagen, S., Petrova, S., White, L., Silman, M., & Morel, A. (2011). Benchmark map of forest carbon stocks in tropical regions across three continents. *Proceedings of the National Academy of Sciences of*

the United States of America, 108, 9899-9904

Sala, O.E., Chapin, F.S., Armesto, J.J., Berlow, E., Bloomfield, J., Dirzo, R., Huber-Sanwald, E., Huenneke, L.F., Jackson, R.B., Kinzig, A., Leemans, R., Lodge, D.M., Mooney, H.A., Oesterheld, M., Poff, N.L., Sykes, M.T., Walker, B.H., Walker, M., & Wall, D.H. (2000). Biodiversity - Global biodiversity scenarios for the year 2100. *Science, 287, 1770-1774*

Sauer, J.R., Hines, J.E., Fallon, J., Pardieck, K., Ziolkowski Jr, D., & Link, W. (2008). The North American breeding bird survey, results and analysis 1966-2007. *Version, 5, 2008*

Schimel, D.S., House, J.I., Hibbard, K.A., Bousquet, P., Ciais, P., Peylin, P., Braswell, B.H., Apps, M.J., Baker, D., Bondeau, A., Canadell, J., Churkina, G., Cramer, W., Denning, A.S., Field, C.B., Friedlingstein, P., Goodale, C., Heimann, M., Houghton, R.A., Melillo, J.M., Moore, B., Murdiyarso, D., Noble, I., Pacala, S.W., Prentice, I.C., Raupach, M.R., Rayner, P.J., Scholes, R.J., Steffen, W.L., & Wirth, C. (2001). Recent patterns and mechanisms of carbon exchange by terrestrial ecosystems. *Nature, 414, 169-172*

Schindler, D.W. (1999). Carbon cycling - The mysterious missing sink. *Nature, 398, 105-+*

Schut, A.G.T., Wardell-Johnson, G.W., Yates, C.J., Keppel, G., Baran, I., Franklin, S.E., Hopper, S.D., Van Niel, K.P., Mucina, L., & Byrne, M. (2014). Rapid Characterisation of Vegetation Structure to Predict Refugia and Climate Change Impacts across a Global Biodiversity Hotspot. *Plos One, 9*

Schutz, B.E., Zwally, H.J., Shuman, C.A., Hancock, D., & DiMarzio, J.P. (2005). Overview of the ICESat Mission. *Geophysical Research Letters, 32*

Sexton, J.O., Bax, T., Siqueira, P., Swenson, J.J., & Hensley, S. (2009). A comparison of lidar, radar, and field measurements of canopy height in pine and hardwood forests of southeastern North America. *Forest Ecology and Management, 257, 1136-1147*

Shabanov, N.V., Huang, D., Yang, W.Z., Tan, B., Knyazikhin, Y., Myneni, R.B., Ahl, D.E., Gower, S.T., Huete, A.R., Aragao, L.E.O.C., & Shimabukuro, Y.E. (2005). Analysis and optimization of the MODIS leaf area index algorithm retrievals over broadleaf forests. *IEEE Transactions on Geoscience and Remote Sensing, 43, 1855-1865*

Simard, M., Pinto, N., Fisher, J.B., & Baccini, A. (2011). Mapping forest canopy height globally with spaceborne lidar. *Journal of Geophysical Research-Biogeosciences, 116*

Solberg, S., Brunner, A., Hanssen, K.H., Lange, H., NÅisset, E., Rautiainen, M., & Stenberg, P. (2009). Mapping LAI in a Norway spruce forest using airborne laser scanning. *Remote Sensing of Environment, 113, 2317-2327*

Sorin, C.P., Randolph, H.W., & John, A.S. (2004). Fusion of Small-Footprint Lidar and Multispectral Data to Estimate Plot- Level Volume and Biomass in

Deciduous and Pine Forests in Virginia, USA. *Forest Science*, 50, 551-565

Spracklen, D.V., Arnold, S.R., & Taylor, C.M. (2012). Observations of increased tropical rainfall preceded by air passage over forests. *Nature*, 489, 282-U127

Sprintsin, M., Chen, J.M., Desai, A., & Gough, C.M. (2012). Evaluation of leaf-to-canopy upscaling methodologies against carbon flux data in North America. *Journal of Geophysical Research-Biogeosciences*, 117

Stahl, G., Holm, S., Gregoire, T.G., Gobakken, T., Naesset, E., & Nelson, R. (2011). Model-based inference for biomass estimation in a LiDAR sample survey in Hedmark County, Norway. *Canadian Journal of Forest Research-Revue Canadienne De Recherche Forestiere*, 41, 96-107

Stark, S.C., Leitold, V., Wu, J.L., Hunter, M.O., de Castilho, C.V., Costa, F.v.R.C., McMahon, S.M., Parker, G.G., Shimabukuro, M.n.T., Lefsky, M.A., Keller, M., Alves, L.F., Schiatti, J., Shimabukuro, Y.E., Brandão, D.O., Woodcock, T.K., Higuchi, N., de Camargo, P.B., de Oliveira, R.C., & Saleska, S.R. (2012). Amazon forest carbon dynamics predicted by profiles of canopy leaf area and light environment. *Ecology Letters*, 15, 1406-1414

Steininger, M.K. (1996). Tropical secondary forest regrowth in the Amazon: Age, area and change estimation with Thematic Mapper data. *International Journal of Remote Sensing*, 17, 9-27

Stoner, E.R., & Baumgardner, M.F. (1981). Characteristic variations in reflectance in surface soils. *Journal Name: Soil Sci. Soc. Am. J.; (United States); Journal Volume: 45:6, Medium: X; Size: Pages: 1161-1165*

Strahler, A.H., Jupp, D.L.B., Woodcock, C.E., Schaaf, C.B., Yao, T., Zhao, F., Yang, X., Lovell, J., Culvenor, D., Newnham, G., Ni-Miester, W., & Boykin-Morris, W. (2008). Retrieval of forest structural parameters using a ground-based lidar instrument (Echidna®). *Canadian Journal of Remote Sensing*, 34

Swatantran, A., Dubayah, R., Goetz, S., Hofton, M., Betts, M.G., Sun, M., Simard, M., & Holmes, R. (2012). Mapping Migratory Bird Prevalence Using Remote Sensing Data Fusion. *Plos One*, 7, e28922

Swatantran, A., Dubayah, R., Roberts, D., Hofton, M., & Blair, J.B. (2011). Mapping biomass and stress in the Sierra Nevada using lidar and hyperspectral data fusion. *Remote Sensing of Environment*, 115, 2917-2930

Tang, H., Brolly, M., Zhao, F., Strahler, A.H., Schaaf, C.L., Ganguly, S., Zhang, G., & Dubayah, R. (2014a). Deriving and validating Leaf Area Index (LAI) at multiple spatial scales through lidar remote sensing: A case study in Sierra National Forest, CA. *Remote Sensing of Environment*, 143, 131-141

Tang, H., Dubayah, R., Brolly, M., Ganguly, S., & Zhang, G. (2014b). Large-scale retrieval of leaf area index and vertical foliage profile from the spaceborne waveform lidar (GLAS/ICESat). *Remote Sensing of Environment*, 154, 8-18

Tang, H., Dubayah, R., Swatantran, A., Hofton, M., Sheldon, S., Clark, D.B., & Blair, B. (2012). Retrieval of vertical LAI profiles over tropical rain forests using waveform lidar at La Selva, Costa Rica. *Remote Sensing of Environment*, 124, 242-250

Tucker, C.J. (1979). Red and Photographic Infrared Linear Combinations for Monitoring Vegetation. *Remote Sensing of Environment*, 8, 127-150

Turner, D.P., Ritts, W.D., Cohen, W.B., Gower, S.T., Running, S.W., Zhao, M.S., Costa, M.H., Kirschbaum, A.A., Ham, J.M., Saleska, S.R., & Ahl, D.E. (2006). Evaluation of MODIS NPP and GPP products across multiple biomes. *Remote Sensing of Environment*, 102, 282-292

Turner, W., Spector, S., Gardiner, N., Fladeland, M., Sterling, E., & Steininger, M. (2003). Remote sensing for biodiversity science and conservation. *Trends in Ecology & Evolution*, 18, 306-314

Vose, J., Peterson, D., & Patel-Weynand, T. (2012). Effects of Climatic Variability and Change on Forest Ecosystems : A Comprehensive Science Synthesis for the U . S . Forest Sector. In, *U.S. Department of Agriculture* (pp. 265-265)

Walker, B.H. (1992). Biodiversity and Ecological Redundancy. *Conservation Biology*, 6, 18-23

Walthall, C., Dulaney, W., Anderson, M., Norman, J., Fang, H.L., & Liang, S.L. (2004). A comparison of empirical and neural network approaches for estimating corn and soybean leaf area index from Landsat ETM+ imagery. *Remote Sensing of Environment*, 92, 465-474

Yang, W.Z., Tan, B., Huang, D., Rautiainen, M., Shabanov, N.V., Wang, Y., Privette, J.L., Huemmrich, K.F., Fensholt, R., Sandholt, I., Weiss, M., Ahl, D.E., Gower, S.T., Nemani, R.R., Knyazikhin, Y., & Myneni, R.B. (2006). MODIS leaf area index products: From validation to algorithm improvement. *IEEE Transactions on Geoscience and Remote Sensing*, 44, 1885-1898

Yang, X.Y., Strahler, A.H., Schaaf, C.B., Jupp, D.L.B., Yao, T., Zhao, F., Wang, Z.S., Culvenor, D.S., Newnham, G.J., Lovell, J.L., Dubayah, R., Woodcock, C.E., & Ni-Meister, W. (2013). Three-dimensional forest reconstruction and structural parameter retrievals using a terrestrial full-waveform lidar instrument (Echidn (R)). *Remote Sensing of Environment*, 135, 36-51

Zhao, F., Strahler, A.H., Schaaf, C.L., Yao, T., Yang, X., Wang, Z., Schull, M.A., Roman, M.O., Woodcock, C.E., Olofsson, P., Ni-Meister, W., Jupp, D.L.B., Lovell, J.L., Culvenor, D.S., & Newnham, G.J. (2012). Measuring gap fraction, element clumping index and LAI in Sierra Forest stands using a full-waveform ground-based lidar. *Remote Sensing of Environment*, 125, 73-79

Zhao, F., Yang, X.Y., Schull, M.A., Roman-Colon, M.O., Yao, T., Wang, Z.S., Zhang, Q.L., Jupp, D.L.B., Lovell, J.L., Culvenor, D.S., Newnham, G.J., Richardson, A.D., Ni-Meister, W., Schaaf, C.L., Woodcock, C.E., & Strahler, A.H. (2011). Measuring effective leaf area index, foliage profile, and stand height in New

England forest stands using a full-waveform ground-based lidar. *Remote Sensing of Environment*, 115, 2954-2964

Zhao, F., Yang, X.Y., Strahler, A.H., Schaaf, C.L., Yao, T., Wang, Z.S., Roman, M.O., Woodcock, C.E., Ni-Meister, W., Jupp, D.L.B., Lovell, J.L., Culvenor, D.S., Newnham, G.J., Tang, H., & Dubayah, R.O. (2013). A comparison of foliage profiles in the Sierra National Forest obtained with a full-waveform under-canopy EVI lidar system with the foliage profiles obtained with an airborne full-waveform LVIS lidar system. *Remote Sensing of Environment*, 136, 330-341

Zhao, K., & Popescu, S. (2009). Lidar-based mapping of leaf area index and its use for validating GLOBCARBON satellite LAI product in a temperate forest of the southern USA. *Remote Sensing of Environment*, 113, 1628-1645

Zhao, M.S., Heinsch, F.A., Nemani, R.R., & Running, S.W. (2005). Improvements of the MODIS terrestrial gross and net primary production global data set. *Remote Sensing of Environment*, 95, 164-176

Zheng, G., & Moskal, L.M. (2012). Computational-Geometry-Based Retrieval of Effective Leaf Area Index Using Terrestrial Laser Scanning. *IEEE Transactions on Geoscience and Remote Sensing*, 50, 3958-3969